Lecture Notes in Physics 873

Gabriele Ghisellini

Radiative Processes in High Energy Astrophysics

Springer

Lecture Notes in Physics

Volume 873

Founding Editors

W. Beiglböck
J. Ehlers
K. Hepp
H. Weidenmüller

Editorial Board

B.-G. Englert, Singapore, Singapore
U. Frisch, Nice, France
P. Hänggi, Augsburg, Germany
W. Hillebrandt, Garching, Germany
M. Hjorth-Jensen, Oslo, Norway
R. A. L. Jones, Sheffield, UK
H. von Löhneysen, Karlsruhe, Germany
M. S. Longair, Cambridge, UK
J.-F. Pinton, Lyon, France
J.-M. Raimond, Paris, France
A. Rubio, Donostia, San Sebastian, Spain
M. Salmhofer, Heidelberg, Germany
D. Sornette, Zurich, Switzerland
S. Theisen, Potsdam, Germany
D. Vollhardt, Augsburg, Germany
W. Weise, Garching, Germany and Trento, Italy
J. D. Wells, Geneva, Switzerland

For further volumes:
www.springer.com/series/5304

The Lecture Notes in Physics

The series Lecture Notes in Physics (LNP), founded in 1969, reports new developments in physics research and teaching—quickly and informally, but with a high quality and the explicit aim to summarize and communicate current knowledge in an accessible way. Books published in this series are conceived as bridging material between advanced graduate textbooks and the forefront of research and to serve three purposes:

- to be a compact and modern up-to-date source of reference on a well-defined topic
- to serve as an accessible introduction to the field to postgraduate students and nonspecialist researchers from related areas
- to be a source of advanced teaching material for specialized seminars, courses and schools

Both monographs and multi-author volumes will be considered for publication. Edited volumes should, however, consist of a very limited number of contributions only. Proceedings will not be considered for LNP.

Volumes published in LNP are disseminated both in print and in electronic formats, the electronic archive being available at springerlink.com. The series content is indexed, abstracted and referenced by many abstracting and information services, bibliographic networks, subscription agencies, library networks, and consortia.

Proposals should be sent to a member of the Editorial Board, or directly to the managing editor at Springer:

Christian Caron
Springer Heidelberg
Physics Editorial Department I
Tiergartenstrasse 17
69121 Heidelberg/Germany
christian.caron@springer.com

Gabriele Ghisellini

Radiative Processes in High Energy Astrophysics

Springer

Gabriele Ghisellini
Osservatorio Astronomico di Brera
INAF
Merate, Italy

ISSN 0075-8450 ISSN 1616-6361 (electronic)
Lecture Notes in Physics
ISBN 978-3-319-00611-6 ISBN 978-3-319-00612-3 (eBook)
DOI 10.1007/978-3-319-00612-3
Springer Cham Heidelberg New York Dordrecht London

Library of Congress Control Number: 2013941386

© Springer International Publishing Switzerland 2013
This work is subject to copyright. All rights are reserved by the Publisher, whether the whole or part of the material is concerned, specifically the rights of translation, reprinting, reuse of illustrations, recitation, broadcasting, reproduction on microfilms or in any other physical way, and transmission or information storage and retrieval, electronic adaptation, computer software, or by similar or dissimilar methodology now known or hereafter developed. Exempted from this legal reservation are brief excerpts in connection with reviews or scholarly analysis or material supplied specifically for the purpose of being entered and executed on a computer system, for exclusive use by the purchaser of the work. Duplication of this publication or parts thereof is permitted only under the provisions of the Copyright Law of the Publisher's location, in its current version, and permission for use must always be obtained from Springer. Permissions for use may be obtained through RightsLink at the Copyright Clearance Center. Violations are liable to prosecution under the respective Copyright Law.
The use of general descriptive names, registered names, trademarks, service marks, etc. in this publication does not imply, even in the absence of a specific statement, that such names are exempt from the relevant protective laws and regulations and therefore free for general use.
While the advice and information in this book are believed to be true and accurate at the date of publication, neither the authors nor the editors nor the publisher can accept any legal responsibility for any errors or omissions that may be made. The publisher makes no warranty, express or implied, with respect to the material contained herein.

Printed on acid-free paper

Springer is part of Springer Science+Business Media (www.springer.com)

Preface

These notes have been written for a University course in Physics and Astronomy, that I taught for some years in Milano. The title is very similar to the one of the famous Rybicki and Lightman book (*Radiative Processes in Astrophysics*), and not by chance, since it hopes to have the same intuitive insight and attention for the physical concepts, rather than for difficult mathematical demonstrations. The aim of the book is to guide the students through the first steps in high energy astrophysics. As such, it requires some, but not much, previous knowledge of general and classical astronomy.

I think that the study of rather violent cosmic phenomena, born when we could open other electromagnetic windows besides the visible band, has been very important, enjoyable and productive, and it will continue to be so in the future, hopefully also when the non-electromagnetic messengers (neutrinos and gravitational waves) will be finally routinely detected. In general, these violent phenomena are associated to strong gravity, but also to fast velocities of extended objects. For this reason I included an entire chapter dedicated to the use of special relativity with extended objects. I hope it helps to clear up some confusing notations and formalisms.

Another field of interests in high energy astrophysics concerns the processes involving electron and positron pairs, to which I dedicate another chapter. The last chapter of the book is dedicated to active galactic nuclei. This is thought as illustrative of all the processes explained in the first part of the book. It is then a good field of research where we can apply the basics just learnt.

The style of the book has been intentionally kept rather informal, hoping that this helps the understanding of the basic concepts, leaving to other books the duty to offer more specialized material for the interested reader.

Finally, I would like to thank the three teachers of my scientific youth: Laura Maraschi, Roland Svensson and Andy Fabian.

Merate, Italy Gabriele Ghisellini

Contents

1 Some Fundamental Definitions 1
1.1 Luminosity 1
1.2 Flux 2
1.3 Intensity 2
1.4 Emissivity 2
1.5 Radiative Energy Density 2
1.6 How to Go from L to u 3
1.6.1 We Are Outside the Source 3
1.6.2 We Are Inside a Uniformly Emitting Source 3
1.6.3 We Are Inside a Uniformly Emitting Shell 4
1.7 How to Go from I to F 4
1.7.1 Flux from a Thick Spherical Source 5
1.8 Radiative Transport: Basics 5
1.8.1 The "$\cos\theta$ Law" 7
1.9 Einstein Coefficients 8
1.9.1 Emissivity, Absorption and Einstein Coefficients 11
1.10 Mean Free Path 11
1.10.1 Random Walk 12
1.11 Thermal and Non-thermal Plasmas 13
1.11.1 Energy Exchange and Thermal Plasmas 14
1.11.2 Non-thermal Plasmas 15
1.12 Coulomb Collisions 15
1.12.1 Cross Section 16
1.13 The Electric Field of a Moving Charge 18
1.13.1 Total Emitted Power: Larmor Formula 20
1.13.2 Pattern 21

2 Bremsstrahlung and Black Body 23
2.1 Bremsstrahlung 23
2.1.1 Free–Free Absorption 25
2.1.2 From Bremsstrahlung to Black Body 26

2.2 Black Body . . . 27
References . . . 29

3 Beaming . . . 31
3.1 Rulers and Clocks . . . 31
3.2 Photographs and Light Curves . . . 32
3.2.1 The Moving Bar . . . 32
3.2.2 The Moving Square . . . 33
3.2.3 Rotation, Not Contraction . . . 34
3.2.4 Time . . . 35
3.2.5 Aberration . . . 36
3.2.6 Intensity . . . 38
3.2.7 Luminosity and Flux . . . 38
3.2.8 Emissivity . . . 39
3.2.9 Brightness Temperature . . . 41
3.2.10 Moving in a Homogeneous Radiation Field . . . 41
3.3 Superluminal Motion . . . 43
3.4 A Question . . . 45
References . . . 46

4 Synchrotron Emission and Absorption . . . 47
4.1 Introduction . . . 47
4.2 Total Losses . . . 47
4.2.1 Synchrotron Cooling Time . . . 50
4.3 Spectrum Emitted by the Single Electron . . . 50
4.3.1 Basics . . . 50
4.3.2 The Real Stuff . . . 52
4.3.3 Limits of Validity . . . 53
4.3.4 From Cyclotron to Synchrotron Emission . . . 54
4.4 Emission from Many Electrons . . . 54
4.5 Synchrotron Absorption: Photons . . . 57
4.5.1 From Thick to Thin . . . 58
4.6 Synchrotron Absorption: Electrons . . . 59
Appendix Useful Formulae . . . 61
A.1 Emissivity . . . 61
A.2 Absorption Coefficient . . . 62
A.3 Specific Intensity . . . 63
A.4 Self-absorption Frequency . . . 63
A.5 Synchrotron Peak . . . 64
References . . . 64

5 Compton Scattering . . . 65
5.1 Introduction . . . 65
5.2 The Thomson Cross Section . . . 65
5.2.1 Why the Peanut Shape? . . . 66
5.3 Direct Compton Scattering . . . 68
5.4 The Klein–Nishina Cross Section . . . 68

5.4.1 Another Limit . . . 70
5.4.2 Pause . . . 71
5.5 Inverse Compton Scattering . . . 72
5.5.1 Thomson Regime . . . 72
5.5.2 Typical Frequencies . . . 72
5.5.3 Cooling Time and Compactness . . . 76
5.5.4 Single Particle Spectrum . . . 77
5.6 Emission from Many Electrons . . . 79
5.6.1 Non-monochromatic Seed Photons . . . 81
5.7 Thermal Comptonization . . . 82
5.7.1 Average Number of Scatterings . . . 83
5.7.2 Average Gain per Scattering . . . 83
5.7.3 Comptonization Spectra: Basics . . . 85
References . . . 88

6 Synchrotron Self-Compton . . . 89
6.1 SSC Emissivity . . . 89
6.2 Diagnostic . . . 90
6.3 Why It Works . . . 92

7 Pairs . . . 95
7.1 Thermal Pairs . . . 96
7.1.1 First Important Result . . . 97
7.1.2 Second Important Result . . . 98
7.2 Non-thermal Pairs . . . 101
7.2.1 Optical Depth and Compactness . . . 101
7.2.2 Photon–Photon Absorption . . . 103
7.2.3 An Illustrative Case: Saturated Pair Production . . . 105
7.2.4 Importance in Astrophysics . . . 107
References . . . 109

8 Active Galactic Nuclei . . . 111
8.1 Introduction . . . 111
8.2 The Discovery . . . 112
8.2.1 Maarten Schmidt Discovers the Redshift of 3C 273 . . . 112
8.3 Basic Components . . . 113
8.4 The Supermassive Black Hole . . . 114
8.5 Accretion Disk: Luminosities and Spectra . . . 115
8.5.1 Spectrum . . . 115
8.6 Emission Lines . . . 117
8.6.1 Broad Emission Lines . . . 118
8.6.2 Narrow Emission Lines . . . 119
8.7 The X-Ray Corona . . . 120
8.7.1 The Power Law: Thermal Comptonization . . . 121
8.7.2 Compton Reflection . . . 122
8.7.3 The Iron Line . . . 123

8.8 The Torus and the Seyfert Unification Scheme 124
8.8.1 The X-Ray Background 127
8.9 The Jet 128
8.9.1 Flat and Steep Radio AGNs 128
8.9.2 Blazars 129
8.9.3 The Power of the Jet 135
8.9.4 Lobes as Energy Reservoirs 137
8.10 Open Issues 138
References 140

Further Reading 141

Index 143

Chapter 1
Some Fundamental Definitions

1.1 Luminosity

By luminosity we mean the quantity of energy irradiated per second [erg s^{-1}]. The luminosity *is not* defined per unit of solid angle. The *monochromatic* luminosity $L(\nu)$ is the luminosity per unit of frequency ν (i.e. per Hz). The *bolometric* luminosity is integrated over frequency:

$$L = \int_0^\infty L(\nu) d\nu \tag{1.1}$$

Often we can define a luminosity integrated in a given energy (or frequency) range, as, for instance, the 2–10 keV luminosity. In general we have:

$$L_{[\nu_1 - \nu_2]} = \int_{\nu_1}^{\nu_2} L(\nu) d\nu \tag{1.2}$$

Examples:

- Sun Luminosity: $L_\odot = 4 \times 10^{33}$ erg s^{-1}
- Luminosity of a typical galaxy: $L_{\rm gal} \sim 10^{11} L_\odot$
- Luminosity of the human body, assuming that we emit as a black-body at a temperature of (273 + 36) K and that our skin has a surface of approximately $S = 2$ m^2:

$$L_{\rm body} = S\sigma T^4 \sim 10^{10} \text{ erg/s} \sim 10^3 \text{ W} \tag{1.3}$$

This *is not* what we loose, since we absorb from the ambient a power $L = S\sigma T_{\rm amb}^4 \sim 8.3 \times 10^9$ erg/s if the ambient temperature is 20 C (=273 + 20 K).

G. Ghisellini, *Radiative Processes in High Energy Astrophysics*,
Lecture Notes in Physics 873, DOI 10.1007/978-3-319-00612-3_1,
© Springer International Publishing Switzerland 2013

1.2 Flux

The flux [erg cm^{-2} s^{-1}] is the energy passing a surface of 1 cm^2 in one second. If a body emits a luminosity L and is located at a distance R, the flux is

$$F = \frac{L}{4\pi R^2}; \quad F(\nu) = \frac{L(\nu)}{4\pi R^2}; \quad F = \int_0^\infty F(\nu) d\nu \tag{1.4}$$

1.3 Intensity

The intensity I is the energy per unit time passing through a unit surface located perpendicularly to the arrival direction of photons, per unit of solid angle. The solid angle appears: [erg cm^{-2} s^{-1} sterad^{-1}]. The monochromatic intensity $I(\nu)$ has units [erg cm^{-2} s^{-1} Hz^{-1} sterad^{-1}]. It always obeys the Lorentz transformation:

$$\frac{I(\nu)}{\nu^3} = \frac{I'(\nu')}{(\nu')^3} = \text{invariant} \tag{1.5}$$

where primed and unprimed quantities refer to two different reference frames. The intensity *does not* depend upon distance. It is the measure of the irradiated energy along a light ray.

1.4 Emissivity

The emissivity j is the quantity of energy emitted by a unit volume, in one unit of time, for a unit solid angle

$$j = \frac{\text{erg}}{dV dt d\Omega} \tag{1.6}$$

If the source is transparent, there is a simple relation between j and I:

$$I = jR \quad \text{(optically thin source)} \tag{1.7}$$

1.5 Radiative Energy Density

We can define it as the energy per unit volume produced by a luminous source, but we have to specify if it is per unit solid angle or not. For simplicity consider the bolometric intensity I. Along the light ray, construct the volume $dV = cdtdA$ where dA (i.e. one cm^2) is the base of the little cylinder of height cdt. The energy contained in this cylinder is

$$dE = I cdtdAd\Omega \tag{1.8}$$

In that cylinder I find the light coming from a given direction, I can also say that:

$$dE = u(\Omega)cdtdAd\Omega \tag{1.9}$$

Therefore

$$u(\Omega) = \frac{I}{c} \tag{1.10}$$

If I want the total u (i.e. summing the light coming from all directions) I must integrate over the entire solid angle.

1.6 How to Go from L to u

There at least 3 possible ways, according if we are outside the source, at a large distance with respect to the size of the source, or if we are inside a source, that in turn can emit uniformly or only in a shell.

1.6.1 We Are Outside the Source

Assume to be at a distance D from the source (see Fig. 1.1). Consider the shell of surface $4\pi D^2$ and height cdt. The volume of this shell is $dV = 4\pi D^2 cdt$. In the time dt the source has emitted an energy $dE = Ldt$. This very same energy is contained in the spherical shell. Therefore the energy density (integrated over the solid angle) is:

$$u = \frac{dE}{dV} = \frac{L}{4\pi D^2 c} \tag{1.11}$$

1.6.2 We Are Inside a Uniformly Emitting Source

Assume that the source is optically thin and homogeneous. In this case the energy density will depend upon the mean escape time from the source. For a given fixed luminosity we have that the longer the escape time, the larger the energy density (more photons accumulate inside the source before escaping). Therefore:

$$u = \frac{L}{V}\langle t_{\rm esc}\rangle \tag{1.12}$$

For a source of size R one can think that the average escape time is $\langle t_{\rm esc}\rangle \sim R/c$, but we should consider that this is true for a photon created at the center. If the photon is created at the border of the sphere, it will have a probability $\sim 1/2$ to escape immediately, and a probability *less* than $1/2$ to pass the entire $2R$ diameter of the

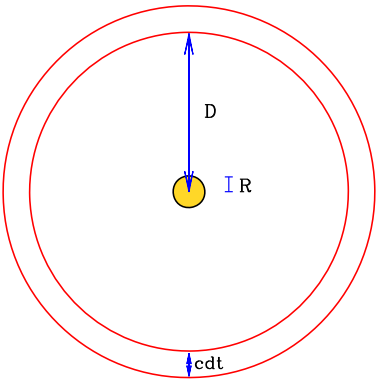


Fig. 1.1 A source of radius R emits a luminosity L. The way to calculate the energy density of the emitted radiation is different if we are outside the source (at the distance D) or inside the source

sphere. Therefore the mean escape time will be less that R/c. Indeed, for a sphere, it is $\langle t_{\rm esc}\rangle \sim (3/4)R/c$ Therefore:

$$u = \frac{3L}{4\pi R^3}\frac{3R}{4c} = \frac{9}{4}\frac{L}{4\pi R^2 c} \tag{1.13}$$

Note that this is more (by a 9/4 factor) than what could be estimated by Eq. 1.11 setting $D = R$. We stress that one can use Eq. 1.13 only for a thin source.

1.6.3 We Are Inside a Uniformly Emitting Shell

Assume that a spherical shell of radius R emits uniformly a luminosity L. In this case the radiation energy density returns to be

$$u = \frac{L}{4\pi R^2 c} \tag{1.14}$$

and it is equal in any location inside the shell.

1.7 How to Go from *I* to *F*

The relation between the intensity I and the total flux F must account for the fact that, in general, each element of the surface is seen under a different angle θ. See Fig. 1.2. We should then consider the projected area, and introduce a $\cos\theta$ term in the integral:

$$F = \int I \cos\theta d\Omega \tag{1.15}$$

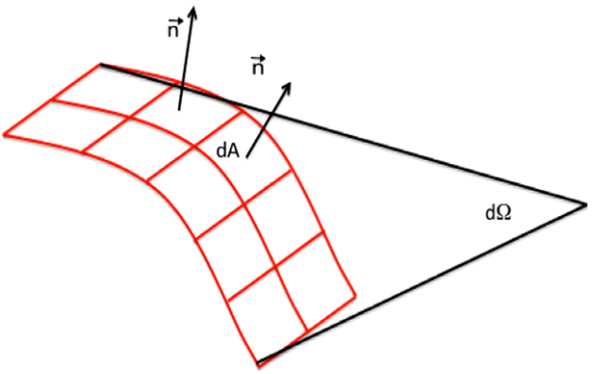


Fig. 1.2 This figure illustrates the fact that each element dA of the surface is seen under a different angle with respect to the normal $\vec{n}$

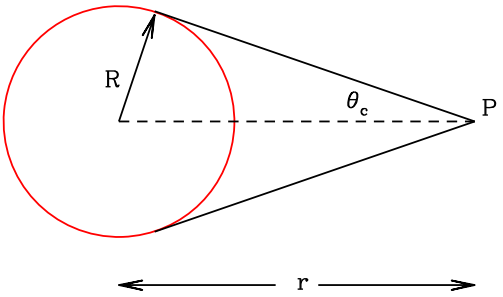


Fig. 1.3 The observer P sees the spherical source as a disk of angular radius θ_c. Each element of the sphere has a different projection

1.7.1 Flux from a Thick Spherical Source

If we see only the surface of a sphere, namely the source is optically thick, and if the intensity is constant along the surface we have symmetry along the ϕ directions and the solid angle $d\Omega = 2\pi \sin\theta d\theta$. See Fig. 1.3. We get:

$$F = \int I \cos\theta d\Omega = 2\pi I \int_0^{\theta_c} \sin\theta \cos\theta d\theta \tag{1.16}$$

Here $R = r \sin\theta_c$. Therefore we have

$$F = 2\pi I \left[\frac{\cos^2\theta}{2}\right]_{\cos\theta_c}^{1} = \pi I \sin^2\theta_c = \pi I \left(\frac{R}{r}\right)^2 \tag{1.17}$$

At the surface, $R = r$, and we have $F = \pi I$.

Very far away, $r \gg R$, and we have $F = \pi\theta_c^2 I = I\Omega_{\text{source}}$.

1.8 Radiative Transport: Basics

Once the radiation is produced in a given location inside the source, we have to see how much of this can leave the source and reach the observer. To calculate that,

we must introduce the **absorption coefficient** α_ν, whose dimension is [length^{-1}]. It is defined by the following equation, describing the decrement of I_ν when passing trough an infinitesimal path of length ds:

$$dI_\nu = -\alpha_\nu I_\nu ds \tag{1.18}$$

The absorption coefficient can be thought as the product of a density of "absorbers" times the cross section of the absorbing process:

$$\alpha_\nu = n\sigma_\nu \tag{1.19}$$

But inside a source, besides absorption, there is a contribution to I_ν coming from the emitters distributed along ds. The increment of I_ν is

$$dI_\nu = j_\nu ds \tag{1.20}$$

Therefore, combining emission and absorption, we have the basic equation of radiative transport:

$$\frac{dI_\nu}{ds} = -\alpha_\nu I_\nu + j_\nu \tag{1.21}$$

We solve it in some specific cases:

1. **Emission only**:

$$\frac{dI_\nu}{ds} = j_\nu \rightarrow I_\nu = I_{\nu,0} + \int_0^S j_\nu ds \tag{1.22}$$

   where S is the total emitting path.
2. **Absorption only**:

$$\frac{dI_\nu}{ds} = -\alpha_\nu I_\nu \rightarrow \frac{dI_\nu}{I_\nu} = -\alpha_\nu ds \tag{1.23}$$

   Note that the form of this relation immediately implies that an exponential is involved:

$$I_\nu(s) = I_\nu(s_0) e^{-\int_{s_0}^{s} \alpha_\nu(s')ds'} \tag{1.24}$$

   Before passing the layer, the intensity was $I_{\nu,0}$. While passing the layer of length s, the intensity decreases exponentially.
3. **Emission plus absorption**: In this case it is convenient to introduce the optical depth τ_ν:

$$d\tau_\nu = \alpha_\nu ds = n\sigma_\nu ds \tag{1.25}$$

   The transport equation then becomes:

$$\frac{dI_\nu}{\alpha_\nu ds} = -I_\nu + \frac{j_\nu}{\alpha_\nu} \rightarrow \frac{dI_\nu}{d\tau_\nu} = -I_\nu + \frac{j_\nu}{\alpha_\nu} \tag{1.26}$$

We can call **source function** the quantity S_ν defined as

$$S_\nu = \frac{j_\nu}{\alpha_\nu} \quad \text{source function} \tag{1.27}$$

Then the formal solution of Eq. 1.26 is

$$I_\nu(\tau_\nu) = I_{\nu,0} e^{-\tau_\nu} + \int_0^{\tau_\nu} e^{-(\tau_\nu - \tau'_\nu)} S_\nu\left(\tau'_\nu\right) d\tau'_\nu \tag{1.28}$$

here τ_ν is the final value of τ'_ν (i.e. when the intensity has traveled the entire distance s). *If* S_ν is constant:

$$I_\nu(\tau_\nu) = I_{\nu,0} e^{-\tau_\nu} + S_\nu\left(1 - e^{-\tau_\nu}\right) \tag{1.29}$$

If $I_{\nu,0} = 0$:

$$I_\nu(\tau_\nu) = \frac{j_\nu}{\alpha_\nu}\left(1 - e^{-\tau_\nu}\right) \tag{1.30}$$

Now, a trick: multiply and divide the RHS by $s = R$ (the dimension of the source) to obtain:

$$I_\nu(\tau_\nu) = \frac{j_\nu R}{\alpha_\nu R}\left(1 - e^{-\tau_\nu}\right) = j_\nu R\left(\frac{1 - e^{-\tau_\nu}}{\tau_\nu}\right) \tag{1.31}$$

In this form it is immediately clear that when the source is optically thin (and $\tau_\nu \ll 1$), we have $1 - e^{-\tau_\nu} \to 1 - 1 + \tau_\nu$ and therefore

$$I_\nu(\tau_\nu) = j_\nu R, \quad (\tau_\nu \ll 1) \tag{1.32}$$

When instead the source becomes optically thick, and $\tau_\nu \gg 1$, then;

$$I_\nu(\tau_\nu) = \frac{j_\nu R}{\tau_\nu}, \quad (\tau_\nu \gg 1) \tag{1.33}$$

Usually, this happens at low frequencies. The above equation explicitly shows that the intensity we see from a thick source comes from a layer of width R/τ_ν, i.e. the layer that is optically thin. In other words we always collect radiation from a layer of the source, down to the depth at which the radiation can escape without being absorbed ($\tau_{\text{layer}} = 1$).

1.8.1 The "$\cos\theta$ Law"

We often say that the radiation of an optically thick source comes from "its surface". Also, we often say that the intensity received from a surface depends on the inclination of that surface, so that the received intensity is maximum for a face-on surface, and negligible for a edge-on one. But can a surface emit? Certainly not! A "surface" has two dimensions, and zero width. There is no room for any atom, inside a surface! So, what do we mean for? Look at Fig. 1.4. Suppose that there is an emitting

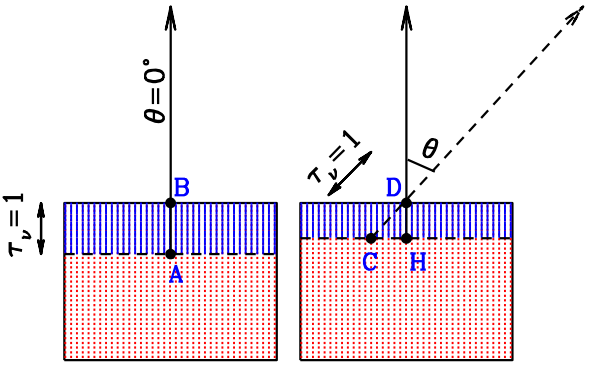


Fig. 1.4 A layer of total optical depth $\tau_\nu \gg 1$ is observed face-on (*left*) and from an *angle* θ from its normal (*right*). The two observers receive always the emission produced in the shell of unit optical depth. But an optical depth of unity corresponds to the length AB (*left*) or CD (*right*). The two lengths are equal ($AB = CD$), but one is inclined, therefore the two volumes are different (by the factor $DH/AB = \cos\theta$)

layer. It is optically thick, but its τ_ν cannot be infinity... The observer looking at the layer face-on receives the radiation produced in a layer of optical depth $\tau_\nu \sim 1$. The optical depth depends on the viewing angle. For a face-on observer, the layer contributing to the emission is maximum, as it is the volume of the layer emitting the unabsorbed radiation. For different viewing angles, the radiation reaching the observer makes a path of the same length inside the layer (of unity optical depth), but inclined. Consequently, the emitting volume is less, by a $\cos\theta$ factor. The radiation we receive is *always* produced in a volume, *never* in a surface...

1.9 Einstein Coefficients

The Einstein coefficients concern intrinsic properties of the emitting particles. As such, they involve more general concepts than the emission or the absorption coefficients. They concern the probability that a particle spontaneously emits a photon, the probability to absorb a photon, and the probability to emit a photon under the influence of another incoming photon (see Fig. 1.6). The latter concept, at first sight, is weird. In the current world we are surrounded by electronic devices using lasers, and therefore we are used to the concept of *stimulated emission*. This was however introduced by Einstein (in 1917) because, without it, he could not recover the black-body formula.

Let us define a system in which the emitting electron can be in one of several energy levels. Each level has a statistical weight g_i. The simple case that comes into mind is an atom. See Fig. 1.5.

Spontaneous Emission A_{21}—This process corresponds to a jump of the electrons from energy level 2 to level 1 by emitting a photon of energy $h\nu$ corresponding

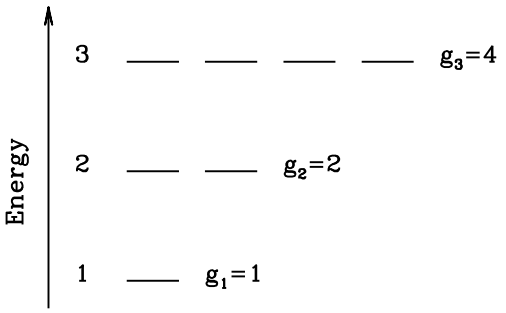


Fig. 1.5 The shown 3 energy levels have different statistical weights g_i

to the jump in energy $E_2 - E_1$. The subscripts 1 and 2 indicate energy levels 1 and 2, but are not important, we can equivalently talk of a jump between the energy levels 5 and 4... and so on. The corresponding Einstein coefficient is A_{21}. Therefore

$$A_{21} = \text{transition probability for spont. emission } \left[\text{s}^{-1}\right] \tag{1.34}$$

Absorption B_{12}—This occurs when the electron is in level 1 and absorb a photon of energy $h\nu$ that corresponds to the energy difference between levels 1 and 2. The probability of one electron to make this transition depends on how many photon there are, and therefore to the intensity J_ν of the radiation field. The latter is averaged over the solid angle: $J_\nu = (1/4\pi) \int I_\nu d\Omega$.

$$B_{12} J_\nu = \text{transition probability for absorption per unit time} \tag{1.35}$$

Stimulated Emission B_{21}—This occurs when the electron is in level 2, and the arrival of a photon of energy $h\nu$ corresponding to the energy difference between levels 2 and 1 makes the electron jump to level 1 by emitting a photon. The energy

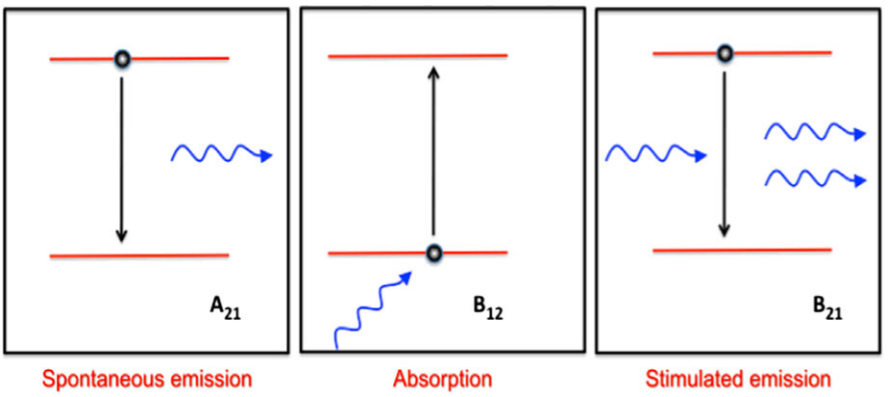


Fig. 1.6 Illustrative sketch for the processes of spontaneous emission, absorption and stimulated emission

of the emitted photon is the same of the energy of the incoming one. It can be shown that also the direction and the phase of the two photons are the same. We then have a coherent emission, at the base of all laser and maser devices. The probability of one electron to make the $2 \rightarrow 1$ transition depends on how many photons there are, and therefore on the radiation intensity:

$$B_{21} J_\nu = \text{transition probability for stimulated emission per unit time} \tag{1.36}$$

The Einstein coefficients are completely general, and are valid for any radiation field (i.e. even out of equilibrium). They are valid even when we have a free particle, (i.e. not an atom), because we can define even in that case the energy state of the particle.

In particular, we can find the relations between the Einstein coefficients in the particular case of equilibrium, that is when the transitions $2 \rightarrow 1$ are equal to the transitions $1 \rightarrow 2$. Assume then that n_1 and n_2 are the number density of electrons in the levels 1 and 2. We must have:

$$n_1 B_{12} J_\nu = n_2 A_{21} + n_2 B_{21} J_\nu \tag{1.37}$$

Solving for J_ν:

$$J_\nu = \frac{A_{21}/B_{21}}{(n_1/n_2)(B_{12}/B_{21}) - 1} \tag{1.38}$$

At equilibrium the ratio n_1/n_2 must be:

$$\frac{n_1}{n_2} = \frac{g_1}{g_2} \frac{e^{-E/kT}}{e^{-(E+h\nu)/kT}} = \frac{g_1}{g_2} e^{h\nu/kT} \tag{1.39}$$

where g_1 and g_2 are the statistical weights of the levels 1 and 2. Inserting in Eq. 1.38 we have

$$J_\nu = \frac{A_{21}/B_{21}}{(g_1 B_{12}/g_2 B_{21}) e^{h\nu/kT} - 1} \tag{1.40}$$

We know that at equilibrium J_ν must be equal to the black-body intensity B_ν. For this to happen it must be that:

$$\begin{aligned} g_1 B_{12} &= g_2 B_{21} \\ A_{21} &= \frac{2h\nu^3}{c^2} B_{21} \end{aligned} \tag{1.41}$$

These are the relations among the Einstein coefficients. Although we have found them in one particular case, these relations are always valid, also out of equilibrium, because they concern intrinsic properties of the system (note for instance that they do no depend on temperature). The relations between the Einstein coefficients imply that we need to know only one of them to find the others.

1.9.1 Emissivity, Absorption and Einstein Coefficients

The emissivity [erg s^{-1} cm^{-2} Hz^{-1} sterad^{-1}] is related to the Einstein coefficient A_{21}. If n_2 is the density of electrons in the state 2, we must have

$$j_\nu = \frac{h\nu}{4\pi} n_2 A_{21} \tag{1.42}$$

The reason of the 4π is because $n_2 A_{21}$ is the probability to emit a photon (for spontaneous emission) *in any direction*, while the emissivity j_ν is for unit of solid angle.

Also the stimulated emission produces photons. Why do we not include it the calculus for the emissivity? Because, to have stimulated emission, we must have the incoming radiation, and it is therefore more convenient to think to stimulated emission as *negative* absorption. For the *total* absorption, consider the quantity $\alpha_\nu I_\nu$. This is the amount of energy absorbed for unit volume, time, frequency and solid angle. We also have that $n_1 B_{12} I_\nu$ is the number of the $1 \to 2$ transitions per unit time, volume and frequency. We must multiply by $h\nu$ to have the energy (per second, Hz, cm^3) and divide by 4π to have the same quantity per unit solid angle. I_ν drops out and we have

$$\begin{aligned}
\alpha_\nu &= \frac{h\nu}{4\pi}(n_1 B_{12} - n_2 B_{21}) \\
&= \frac{h\nu}{4\pi}\left(\frac{n_1 g_2}{g_1} - n_2\right) B_{21} \\
&= \left(\frac{n_1 g_2}{g_1} - n_2\right) \frac{A_{21} c^2}{8\pi \nu^2} \\
&= \left(\frac{n_1 g_2}{n_2 g_1} - 1\right) \frac{c^2}{2h\nu^3} j_\nu
\end{aligned} \tag{1.43}$$

We conclude that absorption and emission are intimately linked, and knowing one process is enough to derive the other one, from first principles. If a particle emits, it can also absorb.

1.10 Mean Free Path

The mean free path (for a photon) is the average distance ℓ traveled by a photon without interacting. It corresponds to a distance for which $\tau_\nu = 1$:

$$\tau_\nu = 1 \to \sigma_\nu n \ell_\nu = 1 \to \ell_\nu = \frac{1}{n\sigma_\nu} \tag{1.44}$$

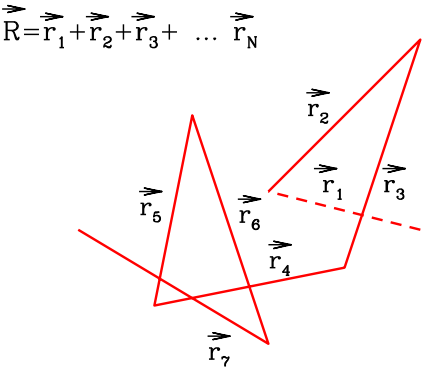


Fig. 1.7 Random walk of a photon inside a source

If a source has radius R and total optical depth $\tau_\nu > 1$ we have:

$$\ell_\nu = \frac{1}{\sigma_\nu n} = \frac{R}{\sigma_\nu n R} = \frac{R}{\tau_\nu} \tag{1.45}$$

1.10.1 Random Walk

Assume that a photon interacts through scattering with electrons inside a source of radius R and optical depth $\tau > 1$. It is a good approximation to assume that the scattering angle is random, so the direction after a collision will be random. The photon will travel "bouncing" from one electron to the next, each time traveling for a mean free path. We then ask: (i) how many scatterings does it have to do before escaping? (ii) How much time does it takes?

Figure 1.7 illustrates the random motion of a photon inside the source. Each segment corresponds to a free path, whose average length is ℓ. The total displacement after N scatterings will be $\vec{R}$, but if we calculate $\vec{R}$ simply summing all the vectors $\vec{r}_1, \vec{r}_2, \vec{r}_3, \ldots, \vec{r}_N$, we obtain 0.

To calculate the distance traveled by the photon we calculate the *square* of $\vec{R}$:

$$\langle \vec{R}^2 \rangle = \langle \vec{r}_1^2 \rangle + \langle \vec{r}_2^2 \rangle + \langle \vec{r}_3^2 \rangle + 2\langle \vec{r}_1 \cdot \vec{r}_2 \rangle + 2\langle \vec{r}_1 \cdot \vec{r}_3 \rangle + \cdots . \tag{1.46}$$

The cross products, on average, vanish, because the $\cos\theta$ between the vectors vanishes, on average. Therefore we remain with the squares only, and each term r_i is, on average, long as a mean free path. We have N of these terms. Therefore

$$\langle \vec{R}^2 \rangle = N\langle \vec{r}_i^2 \rangle = N\ell^2 \rightarrow \sqrt{\langle \vec{R}^2 \rangle} = \sqrt{N}\ell \tag{1.47}$$

If we want to know how many scatterings, on average, a photon undergoes before escaping a source of radius R, we write:

$$\sqrt{N} = \frac{R}{\ell} = R\sigma n = \tau \rightarrow N = \tau^2 \tag{1.48}$$

Remember: this is valid only if $\tau > 1$ (if $\tau < 1$ then the majority of photons escape the source without interacting...).

The other question is how long does it take to escape. If $t_1 = \ell/c$ is the average time for one scattering, we have a total time $t_{\rm tot}$

$$t_{\rm tot} = N t_1 = \tau^2 \frac{\ell}{c} = \tau^2 \frac{R}{R\sigma nc} = \frac{R}{c}\frac{\tau^2}{\tau} = \tau \frac{R}{c} \tag{1.49}$$

So, on average, the photons makes τ^2 scatterings before escaping a source with a scattering optical depth $\tau > 1$. Since each mean free path is long R/τ, the total distance traveled by the photon is τR and of course the total time to escape is $\tau R/c$. Beware that this is true *on average*. As we shall see, the formation of the high energy spectrum through Comptonization involves those photons that make more than τ^2 scatterings, because in this way they can reach higher energies.

Just for fun, suppose that our Sun is uniform and completely ionized. It has a radius $R_\odot = 7 \times 10^{10}$ cm, and a mean density of 1 g cm^{-3}.

- How many scatterings does a photon (created in the center) make before it can escape?
- How long does it take to escape?

1.11 Thermal and Non-thermal Plasmas

By definition, a *thermal plasma* is characterized by a Maxwellian distribution of particles. Therefore a *non-thermal plasma* is anything else. The non-relativistic Maxwellian distribution is:

$$F(v)dv = 4\pi v^2 \left(\frac{m}{2\pi kT}\right)^{3/2} e^{-mv^2/2kT} dv \tag{1.50}$$

In this form, $F(v)$ is normalized, i.e. $\int_0^\infty F(v)dv = 1$. This can be seen changing variable of integration, from v to $x = mv^2/(2kT)$, and remembering that $\int_0^\infty \sqrt{x} e^{-x} dx = \sqrt{\pi}/2$.

It is worth to stress that the physics is in the exponential term, while the $4\pi v^2 dv$ term is simply equal to $dv_x dv_y dv_z$ (in three dimensions). This then suggests the questions: it is possible to have a "Maxwellian-like" distribution in 2 dimensions? And in one dimension?

Instead of the *velocities* we may consider the *momenta* p of the particles. If we write

$$p \equiv \gamma \beta mc \tag{1.51}$$

where $\gamma = 1/(1-\beta^2)^{1/2}$, the above relation is valid both for non-relativistic and for relativistic velocities. The Maxwellian momenta distribution becomes (setting $\Theta \equiv kT/(mc^2)$):

$$F(p)dp = \frac{p^2 e^{-\gamma/\Theta}}{\Theta m^3 c^3 K_2(1/\Theta)} dp \tag{1.52}$$

where $K_2(1/\Theta)$ is the modified Bessel function of the second kind.

Note the following:

- To define a temperature, the distribution of velocities must be *isotropic*.
- Written in terms of momenta, the Maxwellian distribution has the same form in the relativistic limit.
- The Maxwellian distribution is very general, it is a result of statistical mechanics. But to achieve this distribution, it is necessary that the particles *exchange energy among themselves*.
- If competing processes are present (i.e. cooling) it is possible that one has a Maxwellian distribution only in some interval of velocities/momenta (for instance for low velocities).
- The exponential term $e^{-E/kT}$ contains the physics, the term p^2 is simply due to $dp_x dp_y dp_z = 4\pi p^2 dp$.

1.11.1 Energy Exchange and Thermal Plasmas

There are two main ways in which particles can exchange energy among themselves:

1. Collisions
2. Exchange of photons (emission and absorption; scattering)

Traditionally, one thinks to collisions as the main driver, and to Coulomb collisions as the main mechanism. Of course, the more the collisions, the faster the energy exchange and the faster the relaxation towards the thermal equilibrium. We have

$$\begin{aligned} \frac{\#\text{ of collisions of a single particle}}{\text{time}} &\propto \text{density } n \\ \frac{\text{total }\#\text{ of collisions}}{\text{time}} &\propto n^2 \end{aligned} \tag{1.53}$$

However, the density n is not the only factor. The other factor is the energy of the particle: the cross section *decreases* with the velocity of the particle (and then with its energy, or the temperature of the plasma). This means that **it is difficult to have a Maxwellian in hot and rarefied plasmas**.

Ask yourselves: what does it happen if I put particles all of the same energy in a box with reflecting and elastic walls? Why should the energy of a single particle change?

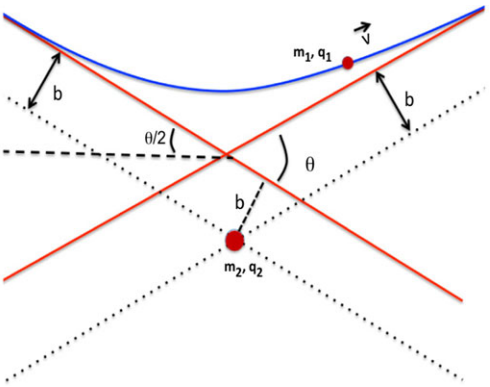


Fig. 1.8 Sketch of the trajectory of the charge q_1 (of mass $m_1 \ll m_2$) that is deflected by the charge q_2

1.11.2 Non-thermal Plasmas

In rarefied and hot plasmas, the *relaxation time* required to go to equilibrium, namely to have sufficient energy exchanges among particles, is long compared to the typical timescales of other processes, such as acceleration, cooling and escape. The particle distribution responsible for the radiation we see is then shaped by these other, more efficient, processes.

The queen of the non-thermal particle distribution is a power law:

$$N(E) = N_0 E^{-p} \tag{1.54}$$

When all particles are relativistic we can equivalently write

$$N(\gamma) = K\gamma^{-p} \tag{1.55}$$

Usually, N is the density [cm^{-3}] of the particles, but sometimes it can indicate the total number. Furthermore, one can also specify if $N(\gamma)$ is per unit of solid angle (when one has a distribution that is not isotropic), or not. One must also specify in what energy range $N(\gamma)$ is valid, so in general $N(\gamma)$ has a low and a high energy cutoff ($\gamma_{\rm min}$ and $\gamma_{\rm max}$). Within these two limits, a power-law particle distribution has no preferred energy (there is no peak or break).

Often one deals with a *broken power-law* distribution, defined by two power-laws of slopes p_1 and p_2 joining at some $\gamma_{\rm break}$.

The main acceleration process leading to a power-law distribution (but not the only one) is shock acceleration. In this process a particle gains energy each time it crosses the shock, and there is a probability, each passage, that the particle escape. This is sufficient to yield a power-law distribution.

1.12 Coulomb Collisions

Figure 1.8 shows the trajectory of a particle of mass m_1 and charge q_1 when it passes near a particle of mass m_2 and charge q_2. For the example in the figure the charges

are of the same sign, and $m_2 \gg m_1$. In general, we can introduce the *reduced mass* μ defined as

$$\mu = \frac{m_1 m_2}{m_1 + m_2}, \quad \mu \longrightarrow m_1 \quad \text{if } m_2 \gg m_1 \tag{1.56}$$

The impact parameter b corresponds to the minimum distance of the *unperturbed trajectory* from the mass m_2. The *deflection angle* θ is the angle between the incoming and outgoing velocity vectors (both measured at large distances from the location of m_2).

One also defines the quantity

$$\tan\theta/2 = \frac{b_0(v)}{b} \rightarrow b = \frac{b_0(v)}{\tan\theta/2} \tag{1.57}$$

where $b_0(v)$ corresponds to the impact parameter for deflection angles of 90° (namely, when $\tan\theta/2 = 1$. In this case $b_0(v) = b$). $b_0(v)$ is related to the electrostatic force. One makes the approximation that the interaction between the two particles is important only when the particle 1 is close to the particle 2. One can then say that the interaction time is of the order of $t \sim b_0/v$. The acceleration can then be approximated by $a \sim v/t \sim v^2/b_0$. On the other hand, the force responsible for this acceleration is $F = q_1 q_2/b_0^2$, and the acceleration is then $a = q_1 q_2/(\mu b_0^2)$. Equating the two expression for the acceleration we have:

$$b_0(v) = \frac{q_1 q_2}{\mu v^2} \tag{1.58}$$

Therefore

$$b = \frac{b_0(v)}{\tan\theta/2} = \frac{q_1 q_2}{\mu v^2 \tan(\theta/2)} \tag{1.59}$$

1.12.1 Cross Section

It is easy to understand that particles with a large impact parameter will be deflected much less than particles that could pass close to q_2. Also, we can understand that particles with larger velocities, thus interacting for a shorter time, will be deflected less. We can simply write the infinitesimal cross section $d\sigma$ as

$$\begin{aligned} d\sigma &= 2\pi b|db| \\ &= 2\pi b\left|\frac{\partial b}{\partial\theta}d\theta\right| \end{aligned} \tag{1.60}$$

The differential cross section (i.e. as a function of deflection angle) is

$$\begin{aligned}\frac{d\sigma}{d\Omega} &= \frac{2\pi b}{2\pi \sin\theta}\left|\frac{\partial b}{\partial\theta}\frac{d\theta}{d\theta}\right| \\ &= \frac{b}{2\sin(\theta/2)\cos(\theta/2)}\left|\frac{\partial}{\partial\theta}\left[\frac{b_0(v)}{\tan(\theta/2)}\right]\right| \\ &= \frac{(q_1 q_2)^2}{4\sin^4(\theta/2)\mu^2 v^4} \end{aligned} \tag{1.61}$$

For electron–proton interactions of non-relativistic particles:

$$\frac{d\sigma}{d\Omega} = \frac{e^4}{4m_e^2 v^4}\frac{1}{\sin^4(\theta/2)}, \quad v \ll c \tag{1.62}$$

In the relativistic case, accounting also for the magnetic moment of the electron:

$$\frac{d\sigma}{d\Omega} = \frac{e^4}{4m_e^2 v^4}\frac{1}{\gamma^2}\frac{1-\beta^2\sin^2(\theta/2)}{\sin^4(\theta/2)}, \quad v \to c \tag{1.63}$$

Note the following:

1.
$$\frac{d\sigma}{d\Omega} \propto v^{-4}$$
The number of collisions in the unit of time is proportional to $\langle\sigma v\rangle \propto v^{-3}$ (a faster electron encounters more protons in the unit of time). For a Maxwellian, $\langle v\rangle \approx T^{1/2}$. Then, for the non-relativistic case:
$$\frac{\#\text{ of collisions}}{\text{time}} \propto v^{-3} \propto T^{-3/2} \tag{1.64}$$
Collisions are then less frequent in hotter plasma.

2.
$$\frac{d\sigma}{d\Omega} \propto \sin^{-4}(\theta/2)$$
Collisions with small deflections are largely favorite. This is because it is more probable to have distant particles, rather than close ones.

3. As a consequence of (2), the field due to the spin (magnetic moment of the electron) is negligible with respect to the Coulomb one. Therefore, in general, the term $(1-\beta^2\sin^2\theta/2)$ is negligible.

4. If we have electron–proton collisions,
$$\frac{d\sigma}{d\Omega} \propto \frac{e^4}{m_e^2 v^4} = \frac{e^4}{m_e^2\beta^4 c^4} = \frac{r_0^2}{\beta^4}$$
where $r_0 \equiv e^2/m_e c^2$ is the classical radius of the electron. We can see that for non-relativistic particles the cross section can be much larger than the scattering cross section $\sigma_T = (8\pi/3)r_0^2$.

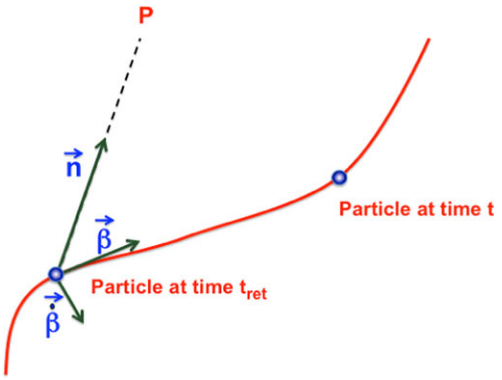


Fig. 1.9 A charge is moving along a trajectory. At the time t we measure the electric field produced by the charge. To find it out, we have to calculate its position, velocity and acceleration at the retarded time t_{ret}

5. In the relativistic case:

$$\frac{d\sigma}{d\Omega} \propto \frac{1}{m^2\gamma^2}$$

This simply flags the fact the relativistic mass is larger (by a factor γ): the particle has more inertia, and deflects less, yielding a smaller cross section.

1.13 The Electric Field of a Moving Charge

The treatment follows Rybicky & Lightman (p. 80) and Jackson (§14.1). The electric and magnetic fields produced by a moving charge is:

$$\begin{aligned}\vec{E}(\vec{r},t) &= \left[\frac{q}{k^2R^2}\frac{(\vec{n}-\vec{\beta})}{\gamma^2}\right]_{t_{\text{ret}}} + \frac{q}{ck^3R}\left\{\vec{n}\times\left[(\vec{n}-\vec{\beta})\times\dot{\vec{\beta}}\right]\right\}_{t_{\text{ret}}} \\ \vec{B}(\vec{r},t) &= \vec{n}\times\vec{E}\end{aligned} \tag{1.65}$$

All the quantities must be evaluated at the *retarded time* (it is called *retarded*, but is really a *earlier* time): at the retarded time the particle was at a distance R such that $t_{\text{ret}} + R/c$ is the time t (the time t is the time of the observer that measures the electric field). See the sketch in Fig. 1.9.

We have the following definitions:

$$\begin{aligned} t_{\text{ret}} &= t - \frac{R(t_{\text{ret}})}{c} \\ k &= 1 - \vec{n}\cdot\vec{\beta} \\ \vec{\beta} &= \frac{\vec{v}}{c} \\ \gamma &= \left(1-\beta^2\right)^{-1/2} \end{aligned} \tag{1.66}$$

We see that Eq. 1.65 for the electric field is made by two pieces.

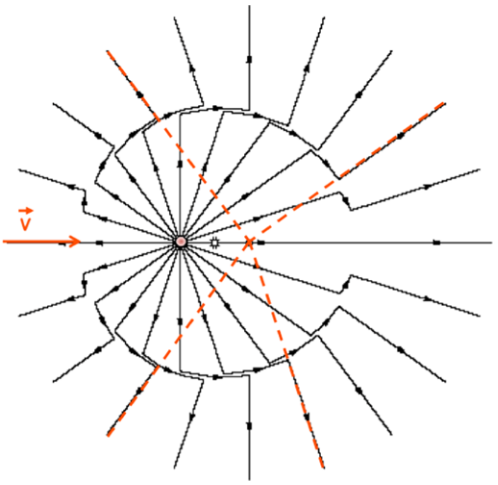


Fig. 1.10 The electric field produced by a charge initially in uniform rectilinear motion that is suddenly stopped. At large distances, the electric field points to where the charge *would be if it had not been stopped*. At closer distances, the electric field had time to "adjust" and points to where the charge is. There is then a region of space where the electric field has to change direction. This corresponds to radiation. The width of this region is $c\Delta t$, where Δt is the time needed to stop the particle, namely, the Δt during which the charge was decelerated

1. The first is called the *velocity field*: acceleration does not appear, and $\vec{E}$ is proportional to R^{-2}.
2. The second is called *acceleration field*: it contains $\dot{\beta}$, i.e. the acceleration, and is proportional to R^{-1}. It is perpendicular to $\vec{n}$ and to $(\vec{n}-\vec{\beta})\times\dot{\vec{\beta}}$.

For a charge moving at a constant speed βc, we have only the velocity field. There is something apparently weird associated to this field: it points at the location of the particle *at time* t, not at the retarded time t_{ret}. This is due to the $(\vec{n}-\vec{\beta})$ term. If the particle does not move, one recovers the usual $\vec{E}=q\vec{n}/R^2$ Coulomb law. But if does move, $\vec{E}$ does not point in the $\vec{n}$ direction, even if we have to calculate the position of the particle at the retarded time. The $(\vec{n}-\vec{\beta})$ term makes the $\vec{E}$ vector to point somewhat along the $\vec{\beta}$ direction.

Figure 1.10 illustrates in a graphic way what the radiation is. Suppose that a charge, in uniform motion along a rectilinear path, is suddenly stopped. Very far way, the observer "does not know" that the particle was stopped, and measures an electric field assuming that the particle has instead continued its motion. The electric vector then points to a point that would be occupied by the particle, if it had not been stopped (dashed lines in Fig. 1.10). In a region closer to the particle, instead, the information: "the particle is now at rest" has been propagated, and the $\vec{E}$ points radially to the actual position of the particle. In between these two regions, $\vec{E}$ must change direction (and value). The change is more pronounced perpendicularly to $\dot{\vec{\beta}}$, and is negligible along $\dot{\vec{\beta}}$ (that here coincides with the direction of the velocity $\vec{\beta}$).

The region where $\vec{E}$ changes direction propagates in time (it goes at c), but its width is always $c\Delta t$.

1.13.1 Total Emitted Power: Larmor Formula

For simplicity, we specialize to the non-relativistic case and consider only the radiative field. For simplicity, we omit the subscript "rad" to E and B. We set:

$$\begin{aligned} \vec{\beta} &\ll 1 \\ k &= 1 - \vec{n}\cdot\vec{\beta} \to 1 \\ \vec{n} - \vec{\beta} &\to \vec{n} \end{aligned} \tag{1.67}$$

With these approximations we have:

$$\begin{aligned} \vec{E}(\vec{r},t) &= \frac{q}{cR}\left[\vec{n}\times(\vec{n}\times\dot{\vec{\beta}})\right]_{t_{\text{ret}}} \\ \vec{B}(\vec{r},t) &= \vec{n}\times\vec{E} \end{aligned} \tag{1.68}$$

To calculate the power per unit solid angle carried by this electromagnetic field let consider the Poynting vector $\vec{S}$ (in cgs units):

$$\vec{S} = \frac{c}{4\pi}\vec{E}\times\vec{B} = \frac{c}{4\pi}|\vec{E}|^2\vec{n} = \frac{c}{4\pi}\frac{q^2}{c^2R^2}\left[\vec{n}\times(\vec{n}\times\dot{\vec{\beta}})\right]^2_{t_{\text{ret}}}\vec{n} \tag{1.69}$$

The power crossing a surface $dA = R^2 d\Omega$ is

$$dP = S dA = SR^2 d\Omega \longrightarrow \frac{dP}{d\Omega} = SR^2 \tag{1.70}$$

Therefore

$$\begin{aligned} \frac{dP}{d\Omega} &= \frac{q^2}{4\pi c}\left|\vec{n}\times(\vec{n}\times\dot{\vec{\beta}})\right|^2_{t_{\text{ret}}} \\ &= \frac{q^2}{4\pi c}\dot{\beta}^2\sin^2\theta \\ &= \frac{q^2}{4\pi c^3}a^2\sin^2\theta \end{aligned} \tag{1.71}$$

This is the Larmor formula for non-relativistic particles. The angle θ is the angle between $\vec{n}$ and the acceleration. The power is null along the acceleration, it is maximum perpendicularly to it. Integrating over the entire solid angle we have the total power:

$$P = \int \frac{dP}{d\Omega}d\Omega = \frac{2\pi q^2 a^2}{4\pi c^3}\int_{-1}^{1}\sin^2\theta d(\cos\theta) = \frac{2q^2}{3c^3}a^2 \tag{1.72}$$

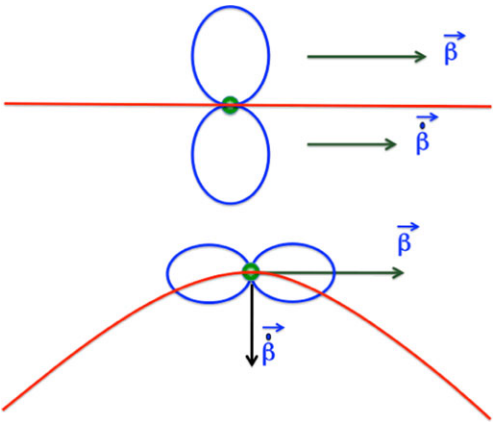


Fig. 1.11 The pattern of the radiation emitted by a charge with its acceleration parallel to the velocity (*top*) and acceleration perpendicular to the velocity (*bottom*)

1.13.2 Pattern

Equation 1.71 shows that the *pattern* of the emitted radiation has a maximum perpendicular to the acceleration, and vanishes in the directions parallel to it. Figure 1.11 shows two examples: in the top part the particle has $\dot{\beta} \parallel \beta$ while in the bottom part $\dot{\beta} \perp \beta$. The particle is non-relativistic.

Just for exercise, consider an antenna consisting of a linear piece of metal. It is called a dipole antenna. What will be the pattern of the emitted radiation? See: http://en.wikipedia.org/wiki/File:Felder_um_Dipol.jpg.

What will be the pattern of an oscillating electron?

We will soon see the modification occurring when the particle becomes relativistic, both for the total emitted power and for the pattern of the emitted radiation.

Chapter 2
Bremsstrahlung and Black Body

2.1 Bremsstrahlung

We will follow an approximate derivation. For a more complete treatment see [2] and [1]. We will consider an electron–proton plasma.

Definitions:

- b: impact parameter
- v: velocity of the electron
- n_{e}: number density of the electrons
- n_{p}: number density of the protons
- T: temperature of the plasma: $mv^2 \sim kT \rightarrow v \sim (kT/m)^{1/2}$.

We here calculate the total power and also the spectrum of bremsstrahlung radiation. We divide the procedure into a few steps:

1. We consider the interaction between the electron and the proton only when the electron passes close to the proton. The characteristic time τ is

$$\tau \approx \frac{b}{v} \tag{2.1}$$

2. During the interaction we assume that the acceleration is constant and equal to

$$a \approx \frac{e^2}{m_e b^2} \tag{2.2}$$

3. From the Larmor formula we get

$$P = \frac{2e^2a^2}{3c^3} \approx \frac{e^2}{c^3}\frac{e^4}{m_{\mathrm{e}}^2 b^4} = \frac{e^6}{m_{\mathrm{e}}^2 c^3 b^4} \tag{2.3}$$

Note that we have dropped the $2/3$ factor, since in this simplified treatment we neglect all the numerical factors of order unity. Later we will give the exact result.

G. Ghisellini, *Radiative Processes in High Energy Astrophysics*,
Lecture Notes in Physics 873, DOI 10.1007/978-3-319-00612-3_2,
© Springer International Publishing Switzerland 2013

4. Since there is a characteristic time, there is also a characteristic frequency, namely τ^{-1}:

$$\omega \approx \frac{1}{\tau} = \frac{v}{b} \tag{2.4}$$

5. Therefore

$$P(\omega) \approx \frac{P}{\omega} = \frac{e^6}{m_e^2 c^3 v b^3} \tag{2.5}$$

6. We can estimate the impact factor b from the density of protons:

$$b \approx n_p^{-1/3} \rightarrow b^3 = \frac{1}{n_p} \tag{2.6}$$

7. The emissivity $j(\omega)$ will be the power emitted by a single electron multiplied by the number density of electrons. If the emission is isotropic we have also to divide by 4π, since the emissivity is for unit solid angle:

$$j(\omega) \approx \frac{n_e n_p}{4\pi} \frac{e^6}{m_e^2 c^3} \left(\frac{m_e}{kT}\right)^{1/2} \tag{2.7}$$

8. We integrate $j(\omega)$ over frequency. The integral will depend upon ω_{max}. What should we use for ω_{max}? One possibility is to set $\hbar\omega_{max} = kT$. This would mean that an electron cannot emit a photon of energy larger than the typical energy of the electron. Seems reasonable, but we are forgetting all the electrons (and the frequencies) that have energies larger than kT. In this way:

$$\begin{aligned} j &= \int_0^{\omega_{max}} j(\omega) d\omega \sim \frac{n_e n_p}{4\pi} \frac{e^6}{m_e^2 c^3} \left(\frac{m_e}{kT}\right)^{1/2} \frac{kT}{\hbar} \\ &= \frac{n_e n_p e^6}{4\pi m_e^2 c^3} \frac{(m_e kT)^{1/2}}{\hbar} \end{aligned} \tag{2.8}$$

   We suspect that in the exact results there will be the contribution of electrons with energy larger than kT: since they belong to the exponential part of the Maxwellian, we suspect that in the exact result there will be an exponential...

9. The exact result, considering also that $\nu = \omega/(2\pi)$, is

$$\begin{aligned} j(\nu) &= \frac{8}{3} \left(\frac{2\pi}{3}\right)^{1/2} \frac{n_e n_p e^6}{m_e^2 c^3} \left(\frac{m_e}{kT}\right)^{1/2} e^{-h\nu/kT} \bar{g}_{ff} \\ j &= \frac{4}{3\pi} \left(\frac{2\pi}{3}\right)^{1/2} \frac{n_e n_p e^6}{m_e^2 c^3} \frac{(m_e kT)^{1/2}}{\hbar} \bar{g}_{ff} \end{aligned} \tag{2.9}$$

The Gaunt factor $\bar{g}_{ff}$ depends on the minimum impact factor which in turn determines the maximum frequency. Details are complicated, but see [2, pp. 158–161] for a more detailed discussion.

We have treated the case of an electron–proton plasma. In the more general case, the plasma will be composed by nuclei with atomic number Z and number density n. The emissivity will then be proportional to Z^2. This is because the acceleration of the electron will be $a = Ze^2/(m_e b^2)$ (see point 2), and we have to square the acceleration to get the power from the Larmor formula. In cgs units we have:

$$\begin{aligned} j(\nu) &= 5.4 \times 10^{-39} Z^2 n_e n_i T^{-1/2} e^{-h\nu/kT} \bar{g} \\ j &= 1.13 \times 10^{-28} Z^2 n_e n_i T^{1/2} \bar{g} \end{aligned} \tag{2.10}$$

2.1.1 Free–Free Absorption

If the underlying particle distribution is a Maxwellian, we can use the Kirchoff law to find out the absorption coefficient. If B_ν is the intensity of black body emission, we must have

$$S_\nu \equiv \frac{j_\nu}{\alpha_\nu} = B_\nu = \frac{2h\nu^3}{c^2} \frac{1}{e^{h\nu/kT} - 1} \tag{2.11}$$

In these cases it is very simple to find α_ν once we know j_ν. Remember: this can be done only if we have a Maxwellian. If the particle distribution is non-thermal, we cannot use the Kirchoff law and we have to go back to a more fundamental level, namely to the Einstein coefficients. Using Eq. 2.11 we have:

$$\alpha_\nu^{\rm ff} = \frac{j_\nu}{B_\nu} = \frac{4}{3}\left(\frac{2\pi}{3}\right)^{1/2} \frac{Z^2 n_e n_i e^6}{h m_e^2 c^2} \left(\frac{m_e c^2}{kT}\right)^{1/2} \frac{1 - e^{-h\nu/kT}}{\nu^3} \bar{g}_{\rm ff} \tag{2.12}$$

In cgs units [cm^{-1}] we have

$$\alpha_\nu^{\rm ff} = 3.7 \times 10^8 \frac{Z^2 n_e n_i}{T^{1/2}} \frac{1 - e^{-h\nu/kT}}{\nu^3} \bar{g}_{\rm ff} \tag{2.13}$$

When $h\nu \ll kT$ (Raleigh–Jeans regime) this simplifies to

$$\alpha_\nu^{\rm ff} = 0.018 \frac{Z^2 n_e n_i}{T^{3/2} \nu^2} \bar{g}_{\rm ff} \tag{2.14}$$

Figure 2.1 shows the bremsstrahlung intensity from a source of radius $R = 10^{15}$ cm and $n_e = n_p = 10^{10}$ cm^{-3}. The three spectra correspond to different temperatures. Note that for smaller temperatures the thin part of I_ν is larger ($I_\nu \propto T^{-1/2}$). On the other hand, at larger T the spectrum extends to larger frequencies, making the frequency integrated intensity to be larger for larger T ($I \propto T^{1/2}$). Note also the self-absorbed part, whose slope is proportional to ν^2. This part ends when the optical depth $\tau = \alpha_\nu R \sim 1$.

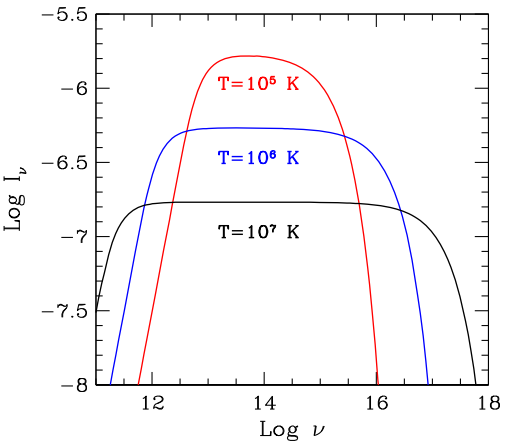


Fig. 2.1 The bremsstrahlung intensity from a source of radius $R = 10^{15}$ cm, density $n_e = n_p = 10^{10}$ cm^{-3} and varying temperature. The Gaunt factor is set to unity for simplicity. At smaller temperatures the thin part of I_ν is larger ($\propto T^{-1/2}$), even if the frequency integrated I is smaller ($\propto T^{1/2}$)

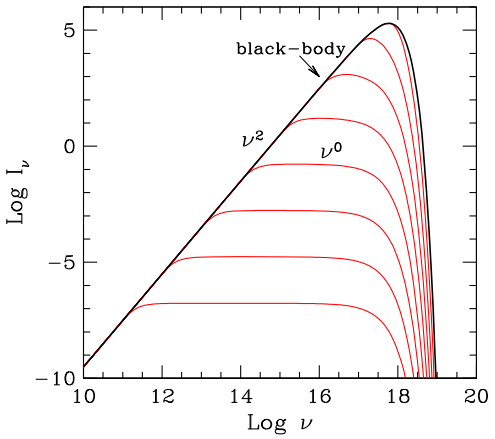


Fig. 2.2 The bremsstrahlung intensity from a source of radius $R = 10^{15}$ cm, temperature $T = 10^7$ K. The Gaunt factor is set to unity for simplicity. The density $n_e = n_p$ varies from 10^{10} cm^{-3} (*bottom curve*) to 10^{18} cm^{-3} (*top curve*), increasing by a factor 10 for each curve. Note the self-absorbed part ($\propto \nu^2$), the flat and the exponential parts. As the density increases, the optical depth also increases, and the spectrum approaches the black-body one

2.1.2 *From Bremsstrahlung to Black Body*

As any other radiation process, the bremsstrahlung emission has a self-absorbed part, clearly visible in Fig. 2.1. This corresponds to optical depths $\tau_\nu \gg 1$. The term ν^{-3} in the absorption coefficient α_ν ensures that the absorption takes place preferentially at low frequencies. By increasing the density of the emitting (and absorbing) particles, the spectrum is self-absorbed up to larger and larger frequencies. When *all* the spectrum is self-absorbed (i.e. $\tau_\nu > 1$ for all ν), *and* the particles belong to a Maxwellian, then we have a black-body. This is illustrated in Fig. 2.2: all spectra are calculated for the same source size ($R = 10^{15}$ cm), same temperature ($T = 10^7$ K), and what varies is the density of electrons and protons (by a factor 10) from $n_e = n_p = 10^{10}$ cm^{-3} to 10^{18} cm^{-3}. As can be seen, the bremsstrahlung intensity becomes more and more self-absorbed as the density increases, until it becomes a black-body. At this point increasing the density does not increase the intensity

any longer. This is because we receive radiation from a layer of unity optical depth. The width of this layer decreases as we increase the densities, but the emissivity increases, so that

$$I_\nu = \frac{j_\nu R}{\tau_\nu} \propto \frac{n_e n_p R}{n_e n_p R} \to \text{constant} \quad (\tau_\nu \gg 1) \tag{2.15}$$

2.2 Black Body

A black body occurs when "the body is black": it is the perfect absorber. But this means that it is also the "perfect" emitter, since absorption and emission are linked. The black body intensity is given by

$$B_\nu(T) = \frac{2}{c^2} \frac{h\nu^3}{e^{h\nu/kT} - 1} \tag{2.16}$$

Expressed in terms of the wavelength λ this is equivalent to:

$$B_\lambda(T) = \frac{2hc^2}{\lambda^5} \frac{1}{e^{hc/\lambda kT} - 1} \tag{2.17}$$

Note the following:

- The black body intensity has a peak. The value of it is different if we ask for the peak of B_ν or the peak of νB_ν.
  The first is at $h\nu_{\text{peak}} = 2.82kT$.
  The second is at $h\nu_{\text{peak}} = 3.93kT$.
- If $T_2 > T_1$, then: $B_\nu(T_2) > B_\nu(T_1)$ for all frequencies.
- When $h\nu \ll kT$ we can expand the exponential term: $e^{h\nu/kT} \to 1 + h\nu/kT \ldots$, and therefor we obtain the **Raleigh–Jeans law**:

$$I_\nu^{\text{RJ}} = \frac{2\nu^2}{c^2} kT \tag{2.18}$$

- When $h\nu \gg kT$ we have $e^{h\nu/kT} - 1 \to e^{h\nu/kT}$ and we obtain the **Wien law**:

$$I_\nu^{\text{W}} = \frac{2h\nu^3}{c^2} e^{-h\nu/kT} \tag{2.19}$$

  See in Fig. 2.3 the Raleigh Jeans and the Wien approximations.
- The integral over frequencies is:

$$\int_0^\infty B_\nu d\nu = \frac{\sigma_{\text{SB}}}{\pi} T^4, \quad \sigma_{\text{SB}} = \frac{2\pi^5 k^4}{15c^2h^3} \tag{2.20}$$

  The constant σ_{SB} is called Stefan–Boltzmann constant.

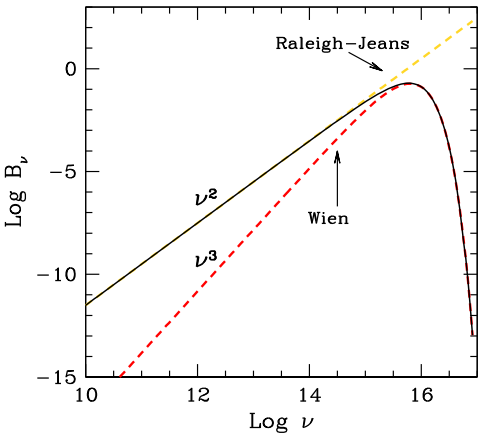


Fig. 2.3 The black body intensity compared with the Raleigh–Jeans and the Wien law

- The energy density u of black body radiation is

$$u = \frac{4\pi}{c}\int_0^\infty B_\nu d\nu = aT^4, \quad a = \frac{4\sigma_{\rm SB}}{c} \tag{2.21}$$

The two constants ($\sigma_{\rm SB}$ and a) have the values:

$$\begin{aligned} \sigma_{\rm SB} &= 5.67 \times 10^{-5}\ {\rm erg\,cm^{-2}\,deg^{-4}\,s^{-1}} \\ a &= 7.65 \times 10^{-15}\ {\rm erg\,cm^{-3}\,deg^{-4}} \end{aligned} \tag{2.22}$$

- The **brightness temperature** is defined using the Raleigh–Jeans law, since $I_\nu^{\rm RJ} = (2\nu^2/c^2)kT$ we have

$$T_{\rm b} = \frac{c^2 I_\nu^{\rm RJ}}{2k\nu^2} \tag{2.23}$$

- A black body is the most efficient radiator, for thermal plasmas and incoherent radiation (we can have coherent processes that are even more efficient). For a given surface and temperature, it is not possible to overtake the luminosity of the black body, at any frequency, for any emission process.
- Let us try to find the temperature of the surface of the Sun. We know its radius (700,000 km) and luminosity ($L_\odot = 4 \times 10^{33}$ erg s^{-1}). Therefore, from

$$L_\odot = \pi 4\pi R^2 \int_0^\infty B_\nu d\nu = 4\pi R^2 \sigma_{\rm SB} T^4 \tag{2.24}$$

we get:

$$T_\odot = \left(\frac{L_\odot}{4\pi R^2 \sigma_{\rm SB}}\right)^{1/4} \sim 5800\ {\rm K} \tag{2.25}$$

- A spherical source emits black body radiation. We know its distance, but not its radius. Find it. Suppose we do not know its distance. Can we predict its angular size? And, if we then observe it, can we then get the distance?

References

1. Blumenthal, G.R., Gould, R.J.: Bremsstrahlung, synchrotron radiation, and Compton scattering of high-energy electrons traversing dilute gases. Rev. Mod. Phys. **42**, 237 (1970)
2. Rybicki, G.B., Lightman, A.P.: Radiative Processes in Astrophysics. Wiley, New York (1979)

Chapter 3
Beaming

3.1 Rulers and Clocks

Special relativity taught us two basic notions: comparing dimensions and flow of times in two different reference frames, we find out that they differ. If we measure a ruler at rest, and then measure the same ruler when is moving, we find that, when moving, the ruler is shorter. If we synchronize two clocks at rest, and then let one move, we see that the moving clock is delaying. Let us see how this can be derived by using the Lorentz transformations, connecting the two reference frames K (that sees the ruler and the clock moving) and K' (that sees the ruler and the clock at rest). For simplicity, but without loss of generality, consider a motion along the x axis, with velocity $v \equiv \beta c$ corresponding to the Lorentz factor $\Gamma = (1-\beta^2)^{-1/2}$. Primed quantities are measured in K'. We have:

$$\begin{aligned} x' &= \Gamma(x - vt) \\ y' &= y \\ z' &= z \\ t' &= \Gamma\left(t - \beta\frac{x}{c}\right) \end{aligned} \tag{3.1}$$

with the inverse relations given by

$$\begin{aligned} x &= \Gamma\left(x' + vt'\right) \\ y &= y' \\ z &= z' \\ t &= \Gamma\left(t' + \beta\frac{x'}{c}\right). \end{aligned} \tag{3.2}$$

The length of a moving ruler has to be measured through the position of its extremes *at the same time* t. Therefore, as $\Delta t = 0$, we have

$$x_2' - x_1' = \Gamma(x_2 - x_1) - \Gamma v \Delta t = \Gamma(x_2 - x_1) \tag{3.3}$$

G. Ghisellini, *Radiative Processes in High Energy Astrophysics*,
Lecture Notes in Physics 873, DOI 10.1007/978-3-319-00612-3_3,
© Springer International Publishing Switzerland 2013

i.e.

$$\Delta x = \frac{\Delta x'}{\Gamma} \rightarrow \text{contraction} \tag{3.4}$$

Similarly, in order to determine a time interval a (lab) clock has to be compared with one in the comoving frame, which has, in this frame, *the same position* x'. Then

$$\Delta t = \Gamma \Delta t' + \Gamma\beta\frac{\Delta x'}{c} = \Gamma \Delta t' \rightarrow \text{dilation} \tag{3.5}$$

An easy way to remember the transformations is to think to mesons produced in collisions of cosmic rays in the high atmosphere, which can be detected even if their lifetime (in the comoving frame) is much shorter than the time needed to reach the earth's surface. For us, on ground, relativistic mesons live longer (for the meson's point of view, instead, it is the length of the traveled distance which is shorter).

All this is correct if we measure lengths by comparing rulers (at the same time in K) and by comparing clocks (at rest in K')—the meson lifetime *is* a clock. In other words, **if we do not use photons** for the measurement process.

3.2 Photographs and Light Curves

If we have an extended moving object and if the information (about position and time) are carried by photons, we **must** take into account their (different) travel paths. When we take a picture, we detect photons arriving at the same time to our camera: if the moving body which emitted them is extended, we must consider that these photons have been emitted at different times, when the moving object occupied different locations in space. This may seem quite obvious. And it is. Nevertheless these facts were pointed out in 1959 [3, 5], more than 50 years after the publication of the theory of special relativity.

3.2.1 The Moving Bar

Let us consider a moving bar, of proper dimension ℓ', moving in the direction of its length at velocity βc and at an angle θ with respect to the line of sight (see Fig. 3.1). The length of the bar in the frame K (according to relativity "without photons") is $\ell = \ell'/\Gamma$. The photon emitted in A_1 reaches the point H in the time interval Δt_e. After Δt_e the extreme B_1 has reached the position B_2, and by this time, photons emitted by the other extreme of the bar can reach the observer simultaneously with the photons emitted by A_1, since the travel paths are equal. The length $B_1B_2 = \beta c\Delta t_e$, while $A_1H = c\Delta t_e$. Therefore

$$A_1H = A_1B_2\cos\theta \rightarrow \Delta t_e = \frac{\ell'\cos\theta}{c\Gamma(1-\beta\cos\theta)} \tag{3.6}$$

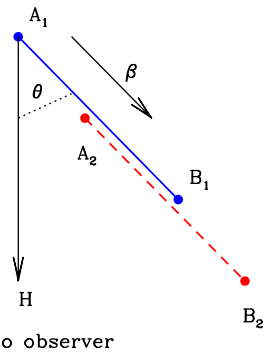


Fig. 3.1 A bar moving with velocity βc in the direction of its length. The path of the photons emitted by the extreme A is longer than the path of photons emitted by B. When we make a picture (or a map) of the bar, we collect photons reaching the detector simultaneously. Therefore the photons from A have to be emitted before those from B, when the bar occupied another position

Note the appearance of the term $\delta = 1/[\Gamma(1 - \beta\cos\theta)]$ in the transformation: this accounts for both the relativistic length contraction $(1/\Gamma)$, and the Doppler effect $[1/(1 - \beta\cos\theta)]$ (see below, Eq. 3.15). The length A_1B_2 is then given by

$$A_1B_2 = \frac{A_1H}{\cos\theta} = \frac{\ell'}{\Gamma(1 - \beta\cos\theta)} = \delta\ell' \tag{3.7}$$

In a real picture, we would see the projection of A_1B_2, i.e.:

$$HB_2 = A_1B_2\sin\theta = \ell'\frac{\sin\theta}{\Gamma(1 - \beta\cos\theta)} = \ell'\delta\sin\theta \tag{3.8}$$

The observed length depends on the viewing angle, and reaches the maximum (equal to ℓ') for $\cos\theta = \beta$.

3.2.2 The Moving Square

Now consider a square of size ℓ' in the comoving frame, moving at 90° to the line of sight (Fig. 3.2). Photons emitted in A, B, C and D have to arrive to the film plate at the same time. But the paths of photons from C and D are longer → they have to be emitted earlier than photons from A and B: when photons from C and D were emitted, the square was in another position.

The interval of time between emission from C and from A is ℓ'/c. During this time the square moves by $\beta\ell'$, i.e. the length CA. Photons from A and B are emitted and received at the same time and therefore $AB = \ell'/\Gamma$. The total observed length is given by

$$CB = CA + AB = \frac{\ell'}{\Gamma}(1 + \Gamma\beta) \tag{3.9}$$

As β increases, the observer sees the side AB increasingly shortened by the Lorentz contraction, but at the same time the length of the side CA increases. The maximum

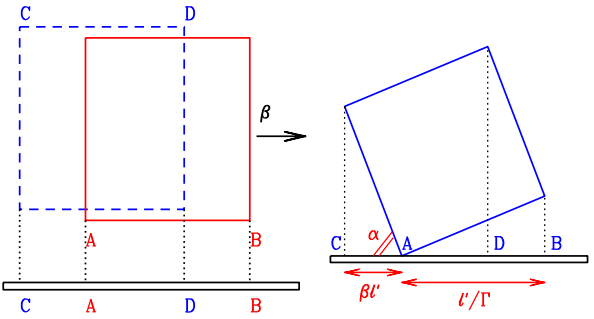


Fig. 3.2 *Left*: A square moving with velocity βc seen at 90°. The observer can see the left side (*segment CA*). Light rays are assumed to be parallel, i.e. the *square* is assumed to be at large distance from the observer. *Right*: The *moving square* is seen as *rotated* by an *angle* α given by $\cos\alpha = \beta$

total length is observed for $\beta = 1/\sqrt{2}$, corresponding to $\Gamma = \sqrt{2}$ and to $CB = \ell'\sqrt{2}$, i.e. equal to *the diagonal* of the square. Note that we have considered the square (and the bar in the previous section) to be at large distances from the observer, so that the emitted light rays are all parallel. If the object is near to the observer, we must take into account that different points of one side of the square (e.g. the side *AB* in Fig. 3.2) have different travel paths to reach the observer, producing additional distortions. See the book by Mook and Vargish [2] for some interesting illustrations.

3.2.3 Rotation, Not Contraction

The net result (taking into account **both** the length contraction **and** the different paths) is an apparent **rotation** of the square, as shown in Fig. 3.2 (right panel). The rotation angle α can be simply derived (even geometrically) and is given by

$$\cos\alpha = \beta \tag{3.10}$$

A few considerations follow:

- If you rotate a sphere you still get a sphere: you **do not** observe a contracted sphere.
- The total length of the projected square, appearing on the film, is $\ell'(\beta + 1/\Gamma)$. It is maximum when the "rotation angle" $\alpha = 45° \rightarrow \beta = 1/\sqrt{2} \rightarrow \Gamma = \sqrt{2}$. This corresponds to the diagonal.
- The appearance of the square *is the same as what seen in a comoving frame for a line of sight making an angle* α' *with respect to the velocity vector, where* α' *is the aberrated angle* given by

$$\sin\alpha' = \frac{\sin\alpha}{\Gamma(1 - \beta\cos\alpha)} = \delta\sin\alpha \tag{3.11}$$

  See Fig. 3.3 for a schematic illustration.

The last point is particularly important, because it introduces a great simplification in calculating not only the appearance of bodies with a complex shape but also the light curves of varying objects.

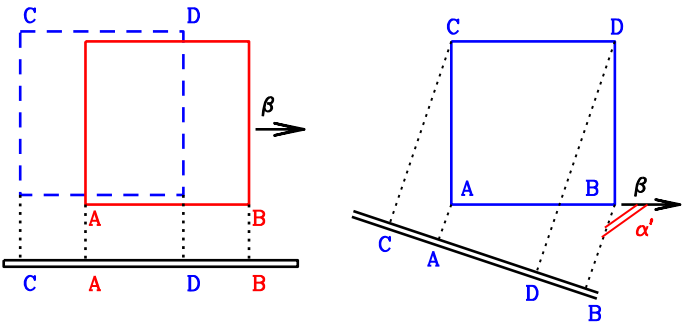


Fig. 3.3 An observer that sees the object at rest at a viewing angle given by $\sin\alpha' = \delta \sin\alpha$, will take the same picture as the observer that sees the object moving and making an *angle* α with his/her line of sight. Note that $\sin\alpha' = \sin(\pi - \alpha')$

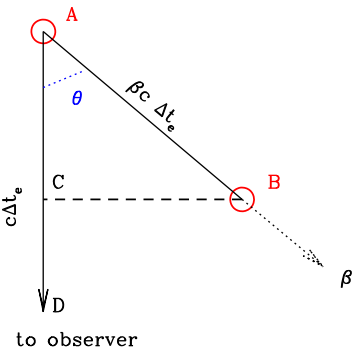


Fig. 3.4 Difference between the proper time and the photons arrival time. A lamp, moving with a velocity βc, emits photons for a time interval $\Delta t'_e$ in its frame K'. The corresponding time interval measured by an observer at an *angle* θ, who receives the photons produced by the lamp is $\Delta t_a = \Delta t'_e/\delta$

3.2.4 Time

Consider a lamp moving with velocity $v = \beta c$ at an angle θ from the line of sight. In K', the lamp remains on for a time $\Delta t'_e$. According to special relativity ("without photons") the measured time in frame K should be $\Delta t_e = \Gamma \Delta t'_e$ (time dilation). However, if we use photons to measure the time interval, we once again must consider that the first and the last photons have been emitted in different locations, and their travel path lengths are different. To find out Δt_a, the time interval between the arrival of the first and last photon, consider Fig. 3.4. The first photon is emitted in A, the last in B. If these points are measured in frame K, then the path AB is

$$AB = \beta c \Delta t_e = \Gamma \beta c \Delta t'_e \tag{3.12}$$

While the lamp moved from A to B, the photon emitted when the lamp was in A has traveled a distance $AD = c\Delta t_e$, and is now in point D. Along the direction of the line of sight, the first and the last photons (the ones emitted in A and in B) are separated by CD. The corresponding time interval, CD/c, is the interval of time Δt_a

between the arrival of the first and the last photon:

$$\begin{aligned}\Delta t_{\rm a} &= \frac{CD}{c} = \frac{AD - AC}{c} = \Delta t_{\rm e} - \beta \Delta t_{\rm e} \cos\theta \\ &= \Delta t_{\rm e}(1 - \beta\cos\theta) \\ &= \Delta t'_{\rm e} \Gamma (1 - \beta\cos\theta) \\ &= \frac{\Delta t'_{\rm e}}{\delta}\end{aligned} \tag{3.13}$$

If θ is small and the velocity is relativistic, then $\delta > 1$, and $\Delta t_{\rm a} < \Delta t_{\rm s}$, i.e. we measure a *time contraction* instead of time dilation. Note also that we recover the usual time dilation (i.e. $\Delta t_{\rm a} = \Gamma \Delta t'_{\rm e}$) if $\theta = 90°$, because in this case all photons have to travel the same distance to reach us.

Since a frequency is the inverse of time, it will transform as

$$\nu = \nu' \delta \tag{3.14}$$

It is because of this that the factor δ is called the relativistic Doppler factor. Its definition is then

$$\delta = \frac{1}{\Gamma(1 - \beta\cos\theta)} \tag{3.15}$$

Note the two terms:

- The term $1/\Gamma$: this corresponds to the usual special relativity term.
- The term $1/(1 - \beta\cos\theta)$: this corresponds to the usual Doppler effect.

The δ factor is the result of the competition of these two terms: for $\theta = 90°$ the usual Doppler term is unity, and only "special relativity" remains: $\delta = 1/\Gamma$. For small θ the term $1/(1 - \beta\cos\theta)$ becomes very large, more than compensating for the $1/\Gamma$ factor. For $\cos\theta = \beta$ (i.e. $\sin\theta = 1/\Gamma$) we have $\delta = \Gamma$. For $\theta = 0°$ we have $\delta = \Gamma(1 + \beta)$.

3.2.5 Aberration

Another very important effect happening when a source is moving is the aberration of light. It is rather simple to understand, if one looks at Fig. 3.5. A source of photons is located perpendicularly to the right wall of a lift. If the lift is not moving, and there is a hole in its right wall, then the light ray enters in A and ends its travel in B. If the lift is not moving, A and B are at the same height. If the lift is moving with a constant velocity v to the top, when the photon smashes the left wall it has a different location, and the point B will have, for a comoving observer, a smaller height than A. The light ray path now appears oblique, tilted. Of course, the greater v, the more tilted the light ray path appears. This immediately stimulate the question: what

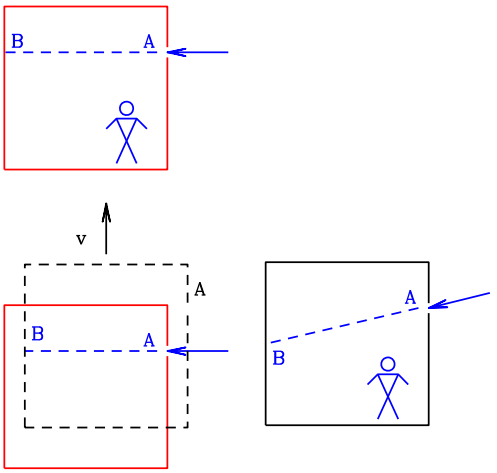


Fig. 3.5 The relativistic lift, to explain relativistic aberration of light. Assume first a non-moving lift, with a hole on the *right wall*. A light ray, coming perpendicularly to the *right wall*, enter through the wall in A and ends its travel in B. If the lift is moving with a constant velocity v to the top, its position is changed when the photon arrives to the *left wall*. For the comoving observer, therefore, it appears that the light path is tilted, since the *point* B where the photon smashes into the left wall is below the *point* A. What happens if the lift, instead to move with a constant velocity, is accelerating?

happens if the lift, instead to move with a constant velocity, is accelerating? With this example one can easily convince him/herself that the "trajectory" of the photon would appear curved. Since, by the equivalence principle, the accelerating lift cannot tell if there is an engine pulling him up or if there is a planet underneath it, we can then say that gravity bends the light rays, and makes the space curved.

This helps to understand why angles, between two inertial frames, change. Calling θ the angle between the direction of the emitted photon and the source velocity vector, we have:

$$\begin{aligned} \sin\theta &= \frac{\sin\theta'}{\Gamma(1+\beta\cos\theta')}; \qquad \sin\theta' = \frac{\sin\theta}{\Gamma(1-\beta\cos\theta)} \\ \cos\theta &= \frac{\cos\theta'+\beta}{1+\beta\cos\theta'}; \qquad \cos\theta' = \frac{\cos\theta-\beta}{1-\beta\cos\theta} \end{aligned} \tag{3.16}$$

Note that, if $\theta' = 90°$, then $\sin\theta = 1/\Gamma$ and $\cos\theta = \beta$. Consider a source emitting isotropically in K'. Half of its photons are emitted in one emisphere, namely, with $\theta' \leq 90°$. Then, in K, the same source will appear to emit half of its photons into a cone of semiaperture $1/\Gamma$.

Assuming symmetry around the angle ϕ, the transformation of the solid angle $d\Omega$ is

$$d\Omega = -2\pi\, d\cos\theta = \frac{d\Omega'}{\Gamma^2(1+\beta\cos\theta')^2} = d\Omega'\Gamma^2(1-\beta\cos\theta)^2 = \frac{d\Omega'}{\delta^2} \tag{3.17}$$

3.2.6 Intensity

We now have all the ingredients necessary to calculate the transformation of the specific (i.e. monochromatic) and bolometric intensity. The specific intensity has the unit of energy per unit surface, time, frequency and solid angle. In cgs, the units are [erg cm^{-2} s^{-1} Hz^{-1} ster^{-1}]. We can then write the specific intensity as

$$\begin{aligned} I(\nu) &= h\nu \frac{dN}{dt\, d\nu\, d\Omega\, dA} \\ &= \delta h\nu' \frac{dN'}{(dt'/\delta)\delta\, d\nu'(d\Omega'/\delta^2)\, dA'} \\ &= \delta^3 I'\left(\nu'\right) = \delta^3 I'(\nu/\delta) \end{aligned} \tag{3.18}$$

Note that $dN = dN'$ because it is a number, and that $dA = dA'$. If we integrate over frequencies we obtain the bolometric intensity which transforms as

$$I = \delta^4 I' \tag{3.19}$$

The fourth power of δ can be understood in a simple way: one power comes from the transformation of the frequencies, one for the time, and two for the solid angle. They all add up. This transformation is at the base of our understanding of relativistic sources, namely radio-loud AGNs, gamma-ray bursts and galactic superluminal sources.

3.2.7 Luminosity and Flux

The transformation of fluxes and luminosities from the comoving to the observer frames is not trivial. The most used formula is $L = \delta^4 L'$, but this assumes that we are dealing with a single, spherical blob. It can be simply derived by noting that $L = 4\pi d_{\rm L}^2 F$, where F is the observed flux, and by considering that the flux, for a distance source, is $F \propto \int_{\Omega_s} I d\Omega$. Since Ω_s is the source solid angle, which is the same in the two K and K' frames, we have that F transforms like I, and so does L. But the emission from jets may come not only by a single spherical blob, but by, for instance, many blobs, or even by a continuous distribution of emitting particles flowing in the jet. If we assume that the walls of the jet are fixed, then the concept of "comoving" frame is somewhat misleading, because if we are comoving with the flowing plasma, then we see the walls of the jet which are moving.

A further complication exists if the velocity is not uni-directional, but radial, like in gamma-ray bursts. In this case, assume that the plasma is contained in a conical narrow shell (width smaller than the distance of the shell from the apex of the cone). The observer which is moving together with a portion of the plasma,

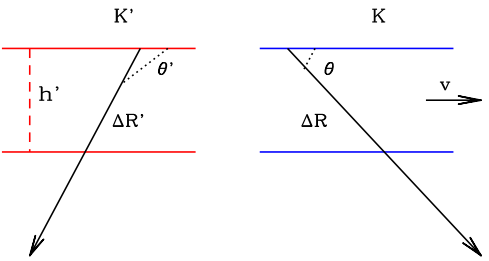


Fig. 3.6 Due to aberration of light, the travel path of the a light ray is different in the two *frames* K and K'

(the nearest case of a "comoving observer") will see the plasma close to her going away from her, and more so for more distant portions of the plasma. Indeed, there could be a limiting distance beyond which the two portions of the shells are causally disconnected.

Useful references are [1] and [4].

3.2.8 Emissivity

The (frequency integrated) emissivity j is the energy emitted per unit time, solid angle and volume. We generally have that the intensity, for an optically thin source, is $I = \int_{\Delta R} j dr$, where ΔR is the length of the region containing the emitting particles. The emissivity transforms like $j = j'\delta^3$, namely with one power of δ less than the intensity.

To understand why, consider a slab with plasma flowing with a velocity parallel to the walls of the slab, as in Fig. 3.6. The observer in K will measure a certain ΔR which depends on her viewing angle. In K' the same path has a different length, because of the aberration of light. The height of the slab $h' = h$, since it is perpendicular to the velocity. The light ray travels a distance $\Delta R = h/\sin\theta$ in K, and the same light ray travels a distance $\Delta R' = h'/\sin\theta'$ in K'. Since $\sin\theta' = \delta\sin\theta$, then $\Delta R' = \Delta R/\delta$. Therefore the column of plasma contributing to the emission, for $\delta > 1$, is less than what the observer in K would guess by measuring ΔR. For simplicity, assume that the plasma is homogeneous, allowing to simply write $I = j\Delta R$. In this case:

$$I = j\Delta R = \delta^4 I' = \delta^4 j'\Delta R' \rightarrow j = \delta^3 j' \tag{3.20}$$

And the corresponding transformation for the specific emissivity is $j(\nu) = \delta^2 j'(\nu')$.

Figure 3.7 illustrates another interesting example, taken from the work of Sikora et al. [4]. Consider that within a distance R from the apex of a jet (R measured in K), at any given time there are N blobs (10 on the specific example of Fig. 3.7), moving with a velocity $v = \beta c$ along the jet. To fix the ideas, let assume that beyond R they switch off. If the viewing angle is $\theta = 90°$, the photons emitted by each

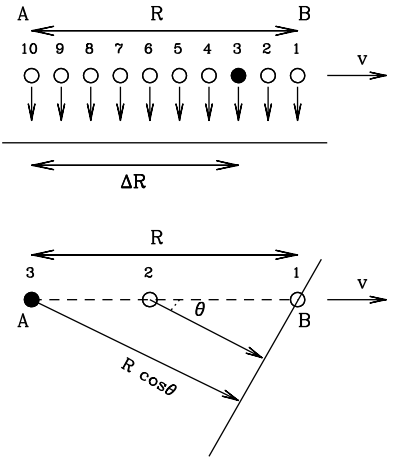


Fig. 3.7 Due to the differences in light travel time, the number of blobs that can be observed simultaneously at any given time depends on the viewing angle and the velocity of the blobs. In the *top panel* the viewing angle is $\theta = 90°$ and all the blobs contained within a certain distance R can be seen. For smaller viewing angles, less blobs are seen. This is because the photons emitted by the rear blobs have more distance to travel, and therefore they have to be emitted before the photons produced by the front blob. Decreasing the viewing angle θ we see less blobs (3 for the case illustrated in the *bottom panel*)

blob travel the same distance to reach the observer, who will see all the 10 blobs. But if $\theta < 90°$, the photons produced by the rear blobs must travel for a longer distance in order to reach the observer, and therefore they have to be emitted before the photons produced by the front blob. The observer will then see *less* blobs. To be more quantitative, consider a viewing angle $\theta < 90°$. Photons emitted by blob number 3 to reach blobs number 1 when it produces its last photon (before to switch off) were emitted when the blobs itself was just born (it was crossing point A). They traveled a distance $R\cos\theta$ in a time Δt. During the same time, the blob number 3 traveled a distance $\Delta R = c\beta\Delta t$ in the forward direction. The fraction f of blobs that can be seen is then

$$f = \frac{R - \Delta R}{R} = 1 - \frac{c\beta\Delta t}{R} = 1 - \beta\cos\theta \tag{3.21}$$

Where we have used the fact that $\Delta t = (R/c)\cos\theta$. This is the usual Doppler factor. We may multiply and divide by Γ to obtain

$$f = \frac{1}{\Gamma\delta} \tag{3.22}$$

The bottom line is the following: even if the flux from a single blob is boosted by δ^4, if the jet is made by many (N) equal blobs, the total flux is not just boosted by $N\delta^4$ times the intrinsic flux of a blob, because the observer will see less blobs if $\theta < 90°$.

3.2.9 Brightness Temperature

The brightness temperature is a quantity used especially in radio astronomy, and it is defined by

$$T_{\rm B} \equiv \frac{I(\nu)}{2k}\frac{c^2}{\nu^2} = \frac{F(\nu)}{2\pi k\theta_{\rm s}^2}\frac{c^2}{\nu^2} \tag{3.23}$$

where we have assumed that the solid angle subtended by the source is $\Delta\Omega_{\rm s} \sim \pi\theta_{\rm s}^2$, and that the received flux is $F(\nu) = \Delta\Omega_{\rm s} I(\nu)$. There are 2 ways to measure $\theta_{\rm s}$:

1. from VLBI observations, one can often resolve the source and hence directly measure the angular size. In this case the relation between the brightness temperature measured in the K and K' frames is

$$T_{\rm B} = \frac{\delta^3 F'(\nu')}{2\pi k\theta_{\rm s}^2}\frac{c^2}{\delta^2(\nu')^2} = \delta T'_{\rm B} \tag{3.24}$$

2. If the source is varying, we can estimate its size by requiring that the observed variability time-scale $\Delta t_{\rm var}$ is longer than the light travel time R/c, where R is the typical radius of the emission region. In this case

$$T_{\rm B} > \frac{\delta^3 F'(\nu')}{2\pi k}\frac{d_{\rm A}^2\delta^2}{(c\Delta t'_{\rm var})^2}\frac{c^2}{\delta^2(\nu')^2} = \delta^3 T'_{\rm B} \tag{3.25}$$

where $d_{\rm A}$ is the angular distance, related to the luminosity distance $d_{\rm L}$ by $d_{\rm A} = d_{\rm L}/(1+z)^2$.

There is a particular class of extragalactic radio sources, called Intra-Day Variable (IDV) sources, showing variability time-scales of hours in the radio band. For them, the corresponding observed brightness temperature can exceed 10^{16} K, a value much larger than the theoretical limit for an incoherent synchrotron source, which is between 10^{11} and 10^{12} K. If the variability is indeed intrinsic, namely not produced by interstellar scintillation, then one would derive a limit on the beaming factor δ, which should be larger than about 100.

3.2.10 Moving in a Homogeneous Radiation Field

Jets in AGNs often moves in an external radiation field, produced by, e.g. the accretion disk, or by the Broad Line Region (BLR) which intercepts a fraction of the radiation produced by the disk and re-emits it in the form of emission lines. It is therefore interesting to calculate what is the energy density seen by an observer which is comoving with the jet plasma.

To make a specific example, as illustrated by Fig. 3.8, assume that a portion of the jet is moving with a bulk Lorentz factor Γ, velocity βc and that it is surrounded

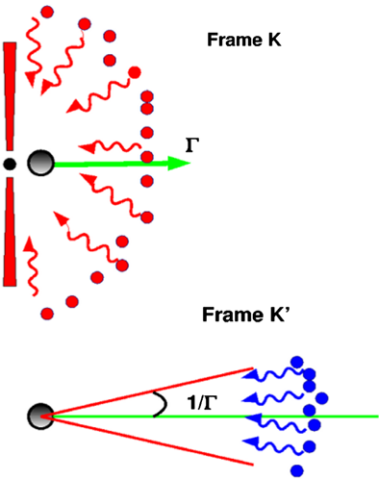


Fig. 3.8 A real case: A relativistic bob is moving within the Broad Line Region of a radio loud AGN, with Lorentz factor Γ. In the rest *frame* K' of the blob the photons coming from 90° in *frame* K are seen to come at an *angle* $1/\Gamma$. The energy density as seen by the blob is enhanced by a factor $\sim\Gamma^2$

by a shell of broad line clouds. For simplicity, assume that the broad line photons are produced by the surface of a sphere of radius R and that the jet is within it. Assume also that the radiation is monochromatic at some frequency ν_0 (in frame K). The comoving (in frame K') observer will see photons coming from a cone of semi-aperture $1/\Gamma$ (the other half may be hidden by the accretion disk): photons coming from the forward direction are seen blue-shifted by a factor $(1+\beta)\Gamma$, while photons that the observer in K sees as coming from the side (i.e. 90° degrees) will be observed in K' as coming from an angle given by $\sin\theta' = 1/\Gamma$ (and $\cos\theta' = \beta$) and will be blue-shifted by a factor Γ. As seen in K', each element of the BLR surface is moving in the opposite direction of the actual jet velocity, and the photons emitted by this element form an angle θ' with respect the element velocity. The Doppler factor used by K' is then

$$\delta' = \frac{1}{\Gamma(1-\beta\cos\theta')} \tag{3.26}$$

The intensity coming from each element is seen boosted as (cf. Eq. 3.19):

$$I' = \delta'^4 I \tag{3.27}$$

The radiation energy density is the integral over the solid angle of the intensity, divided by c:

$$\begin{aligned} U' &= \frac{2\pi}{c}\int_\beta^1 I' d\cos\theta' \\ &= \frac{2\pi}{c}\int_\beta^1 \frac{I}{\Gamma^4(1-\beta\cos\theta')^4} d\cos\theta' \\ &= \left(1+\beta+\frac{\beta^2}{3}\right)\Gamma^2\frac{2\pi I}{c} \end{aligned}$$

$$= \left(1 + \beta + \frac{\beta^2}{3}\right)\Gamma^2 U \tag{3.28}$$

Note that the limits of the integral correspond to the angles $0'$ and $90°$ in frame K. The radiation energy density, in frame K', is then boosted by a factor $(7/3)\Gamma^2$ when $\beta \sim 1$. Doing the same calculation for a sphere, one would obtain $U' = \Gamma^2 U$.

Furthermore a (monochromatic) flux in K is seen, in K', at different frequencies, between $\Gamma\nu_0$ and $(1+\beta)\Gamma\nu_0$, with a slope $F'(\nu') \propto \nu'^2$. Why the slope ν'^2? This can be derived as follows: we already know that $I'(\nu') = \delta'^3 I(\nu) = (\nu'/\nu)^3 I(\nu)$. The flux at a specific frequency is

$$F'(\nu') = 2\pi \int_{\mu'_1}^{\mu'_2} d\mu' \left(\frac{\nu'}{\nu}\right)^3 I(\nu) \tag{3.29}$$

where $\mu' \equiv \cos\theta'$, and the integral is over those μ' contributing at ν'. Since

$$\frac{\nu'}{\nu} = \delta' = \frac{1}{\Gamma(1 - \beta\mu')} \rightarrow \mu' = \frac{1}{\beta}\left(1 - \frac{\nu}{\Gamma\nu'}\right) \tag{3.30}$$

we have

$$d\mu' = -\frac{d\nu}{\beta\Gamma\nu'} \tag{3.31}$$

Therefore, if the intensity is monochromatic in frame K, i.e. $I(\nu) = I_0\delta(\nu - \nu_0)$, the flux density in the comoving frame is

$$\begin{aligned} F'(\nu') &= 2\pi \int_{\nu_2}^{\nu_1} \frac{d\nu}{\beta\Gamma\nu'} \left(\frac{\nu'}{\nu}\right)^3 I_0\delta(\nu - \nu_0) \\ &= \frac{2\pi}{\Gamma\beta}\frac{I_0}{\nu_0^3}\nu'^2; \qquad \Gamma\nu_0 \le \nu' \le (1+\beta)\Gamma\nu_0 \end{aligned} \tag{3.32}$$

where the frequency limits corresponds to photons produced in an emisphere in frame K, and between $0°$ and $\sin\theta' = 1/\Gamma$ in frame K'. Integrating Eq. 3.32 over frequency, one obtains

$$F' = 2\pi I_0 \Gamma^2 \left(1 + \beta + \frac{\beta^2}{3}\right) = \Gamma^2 \left(1 + \beta + \frac{\beta^2}{3}\right) F \tag{3.33}$$

in agreement with Eq. 3.28.

3.3 Superluminal Motion

In 1971 the Very Long Baseline Interferometry began, linking different radio-telescopes that where distant even thousands of km. The resolving power of a tele-

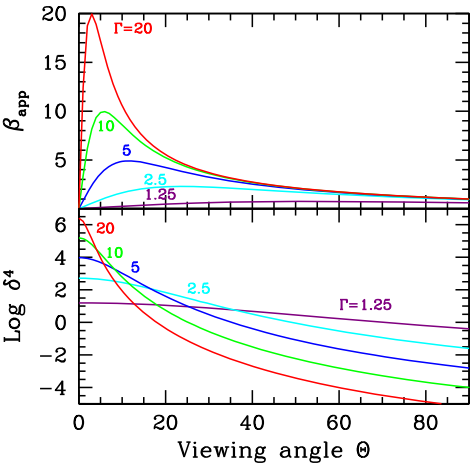


Fig. 3.9 *Top*: The apparent velocity $\beta_{\rm app}$ as a function of the viewing angle θ for different values of Γ, as labeled. *Bottom*: The amplification δ^4 as a function of the viewing angle, for the same Γ as in the *top panel*

scope is of the order of

$$\phi \sim \frac{\lambda}{D} \tag{3.34}$$

where λ is the wavelength to be observed, and D is the diameter of the telescope or the distance of two connected telescopes. Observing at 1 cm, with two telescopes separated by 1000 km (i.e.10^8 cm), means that we can observe details of the source down to the milli-arcsec level (m.a.s.). The first observations of the inner jet of radio-loud quasars revealed that the jet structure was not continuous, but blobby, with several radio knots. Repeating the observations allowed us to discover that the blobs were not stationary, but were moving. Comparing radio maps taken at different times one could measure the angular displacement $\Delta\theta$ between the position of the blob. Knowing the distance d, one could then transform $\Delta\theta$ is a linear size: $\Delta R = d\Delta\theta$. Dividing by the time interval $\Delta t_{\rm a}$ between the two radio maps, one obtains a velocity

$$v_{\rm app} = \frac{d\Delta\theta}{\Delta t_{\rm A}} \tag{3.35}$$

With some surprise, in several objects this turned out to be larger than the light speed c. Therefore these sources were called *superluminal*. The explanation of this apparent violation of special relativity is in Fig. 3.4: the time interval $\Delta t_{\rm a}$ can be much shorter than the emission time $\Delta t_{\rm e}$. With reference to Fig. 3.4, what the observer measures in the two radio maps is the position of the blob in point A (first map) and B (second map), projected in the plane of the sky. The observed displacement is then:

$$CB = \beta c \Delta t_{\rm e} \sin\theta \tag{3.36}$$

Table 3.1 Useful relativistic transformations

$\nu = \nu'\delta$	frequency
$t = t'/\delta$	time
$V = V'\delta$	volume
$\sin\theta = \sin\theta'/\delta$	sine
$\cos\theta = (\cos\theta' + \beta)/(1 + \beta\cos\theta')$	cosine
$I(\nu) = \delta^3 I'(\nu')$	specific intensity
$I = \delta^4 I'$	total intensity
$j(\nu) = j'(\nu')\delta^2$	specific emissivity
$\kappa(\nu) = \kappa'(\nu')/\delta$	absorption coefficient
$T_B = T'_B\delta$	brightn. temp. (size directly measured)
$T_B = T'_B\delta^3$	brightn. temp. (size from variability)
$U' = (1 + \beta + \beta^2/3)\Gamma^2 U$	radiation energy density within an emisphere

Dividing by $\Delta t_\mathrm{a} = \Delta t_\mathrm{e}(1 - \beta\cos\theta)$ we have the measured apparent velocity as

$$v_\mathrm{app} = \frac{\beta c \Delta t_\mathrm{e}\sin\theta}{\Delta t_\mathrm{a}} \longrightarrow \beta_\mathrm{app} = \frac{\beta\sin\theta}{1 - \beta\cos\theta} \tag{3.37}$$

Ask yourself: Γ does not appear. Is it ok? At 0° the apparent velocity is zero. Is it ok? At what angle β_app is maximized? What is its maximum value? Figure 3.9 shows β_app as a function of the viewing angle (angle between the line of sight and the velocity) for different Γ. Is the apparent superluminal speed given by a real motion of the emitting material? Can it be something else? If there are other possibilities, how to discriminate among them?

Table 3.1 collects some of the most common Lorentz transformation, useful when dealing with high energy cosmic sources.

3.4 A Question

Suppose that some optically thin plasma of mass m is falling onto a central object with a velocity v and bulk Lorentz factor Γ. The central object has mass M and produces a luminosity L. Assume that the interaction is through Thomson scattering and that there are no electron–positron pairs.

(a) What is the radiation force acting on the electrons?
(b) What is the gravity force acting on the protons?
(c) What definition of limiting ("Eddington") luminosity would you give in this case?
(d) What happens if the plasma is instead going outward?

References

1. Lind, K.R., Blandford, R.D.: Semidynamical models of radio jets – relativistic beaming and source counts. Astrophys. J. **295**, 358 (1985)
2. Mook, D.E., Vargish, T.: Inside Relativity. Princeton University Press, Princeton (1991)
3. Penrose, R.: The apparent shape of a relativistically moving sphere. Proc. Camb. Philos. Soc. **55**, 137 (1959)
4. Sikora, M., Madejski, G., Moderski, R., Poutanen, J.: Learning about active galactic nucleus jets from spectral properties of blazars. Astrophys. J. **484**, 108 (1997)
5. Terrel, J.: Invisibility of the Lorentz contraction. Phys. Rev. **116**, 1041 (1959)

Chapter 4
Synchrotron Emission and Absorption

4.1 Introduction

We now know for sure that many astrophysical sources are magnetized and have relativistic leptons. Magnetic field and relativistic particles are the two ingredients to have synchrotron radiation. What is responsible for this kind of radiation is the Lorentz force, making the particle to gyrate around the magnetic field lines. Curiously enough, this force *does not work*, but makes the particles to accelerate even if their velocity modulus hardly changes.

The outline of this section is:

1. We will derive the total power emitted by the single electron. Total means integrated over frequency and over emission angles. This will require to generalize the Larmor formula to the relativistic case;
2. We will then outline the basics of the spectrum emitted by the single electron. This is treated in several text-books, so we will concentrate on the basic concepts;
3. Spectrum from an ensemble of electrons. Again, only the basics;
4. Synchrotron self absorption. We will try to discuss things from the point of view of a photon, that wants to calculate its survival probability, and also the point of view of the electron, that wants to calculate the probability to absorb the photon, and then increase its energy and momentum.

4.2 Total Losses

To calculate the total (=integrated over frequencies and emission angles) synchrotron losses we go into the frame that is instantaneously at rest with the particle (in this frame v is zero, but not the acceleration!). This is because we will use the fact that the *emitted* power is Lorentz invariant:

$$P_{\rm e} = P'_{\rm e} = \frac{2e^2}{3c^3} a'^2 = \frac{2e^2}{3c^3}\left[a'^2_{\parallel} + a'^2_{\perp}\right] \tag{4.1}$$

G. Ghisellini, *Radiative Processes in High Energy Astrophysics*,
Lecture Notes in Physics 873, DOI 10.1007/978-3-319-00612-3_4,
© Springer International Publishing Switzerland 2013

where the subscript "e" stands for "emitted". The fact that the power is invariant sounds natural, since after all, power is energy over time, and both energy and time transforms the same way (in special relativity with rulers and clocks). But be aware that this *does not mean* that the emitted and *received* power are the same. They are not!

The problem is now to find how the parallel (to the velocity vector) and perpendicular components of the acceleration Lorentz transform. This is done in text books, so we report the results:

$$\begin{aligned} a'_{\parallel} &= \gamma^3 a_{\parallel} \\ a'_{\perp} &= \gamma^2 a_{\perp} \end{aligned} \tag{4.2}$$

where γ is the particle Lorentz factor. One easy way to understand and remember these transformations is to recall that the acceleration is the second derivative of space with respect to time. The perpendicular component of the displacement is invariant, so we have only to transform (twice) the time (factor γ^2). The parallel displacement instead transforms like γ, hence the γ^3 factor.

The generalization of the Larmor formula is then:

$$P_{\mathrm{e}} = P'_{\mathrm{e}} = \frac{2e^2}{3c^3}\left[a'^2_{\parallel} + a'^2_{\perp}\right] = \frac{2e^2}{3c^3}\gamma^4\left[\gamma^2 a^2_{\parallel} + a^2_{\perp}\right] \tag{4.3}$$

Don't be fooled by the γ^2 factor in front of $a^2_{\parallel}\ldots$ this component of the power is hardly important: since the velocity, for relativistic particles, is always close to c, it implies that one can get very very small acceleration in the same direction of the velocity. This is why linear accelerators minimize radiation losses. For synchrotron machines, instead, the losses due to radiation can be the limiting factor, and they are of course due to $a_{\perp}$: changing the *direction* of the velocity means large accelerations, even without any change in the velocity modulus. To go further, we have to calculate the two components of the acceleration for an electron moving in a magnetic field. Its trajectory, in general, will have a helical shape of radius r_{L} (the Larmor radius). The angle that the velocity vector makes with the magnetic field line is called *pitch angle*. See Fig. 4.1. Let us denote it with θ. We can anticipate that, in the absence of electric field and for a homogeneous magnetic field, the modulus of the velocity will not change: the magnetic field does not work, and so there is no change of energy, except for the losses due to the synchrotron radiation itself. So one important assumption is that *at least during one gyration, the losses are not important*. This is almost always satisfied in astrophysical settings, but there are indeed some cases where this is not true.

When there is no electric field the only acting force is the (relativistic) Lorentz force:

$$\mathbf{F}_{\mathrm{L}} = \frac{d}{dt}(\gamma m \mathbf{v}) = \frac{e}{c}\mathbf{v} \times \mathbf{B} \tag{4.4}$$

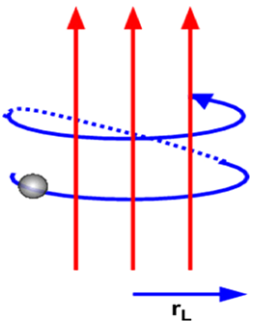


Fig. 4.1 A particle gyrates along the magnetic field lines. Its trajectory has a helicoidal shape, with Larmor radius $r_{\rm L}$ and pitch angle θ

The parallel and perpendicular components are

$$\begin{aligned} F_{\rm L\parallel} &= \gamma m \frac{dv_\parallel}{dt} = 0 \quad \rightarrow \quad a_\parallel = 0 \\ F_{\rm L\perp} &= \gamma m \frac{dv_\perp}{dt} = e\frac{v_\perp}{c} B \quad \rightarrow \quad a_\perp = \frac{evB\sin\theta}{\gamma mc} \end{aligned} \tag{4.5}$$

We can also derive the Larmor radius $r_{\rm L}$ by setting $a_\perp = v_\perp^2/r_{\rm L}$, and so

$$r_{\rm L} = \frac{v_\perp^2}{a_\perp} = \frac{\gamma mc^2\beta\sin\theta}{eB} \tag{4.6}$$

The fundamental frequency is the inverse of the time occurring to complete one orbit (gyration frequency), so $\nu_{\rm B} = c\beta\sin\theta/(2\pi r_{\rm L})$, giving

$$\nu_{\rm B} = \frac{eB}{2\pi\gamma mc} = \frac{\nu_{\rm L}}{\gamma} \tag{4.7}$$

where $\nu_{\rm L}$ is the Larmor frequency, namely the gyration frequency for sub-relativistic particles. Larger B means smaller $r_{\rm L}$, hence greater gyration frequencies. Vice-versa, larger γ means larger inertia, thus larger $r_{\rm L}$, and smaller gyration frequencies. Substituting $a_\perp$ given in Eq. 4.5 in the generalized Larmor formula (Eq. 4.3) we get:

$$P_{\rm S} = \frac{2e^4}{3m^2c^3} B^2\gamma^2\beta^2\sin^2\theta \tag{4.8}$$

We can make it nicer (for future use) by recalling that:

- The magnetic energy density is $U_B \equiv B^2/(8\pi)$.
- The quantity $e^2/(m_{\rm e}c^2)$, in the case of electrons, is the classical electron radius r_0.
- The square of the electron radius is proportional to the Thomson scattering cross section $\sigma_{\rm T}$, i.e. $\sigma_{\rm T} = 8\pi r_0^2/3 = 6.65 \times 10^{-25}$ cm^2.

Making these substitutions, we have that the synchrotron power emitted by a single electron of given pitch angle is:

$$P_{\rm S}(\theta) = 2\sigma_{\rm T} c U_B \gamma^2\beta^2\sin^2\theta \tag{4.9}$$

In the case of an *isotropic distribution of pitch angles* we can average the term $\sin^2\theta$ over the solid angle. The result is $2/3$, giving

$$\langle P_{\rm S}\rangle = \frac{4}{3}\sigma_{\rm T} c U_B \gamma^2 \beta^2 \tag{4.10}$$

Now pause, and ask yourself:

- Is P_S valid only for relativistic particles, or does it describe correctly the radiative losses also for sub-relativistic ones?
- In the relativistic case the losses are proportional to the *square* of the electron energy. Do you understand why? And for sub-relativistic particles?
- What happens of we have protons, instead of electrons?
- What happens for $\theta \to 0$? Are you sure? (that losses vanishes...) Ok, but what happens to the *received* power when you have the lines of the magnetic field along the line of sight, and a beam of particles, all with a small pitch angles, shooting at you?
- Why on earth there is the scattering cross section? Is this a coincidence or does it hide a deeper fact?

4.2.1 Synchrotron Cooling Time

When you want to estimate a timescale of a quantity A, you can always write $t = A/\dot{A}$. In our case A is the energy of the particle. For electrons with an isotropic pitch angle distribution we have

$$t_{\rm syn} = \frac{E}{\langle P_{\rm S}\rangle} = \frac{\gamma m_{\rm e} c^2}{(4/3)\sigma_{\rm T} c U_B \gamma^2 \beta^2} \sim \frac{7.75\times 10^8}{B^2\gamma}\ {\rm s} = \frac{24.57}{B^2\gamma}\ {\rm yr} \tag{4.11}$$

In the vicinity of a supermassive AGN black hole we can have $B = 10^3 B_3$ Gauss and $\gamma = 10^3\gamma_3$, yielding $t_{\rm syn} = 0.75/(B_3^2\gamma_3)$ s. The same electron, in the radio lobes of a radio loud quasar with $B = 10^{-5}B_{-5}$ Gauss, cools in $t_{\rm syn} = 246$ million years.

4.3 Spectrum Emitted by the Single Electron

4.3.1 Basics

There exists a typical frequency associated to the synchrotron process. This is related to the inverse of a typical time. If the electron is relativistic, this is *not* the revolution period. Instead, it is the fraction of the time, for each orbit, during which the observer *receives* some radiation. To simplify, consider an electron with a pitch angle of 90°, and look at Fig. 4.2, illustrating the typical patterns of the produced

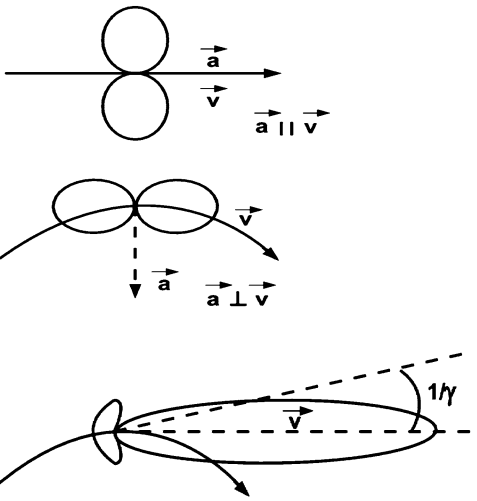


Fig. 4.2 Radiation patterns for a non-relativistic particle with the velocity parallel (*top*) or perpendicular (*mid*) to the acceleration. When the particle is relativistic, the pattern strongly changes due to the aberration of light, and is strongly beamed in the forward direction

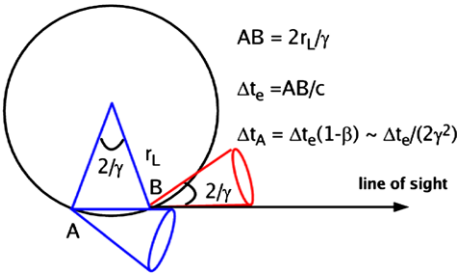


Fig. 4.3 A relativistic electron is gyrating along a magnetic field line with pitch angle 90°. Its trajectory is then a *circle of radius* $r_{\rm L}$. Due to aberration, an observer will "see it" (i.e. will measure an electric field) when the beaming cone of total aperture *angle* $2/\gamma$ is pointing at him

radiation for sub-relativistic electrons moving with a velocity parallel (top panel) or perpendicular (mid panel) to the acceleration. In the bottom panel we see the pattern for a relativistic electron (with $\mathbf{v} \perp \mathbf{a}$): it is strongly beamed in the forward direction. This is the direct consequence of the aberration of light, making half of the photons be emitted in a cone of semi-aperture angle $1/\gamma$ (which is called *the beaming angle*). Note that this *does not* mean that *half of the power* is emitted within $1/\gamma$, because the photons inside the beaming cone are more energetic than those outside, and are more tightly packed (do you remember the δ^4 factor when studying beaming?).

To go further, recall what we do when we study a time series and we want to find the power spectrum: we Fourier transform it. In this case we must do the same. Therefore if there is a typical timescale during which we *receive* most of the signal, we can say that most of the power is emitted at a frequency that is the inverse of that time.

Look at Fig. 4.3: the relativistic electron emits photons all along its orbit, but it will "shoot" in a particular direction only for the time

$$\Delta t_{\rm e} \sim \frac{AB}{v} = \frac{2}{\gamma}\frac{r_{\rm L}}{v} = \frac{1}{v}\frac{2mcv}{eB} = \frac{2}{2\pi}\frac{1}{\nu_{\rm L}} = \frac{2}{2\pi}\frac{1}{\gamma\nu_{\rm B}} \tag{4.12}$$

This is the *emitting* time during which the electron emits photons that will reach the observer. We can approximate the arc AB with a straight segment if the electron is relativistic, and the observer will then measure an *arrival* time Δt_A that is shorter than Δt_e:

$$\Delta t_{\rm A} = \Delta t_{\rm e}(1-\beta) = \Delta t_{\rm e}\frac{(1-\beta^2)}{1+\beta} \sim \frac{\Delta t_{\rm e}}{2\gamma^2} = \frac{1}{2\pi\gamma^3\nu_{\rm B}} \tag{4.13}$$

The inverse of this time is the typical synchrotron (angular) frequency $\omega_{\rm s} = 2\pi\nu_{\rm s}$, so that:

$$\nu_{\rm s} = \frac{1}{2\pi\,\Delta t_{\rm A}} = \gamma^3\nu_{\rm B} = \gamma^2\nu_{\rm L} = \gamma^2\frac{eB}{2\pi m_e c} \tag{4.14}$$

This is a factor γ^3 greater than the fundamental frequency, and a factor γ^2 greater than the Larmor frequency, defined as the typical frequency of non-relativistic particles. We expect that the particle emits most of its power at this frequency.

4.3.2 The Real Stuff

One can look at any text book for a detailed discussion of the procedure to calculate the spectrum emitted by the single particle. Here we report the results: the power per unit frequency emitted by an electron of given Lorentz factor and pitch angle is:

$$\begin{aligned} P_{\rm s}(\nu,\gamma,\theta) &= \frac{\sqrt{3}e^3 B\sin\theta}{m_{\rm e}c^2}F(\nu/\nu_c) \\ F(\nu/\nu_c) &\equiv \frac{\nu}{\nu_c}\int_{\nu/\nu_c}^{\infty} K_{5/3}(y)dy \\ \nu_c &\equiv \frac{3}{2}\nu_{\rm s}\sin\theta \end{aligned} \tag{4.15}$$

This is the power integrated over the emission pattern. $K_{5/3}(y)$ is the modified Bessel function of order 5/3. The dependence upon frequency is contained in $F(\nu/\nu_c)$, that is plotted in Fig. 4.4. This function peaks at $\nu \sim 0.29\nu_c$, therefore very close to what we have estimated before, in our very approximate treatment. The low frequency part is well approximated by a power law of slope 1/3:

$$F(\nu/\nu_c) \to \frac{4\pi}{\sqrt{3}\Gamma(1/3)}\left(\frac{\nu}{2\nu_c}\right)^{1/3} \quad (\nu \ll \nu_c) \tag{4.16}$$

At $\nu \gg \nu_c$ the function decays exponentially, and can be approximated by:

$$F(\nu/\nu_c) \to \left(\frac{\pi}{2}\right)^{1/2}\left(\frac{\nu}{\nu_c}\right)^{1/2} e^{-\nu/\nu_c} \quad (\nu \gg \nu_c) \tag{4.17}$$

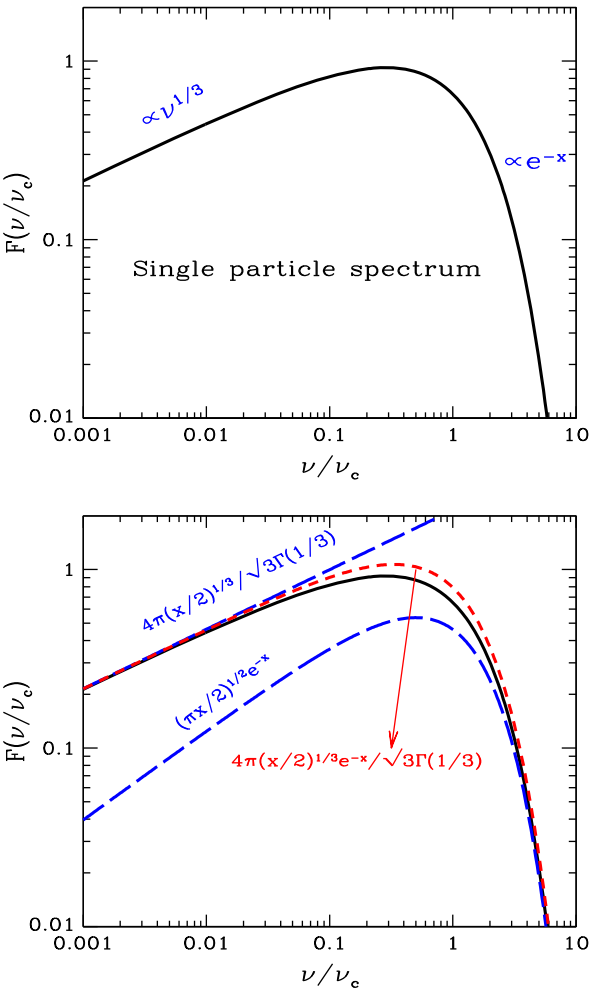


Fig. 4.4 *Top panel*: The function $F(\nu/\nu_c)$ describing the synchrotron spectrum emitted by the single electron. *Bottom panel*: $F(\nu/\nu_c)$ is compared with some approximating formulae, as labeled. We have defined $x \equiv \nu/\nu_c$

Another approximation valid for all frequency, but overestimating F around the peak, is:

$$F(\nu/\nu_c) \sim \frac{4\pi}{\sqrt{3}\Gamma(1/3)} \left(\frac{\nu}{2\nu_c}\right)^{1/3} e^{-\nu/\nu_c} \tag{4.18}$$

4.3.3 Limits of Validity

One limit can be obtained by requiring that, during one orbit, the emitted energy is much smaller than the electron energy. If not, the orbit is modified, and our calculations are no more valid. For non-relativistic electrons this translates in demanding

that

$$h\nu_{\rm L} < m_{\rm e}c^2 \rightarrow B < \frac{2\pi m_{\rm e}^2 c^3}{he} \equiv B_{\rm c} \tag{4.19}$$

where $B_{\rm c} \sim 4.4 \times 10^{13}$ Gauss is the critical magnetic field, around and above which quantum effects appears (i.e. quantized orbits, Landau levels and so on).

For relativistic particles we demand that the energy emitted during one orbit does not exceed the energy of the particle.

$$P_{\rm s}\frac{2\pi r_{\rm L}}{\beta c} < \gamma m_{\rm e}c^2 \rightarrow B < \frac{2e/\sigma_{\rm T}}{\gamma^2 \sin^3\theta} \sim \frac{1.4 \times 10^{15}}{\gamma^2 \sin^3\theta}\ \text{Gauss} \tag{4.20}$$

Therefore for large γ we reach the validity limit even if the magnetic field is sub-critical.

For very small pitch angles beware that the spectrum is not described by $F(\nu/\nu_c)$, but consists of a blue-shifted cyclotron line. This is because, in the gyroframe, the particle is sub-relativistic, and so it emits only one (or very few) harmonics, that the observer sees blueshifted.

4.3.4 From Cyclotron to Synchrotron Emission

A look at Fig. 4.5 helps to understand the difference between cyclotron and synchrotron emission. When the particle is very sub-relativistic, the observed electric field is sinusoidal in time. Correspondingly, the Fourier transform of $E(t)$ gives only one frequency, the first harmonic. Increasing somewhat the velocity (say, $\beta \sim 0.01$) the emission pattern starts to be asymmetric (for light aberration) and as a consequence $E(t)$ must be described by more than just one sinusoid, and higher order harmonics appear. In these cases the ratio of the power contained in successive harmonics goes as β^2.

Finally, for relativistic (i.e. $\gamma \gg 1$) particles, the pattern is so asymmetric that the observers sees only spikes of electric field. They repeat themselves with the gyration period, but all the power is concentrated into $\Delta t_{\rm A}$. To reproduce $E(t)$ in this case with sinusoids requires a large number of them, with frequencies going at least up to $1/\Delta t_{\rm A}$. In this case the harmonics are many, guaranteeing that the spectrum becomes continuous with any reasonable line broadening effect, and the power is concentrated at high frequencies.

4.4 Emission from Many Electrons

Again, this problem is treated in several text books, so we repeat the basic results using some approximations, tricks and shortcuts.

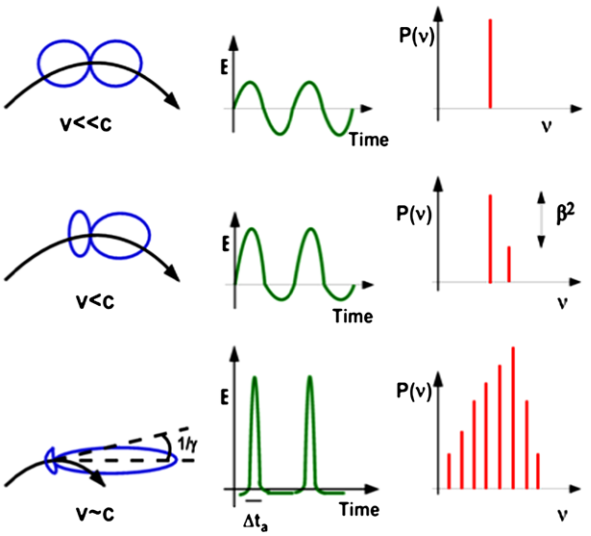


Fig. 4.5 From cyclo to synchro: If the emitting particle has a very small velocity, the observer sees a sinusoidal (in time) electric field $E(t)$. Increasing the velocity the pattern becomes asymmetric, and the second harmonic appears. For $0 < \beta \ll 1$ the power in the second harmonic is a factor β^2 less than the power in the first. For relativistic particles, the pattern becomes strongly beamed, the emission is concentrated in the time Δt_A. As a consequence the Fourier transformation of $E(t)$ must contain many harmonics, and the power is concentrated in the harmonics of frequencies $\nu \sim 1/\Delta t_A$. Broadening of the harmonics due to several effects ensures that the spectrum in this case becomes continuous. Note that the fundamental harmonic becomes *smaller* increasing γ (since $\nu_B \propto 1/\gamma$)

The queen of the particle energy distributions in high energy astrophysics is the *power law* distribution:

$$N(\gamma) = K\gamma^{-p} = N(E)\frac{dE}{d\gamma}; \quad \gamma_{\min} < \gamma < \gamma_{\max} \tag{4.21}$$

Now, assuming that the distribution of pitch angles is the same at low and high γ, we want to obtain the synchrotron emissivity produced by these particles. Beware that the *emissivity* is the power per unit *solid angle* produced within 1 cm^3. The specific emissivity is also per unit of frequency. So, if Eq. 4.21 represents a density, we should integrate over γ the power produced by the single electron (of a given γ) times $N(\gamma)$, and divide all it by 4π, if the emission is isotropic:

$$j_s(\nu, \theta) = \frac{1}{4\pi}\int_{\gamma_{\min}}^{\gamma_{\max}} N(\gamma)P(\gamma, \nu, \theta)d\gamma \tag{4.22}$$

Doing the integral one easily finds that, in an appropriate range of frequencies:

$$j_s(\nu, \theta) \propto K B^{(p+1)/2}\nu^{-(p-1)/2} \tag{4.23}$$

The important thing is that a power law electron distribution produces a power law spectrum, and the two spectral indices are related. We traditionally call α the spectral index of the radiation, namely $j_\mathrm{s} \propto \nu^{-\alpha}$. We then have

$$\alpha = \frac{p-1}{2} \tag{4.24}$$

This result is so important that it is worth to try to derive it in a way as simple as possible, even without doing the integral of Eq. 4.22. We can in fact use the fact that the synchrotron spectrum emitted by the single particle is peaked. We can then say, without being badly wrong, that all the power is emitted at the typical synchrotron frequency:

$$\nu_\mathrm{s} = \gamma^2 \nu_\mathrm{L}; \quad \nu_\mathrm{L} \equiv \frac{eB}{2\pi m_\mathrm{e} c} \tag{4.25}$$

In other words, there is a tight correspondence between the energy of the electron and the frequency it emits. To simplify further, let us assume that the pitch angle is 90°. The emissivity at a given frequency, within an interval $d\nu$, is then the result of the emission of electrons having the appropriate energy γ, within the interval $d\gamma$

$$j_\mathrm{s}(\nu)d\nu = \frac{1}{4\pi} P_\mathrm{s} N(\gamma) d\gamma; \quad \gamma = \left(\frac{\nu}{\nu_\mathrm{L}}\right)^{1/2}; \quad \frac{d\gamma}{d\nu} = \frac{\nu^{-1/2}}{2\nu_\mathrm{L}^{1/2}} \tag{4.26}$$

we then have

$$\begin{aligned} j_\mathrm{s}(\nu) &\propto B^2 \gamma^2 K \gamma^{-p} \frac{d\gamma}{d\nu} \\ &\propto B^2 K \left(\frac{\nu}{\nu_\mathrm{L}}\right)^{(2-p)/2} \frac{\nu^{-1/2}}{\nu_\mathrm{L}^{1/2}} \\ &\propto K B^{(p+1)/2} \nu^{-(p-1)/2} \end{aligned} \tag{4.27}$$

where we have used $\nu_\mathrm{L} \propto B$.

The synchrotron flux received from a homogeneous and thin source of volume $V \propto R^3$, at a distance d_L, is

$$\begin{aligned} F_\mathrm{s}(\nu) &= 4\pi j_\mathrm{s}(\nu) \frac{V}{4\pi d_\mathrm{L}^2} \\ &\propto \frac{R^3}{d_\mathrm{L}^2} K B^{1+\alpha} \nu^{-\alpha} \\ &\propto \theta_s^2 R K B^{1+\alpha} \nu^{-\alpha} \end{aligned} \tag{4.28}$$

where θ_s is the angular radius of the source (not the pitch angle!). Observing the source at two different frequencies allows to determine α, hence the slope of the

particle energy distribution. Furthermore, if we know the distance and R, the normalization depends on the particle density and the magnetic field: two unknowns and only one equation. We need another relation to close the system. As we will see in the following, this is provided by the self-absorbed flux.

4.5 Synchrotron Absorption: Photons

All emission processes have their absorption counterpart, and the synchrotron emission is no exception. What makes synchrotron special is really the fact that it is done by relativistic particles, and they are almost never distributed in energy as a Maxwellian. If they were, we could use the well known fact that the ratio between the emissivity and the absorption coefficient is equal to the black body (Kirchoff law) and then we could easily find the absorption coefficient. But in the case of a non-thermal particle distribution we cannot do that. Instead we are obliged to go back to more fundamental relations, the one between the A and B Einstein coefficients relating spontaneous and stimulated emission and "true" absorption (by the way, recall that the absorption coefficient is what remains subtracting stimulated emission from "true" absorption). But we once again will use some tricks, in order to be as simple as possible. These are the steps:

1. The first trick is to think to our power law energy distribution as a superposition of Maxwellians, of different temperatures. So, we will relate the energy $\gamma m_e c^2$ of a given electron to the energy kT of a Maxwellian.
2. We have already seen that there is a tight relation between the emitted frequency and γ. Since the emission and absorption processes are related, we will assume that a particular frequency ν is preferentially absorbed by those electrons that can emit it.
3. As a consequence, we can associate our "fake" temperature to the frequency:

$$kT \sim \gamma m_e c^2 \sim m_e c^2 \left(\frac{\nu}{\nu_L}\right)^{1/2} \tag{4.29}$$

4. For an absorbed source the *brightness temperature* T_b, defined by

$$I(\nu) \equiv 2kT_b \frac{\nu^2}{c^2} \tag{4.30}$$

must be equal to the kinetic "temperature" of the electrons, and so

$$I(\nu) \equiv 2kT \frac{\nu^2}{c^2} \sim 2m_e \nu^2 \left(\frac{\nu}{\nu_L}\right)^{1/2} \propto \frac{\nu^{5/2}}{B^{1/2}} \tag{4.31}$$

These are the right dependencies. Note that the spectrum is $\propto \nu^{5/2}$, not ν^2, and this is the consequence of having "different temperatures". Note also that the particle density disappeared: if you think about it is natural: the more electrons you have, the more you emit, but the more you absorb. Finally, even the *slope* of the particle distribution is not important, it controls (up to a factor of order unity) only the normalization of $I(\nu)$ (our ultra-simple derivation cannot account for it, see the Appendix).

The above is valid as long as we can associate a specific γ to any ν. This is not always the case. Think for instance to a cut-off distribution, with $\gamma_{\rm min} \gg 1$. In this case the electrons with $\gamma_{\rm min}$ are the most efficient emitters and absorbers of all photons with $\nu < \nu_{\rm min} \equiv \gamma_{\rm min}^2 \nu_{\rm L}$. So in this case we *should not* associate a different temperature when dealing with different $\nu < \nu_{\rm min}$. But if do not change T, we recover a self-absorbed intensity $I(\nu) \propto \nu^2$ (i.e. Raleigh–Jeans like).

Now, going from the intensity to the flux, we must integrate $I(\nu)$ over the angular dimension of the source (i.e. θ_s), obtaining

$$F(\nu) \propto \theta_s^2 \frac{\nu^{5/2}}{B^{1/2}} \tag{4.32}$$

if we could observe a self-absorbed source, of known angular size, we could then derive its magnetic field *even without knowing its distance* (apart from k-corrections: here all frequencies are in the rest frame of the source, therefore $\nu = (1+z)\nu_{\rm obs}$).

4.5.1 From Thick to Thin

To describe the transition from the self-absorbed to the thin regime we have to write the radiation transfer equation. The easiest one is for a slab. Calling α_ν the specific absorption coefficient [cm^{-1}] we have

$$I(\nu) = \frac{j(\nu)}{\alpha_\nu}\left(1 - e^{-\tau_\nu}\right); \quad \tau_\nu \equiv R\alpha_\nu \tag{4.33}$$

it is instructive to write Eq. 4.33 in the form:

$$I(\nu) = j(\nu) R \frac{1 - e^{-\tau_\nu}}{\tau_\nu} \tag{4.34}$$

because in this way it is evident that when $\tau_\nu \gg 1$ (self-absorbed regime), we simply have

$$I(\nu) = \frac{j(\nu)R}{\tau_\nu} = \frac{j(\nu)}{\alpha_\nu}; \quad \tau_\nu \gg 1 \tag{4.35}$$

One can interpret it saying that the intensity is coming from electrons lying in a shell within R/τ_ν from the surface.

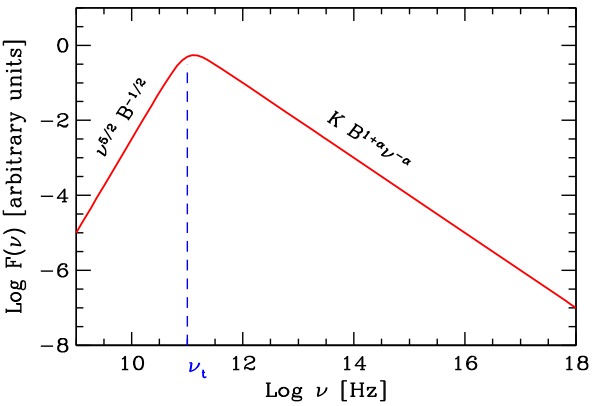


Fig. 4.6 The synchrotron spectrum from a partially self-absorbed source. Observations of the self-absorbed part could determine B. Observations of the thin part can then determine K and the electron slope p

Since we have already obtained $I(\nu) \propto \nu^{5/2} B^{-1/2}$ in the absorbed regime, we can derive the dependencies of the absorption coefficient:

$$\alpha_\nu = \frac{j(\nu)}{I(\nu)} \propto \frac{K B^{(p+1)/2} \nu^{-(p-1)/2}}{\nu^{5/2} B^{-1/2}} = K B^{(p+2)/2} \nu^{-(p+4)/2} \tag{4.36}$$

Note the rather strong dependence upon frequency: at large frequencies, absorption is small.

The obvious division between the thick and thin regime is when $\tau_\nu = 1$. We call *self-absorption frequency*, ν_t, the frequency when this occurs. We then have:

$$\tau_{\nu_t} = R\alpha_{\nu_t} = 1 \rightarrow \nu_t \propto \left[RKB^{(p+2)/2}\right]^{2/(p+4)} \tag{4.37}$$

The self-absorption frequency is a crucial quantity for studying synchrotron sources: part of the reason is that it can be thought to belong to both regimes (thin and thick), the other reason is that the synchrotron spectrum peaks very close to ν_t (see Fig. 4.6) even if not exactly at ν_t (see the Appendix).

4.6 Synchrotron Absorption: Electrons

In the previous section we have considered what happens to the emitted spectrum when photons are emitted and absorbed. This is described by the absorption coefficient. But now imagine to be an electron, that emits and absorbs synchrotron photons. You would probably be interested if your budget is positive or negative, that is, if you are loosing or gaining energy. This is most efficiently described by a cross section, that tells you the probability to absorb a photon. Surprisingly, the synchrotron absorption cross section has been derived relatively recently [1], and its expression is:

$$\sigma_s(\nu, \gamma, \theta) = \frac{16\pi^2}{3\sqrt{3}} \frac{e}{B} \frac{1}{\gamma^5 \sin\theta} K_{5/3}\left(\frac{\nu}{\nu_c \sin\theta}\right) \tag{4.38}$$

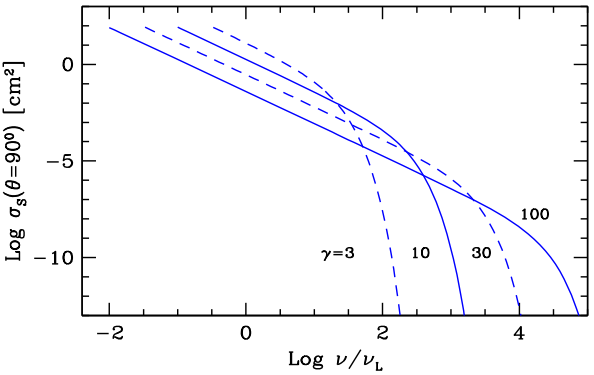


Fig. 4.7 The synchrotron absorption cross section as a function of ν/ν_L for different values of γ, as labeled, assuming a pitch angle of $\theta = 90°$ and a magnetic field of 1 Gauss

For frequencies $\nu \ll \nu_c$ this expression can be approximated by:

$$\sigma_s(\nu, \gamma, \theta) = \frac{8\pi^2 (3\sin\theta)^{2/3} \Gamma(5/3)}{3\sqrt{3}} \frac{e}{B} \left(\frac{\nu}{\nu_L/\gamma} \right)^{-5/3} ; \quad \nu \ll \nu_c \tag{4.39}$$

Note these features:

- At the fundamental frequency ν_L/γ, the cross section does not depend on γ.
- The dimensions are given by e/B: this factor is proportional to the product of the classical electron radius and the Larmor wavelength (or radius). Imagine an electron with 90° pitch angle, and to see its orbit from the side: you would see a rectangle of base r_L and height r_0. The area of this rectangle is of the order of e/B. At low frequencies, σ_s can be orders of magnitudes larger than the Thomson scattering cross section.
- There is no explicit dependence on the particle mass. However, protons have much smaller ν_L, and the dependence on mass is hidden there. Nevertheless, electrons and protons have the same cross section (of order e/B) at their respective fundamental frequencies.

Figure 4.7 shows σ_s as a function of ν/ν_L for different γ. The thing it should be noticed is that this cross section is really large. Can we make some useful use of it? Well, there are at least two issues, one concerning energy, and the other concerning momentum.

First, electrons emitting and absorbing synchrotron photons do so with a large efficiency. *They can talk each other by exchanging photons*. Therefore, even if they are distributed as a power law in energy at the beginning, they will try to form a Maxwellian. They will form it, as long as other competing processes are not important, such as inverse Compton scatterings. The formation of the Maxwellian will interest only the low energy part of the electron distribution, where absorption is important. Note that this thermalization process works exactly when Coulomb collisions fail: they are inefficient at low density and high temperature, while synchrotron absorption can work for relativistic electrons even if they are not very dense.

The second issue concerns exchange of momentum between photons and electrons. Suppose that a magnetized region with relativistic electrons is illuminated by

low frequency radiation by another source, located aside. The electrons will efficiently absorb this radiation, and thus its momentum. The magnetized region will then accelerate.

Appendix: Useful Formulae

In this section we collect several useful formulae concerning the synchrotron emission. When possible, we give also simplified analytical expressions. We will often consider that the emitting electrons have a distribution in energy which is a power law between some limits γ_1 and γ_2. Electrons are assumed to be isotropically distributed in the comoving frame of the emitting source. Their density is

$$N(\gamma) = K\gamma^{-p}; \quad \gamma_1 < \gamma < \gamma_2 \tag{4.40}$$

The Larmor frequency is defined as:

$$\nu_L \equiv \frac{eB}{2\pi m_e c} \tag{4.41}$$

A.1 Emissivity

The synchrotron emissivity $j_s(\nu, \theta)$ [erg cm^{-3} s^{-1} sterad^{-1}] is

$$j_s(\nu, \theta) \equiv \frac{1}{4\pi} \int_{\gamma_1}^{\gamma_2} N(\gamma) P_s(\nu, \gamma, \theta) d\gamma \tag{4.42}$$

where $P_s(\nu, \gamma, \theta)$ is the power emitted at the frequency ν (integrated over all directions) by the single electron of energy $\gamma m_e c^2$ and pitch angle θ. For electrons making the same pitch angle θ with the magnetic field, the emissivity is

$$j_s(\nu, \theta) = \frac{3\sigma_T c K U_B}{8\pi^2 \nu_L} \left(\frac{\nu}{\nu_L}\right)^{-\frac{p-1}{2}} (\sin\theta)^{\frac{p+1}{2}} 3^{\frac{p}{2}} \frac{\Gamma(\frac{3p-1}{12})\Gamma(\frac{3p+19}{12})}{p+1} \tag{4.43}$$

between $\nu_1 \gg \gamma_1^2 \nu_L$ and $\nu_2 \ll \gamma_2^2 \nu_L$. If the distribution of pitch angles is isotropic, we must average the $(\sin\theta)^{\frac{p+1}{2}}$ term, obtaining

$$\left\langle (\sin\theta)^{\frac{p+1}{2}} \right\rangle = \int_0^{\frac{\pi}{2}} (\sin\theta)^{\frac{p+1}{2}} \sin\theta d\theta = \frac{\sqrt{\pi}}{2} \frac{\Gamma(\frac{p+5}{4})}{\Gamma(\frac{p+7}{4})} \tag{4.44}$$

Therefore the pitch angle averaged synchrotron emissivity is

$$j_s(\nu) = \frac{3\sigma_T c K U_B}{16\pi\sqrt{\pi}\nu_L} \left(\frac{\nu}{\nu_L}\right)^{-\frac{p-1}{2}} f_j(p) \tag{4.45}$$

The function $f_j(p)$ includes all the products of the Γ-functions:

$$f_j(p) = \frac{3^{\frac{p}{2}}}{p+1} \frac{\Gamma(\frac{3p-1}{12})\Gamma(\frac{3p+19}{12})\Gamma(\frac{p+5}{4})}{\Gamma(\frac{p+7}{4})}$$
$$\sim 3^{\frac{p}{2}} \left(\frac{2.25}{p^{2.2}} + 0.105 \right) \tag{4.46}$$

where the simplified fitting function is accurate at the per cent level.

A.2 Absorption Coefficient

The absorption coefficient $\alpha_\nu(\theta)$ [cm^{-1}] is defined as:

$$\alpha_\nu(\theta) \equiv \frac{1}{8\pi m_e \nu^2} \int_{\gamma_1}^{\gamma_2} \frac{N(\gamma)}{\gamma^2} \frac{d}{d\gamma} \left[\gamma^2 P(\nu, \theta) \right] d\gamma \tag{4.47}$$

Written in this way, the above formula is valid even when the electron distribution is truncated. For our power law electron distribution $\alpha_\nu(\theta)$ becomes:

$$\alpha_\nu(\theta) \equiv \frac{1}{8\pi m_e \nu^2} \int_{\gamma_1}^{\gamma_2} \frac{N(\gamma)}{\gamma^2} \frac{d}{d\gamma} \left[\gamma^2 P(\nu, \theta) \right] d\gamma \tag{4.48}$$

Above $\nu = \gamma_1^2 \nu_L$, we have:

$$\alpha_\nu(\theta) = \frac{e^2 K}{4 m_e c^2} (\nu_L \sin\theta)^{\frac{p+2}{2}} \nu^{-\frac{p+4}{2}} 3^{\frac{p+1}{2}} \Gamma\left(\frac{3p+22}{12} \right) \Gamma\left(\frac{3p+2}{12} \right) \tag{4.49}$$

Averaging over the pitch angles we have:

$$\left\langle (\sin\theta)^{\frac{p+2}{2}} \right\rangle = \int_0^{\frac{\pi}{2}} (\sin\theta)^{\frac{p+2}{2}} \sin\theta d\theta = \frac{\sqrt{\pi}}{2} \frac{\Gamma(\frac{p+6}{4})}{\Gamma(\frac{p+8}{4})} \tag{4.50}$$

resulting in a pitch angle averaged absorption coefficient:

$$\alpha_\nu = \frac{\sqrt{\pi} e^2 K}{8 m_e c} \nu_L^{\frac{p+2}{2}} \nu^{-\frac{p+4}{2}} f_\alpha(p) \tag{4.51}$$

where the function $f_\alpha(p)$ is:

$$f_\alpha(p) = 3^{\frac{p+1}{2}} \frac{\Gamma(\frac{3p+22}{12})\Gamma(\frac{3p+2}{12})\Gamma(\frac{p+6}{4})}{\Gamma(\frac{p+8}{4})}$$
$$\sim 3^{\frac{p+1}{2}} \left(\frac{1.8}{p^{0.7}} + \frac{p^2}{40} \right) \tag{4.52}$$

The simple fitting function is accurate at the per cent level.

A.3 Specific Intensity

Simple radiative transfer allows to calculate the specific intensity:

$$I(\nu) = \frac{j_{\rm s}(\nu)}{\alpha_\nu}\left(1 - e^{-\tau_\nu}\right) \tag{4.53}$$

where the absorption optical depth $\tau_\nu \equiv \alpha_\nu R$ and R is the size of the emitting region. When $\tau_\nu \gg 1$, the exponential term vanishes, and the intensity is simply the ratio between the emissivity and the absorption coefficient. This is the self-absorbed, or thick, regime. In this case, since both $j_{\rm s}(\nu)$ and α_ν depends linearly upon K, the resulting self-absorbed intensity does not depend on the normalization of the particle density K:

$$I(\nu) = \frac{2m_{\rm e}}{\sqrt{3}\nu_L^{1/2}} f_I(p)\left(1 - e^{-\tau_\nu}\right) \tag{4.54}$$

we can thus see that the slope of the self-absorbed intensity does not depend on p. Its normalization, however, does (albeit weakly) depend on p through the function $f_I(p)$, which in the case of averaging over an isotropic pitch angle distribution is given by:

$$\begin{aligned} f_I(p) = \frac{1}{p+1} &= \frac{\Gamma(\frac{3p-1}{12})\Gamma(\frac{3p+19}{12})\Gamma(\frac{p+5}{4})\Gamma(\frac{p+8}{4})}{\Gamma(\frac{3p+22}{12})\Gamma(\frac{3p+2}{12})\Gamma(\frac{p+7}{4})\Gamma(\frac{p+6}{4})} \\ &\sim \frac{5}{4p^{4/3}} \end{aligned} \tag{4.55}$$

where again the simple fitting function is accurate at the level of 1 per cent.

A.4 Self-absorption Frequency

The self-absorption frequency $\nu_{\rm t}$ is defined by $\tau_{\nu_{\rm t}} = 1$:

$$\nu_{\rm t} = \nu_L\left[\frac{\sqrt{\pi}e^2RK}{8m_{\rm e}c\nu_L} f_\alpha(p)\right]^{\frac{4}{p+4}} = \nu_L\left[\frac{\pi\sqrt{\pi}}{4}\frac{eRK}{B} f_\alpha(p)\right]^{\frac{2}{p+4}} \tag{4.56}$$

Note that the term in parenthesis is dimensionless, and since RK has units of the inverse of a surface, then e/B has the dimension of a surface. In fact we have already discussed that this is the synchrotron absorption cross section of a relativistic electron of energy $\gamma m_{\rm e}c^2$ absorbing photons at the fundamental frequency ν_L/γ.

The random Lorentz factor $\gamma_{\rm t}$ of the electrons absorbing (and emitting) photons with frequency $\nu_{\rm t}$ is $\gamma_{\rm t} \sim [3\nu_{\rm t}/(4\nu_L)]^{1/2}$.

A.5 Synchrotron Peak

In an $F(\nu)$ plot, the synchrotron spectrum peaks close to ν_t, at a frequency $\nu_{s,p}$ given by solving

$$\frac{dI(\nu)}{d\nu} = 0 \rightarrow \frac{d}{d\nu}\left[\nu^{5/2}\left(1 - e^{-\tau_\nu}\right)\right] = 0 \tag{4.57}$$

which is equivalent to solve the equation:

$$\exp(\tau_{\nu_{s,p}}) - \frac{p+4}{5}\tau_{\nu_{s,p}} - 1 = 0 \tag{4.58}$$

whose solution can be approximated by

$$\tau_{\nu_{s,p}} \sim \frac{2}{5} p^{1/3} \ln p \tag{4.59}$$

References

1. Ghisellini, G., Svensson, R.: The synchrotron and cyclo-synchrotron absorption cross-section. Mon. Not. R. Astron. Soc. **252**, 313 (1991)

Chapter 5
Compton Scattering

5.1 Introduction

The simplest interaction between photons and free electrons is *scattering*. When the energy of the incoming photons (as seen in the comoving frame of the electron) is small with respect to the electron rest mass-energy, the process is called *Thomson scattering*, which can be described in terms of classical electro-dynamics. As the energy of the incoming photons increases and becomes comparable or greater than $m_e c^2$, a quantum treatment is necessary (Klein–Nishina regime).

5.2 The Thomson Cross Section

Assume an electron at rest, and an electromagnetic wave of frequency $\nu \ll m_e c^2/h$. Assume also that the incoming wave is completely linearly polarized. In order to neglect the magnetic force $(e/c)(\mathbf{v} \times \mathbf{B})$ we must also require that the oscillation velocity $v \ll c$. This in turn implies that the incoming wave has a sufficiently low amplitude. The electron starts to oscillate in response to the varying electric force eE, and the average square acceleration during one cycle of duration $T = 1/\nu$ is

$$\langle a^2 \rangle = \frac{1}{T} \int_0^T \frac{e^2 E_0^2}{m_e^2} \sin^2(2\pi \nu t) dt = \frac{e^2 E_0^2}{2 m_e^2} \tag{5.1}$$

The emitted power per unit solid angle is given by the Larmor formula $dP/d\Omega = e^2 a^2 \sin^2 \Theta/(4\pi c^3)$ where Θ is the angle between the acceleration vector and the propagation vector of the emitted radiation. Please note that Θ is *not* the scattering angle, which is instead the angle between the incoming and the scattered wave (or photon). We then have

$$\frac{dP_e}{d\Omega} = \frac{e^4 E_0^2}{8\pi m_e^2 c^3} \sin^2 \Theta \tag{5.2}$$

G. Ghisellini, *Radiative Processes in High Energy Astrophysics*,
Lecture Notes in Physics 873, DOI 10.1007/978-3-319-00612-3_5,
© Springer International Publishing Switzerland 2013

The scattered radiation is completely linearly polarized in the plane defined by the incident polarization vector and the scattering direction. The flux of the incoming wave is $S_i = cE_0^2/(8\pi)$. The differential cross section of the process is then

$$\left(\frac{d\sigma}{d\Omega}\right)_{\text{pol}} = \frac{dP_e/d\Omega}{S_i} = r_0^2 \sin^2\Theta \tag{5.3}$$

where $r_0 \equiv e^2/(m_e c^2)$ is the *classic electron radius*, $r_0 = 2.82 \times 10^{-13}$ cm. We see that the scattered pattern of a completely polarized incoming wave is a torus, with axis along the acceleration direction. The total cross section can be derived in a similar way, but considering the Larmor formula integrated over the solid angle $[P = 2e^2a^2/(3c^3)]$. In this way the total cross section is

$$\sigma_{\text{pol}} = \frac{P_e}{S_i} = \frac{8\pi}{3} r_0^2 \tag{5.4}$$

Note that the classical electron radius can also be derived by equating the energy of the associated electric field to the electron rest mass-energy:

$$m_{\text{e}}c^2 = \int_{a_o}^{\infty} \frac{E^2}{8\pi} 4\pi r^2 dr = \int_{a_o}^{\infty} \frac{e^2}{2r^2} dr \rightarrow a_0 = \frac{1}{2}\frac{e^2}{m_{\text{e}}c^2} \tag{5.5}$$

Why is a_0 slightly different from r_0? Because there is an intrinsic uncertainty related to the distribution of the charge within (or throughout the surface of) the electron. See the discussion in Vol. 2, Chap. 28.3 of "The Feynman Lectures on Physics", about the fascinating idea that the mass of the electron is all electromagnetic.

5.2.1 Why the Peanut Shape?

The scattering of a completely unpolarized incoming wave can be derived by assuming that the incoming radiation is the sum of two orthogonal completely linearly polarized waves, and then summing the associated scattering patterns. Since we have the freedom to chose the orientations of the two polarization planes, it is convenient to chose one of these planes as the one defined by the incident and scattered directions, and the other one perpendicular to this plane. The scattering can be then regarded as the sum of two independent scattering processes, one with emission angle Θ, the other with $\pi/2$. If we note that the scattering angle (i.e. the angle between the scattered wave and the incident wave) is $\theta = \pi/2 - \Theta$, we have

$$\begin{aligned}\left(\frac{d\sigma}{d\Omega}\right)_{\text{unpol}} &= \frac{1}{2}\left[\left(\frac{d\sigma(\Theta)}{d\Omega}\right)_{\text{pol}} + \left(\frac{d\sigma(\pi/2)}{d\Omega}\right)_{\text{pol}}\right] \\ &= \frac{1}{2} r_0^2 \left(1 + \sin^2\Theta\right) \\ &= \frac{1}{2} r_0^2 \left(1 + \cos^2\theta\right)\end{aligned} \tag{5.6}$$

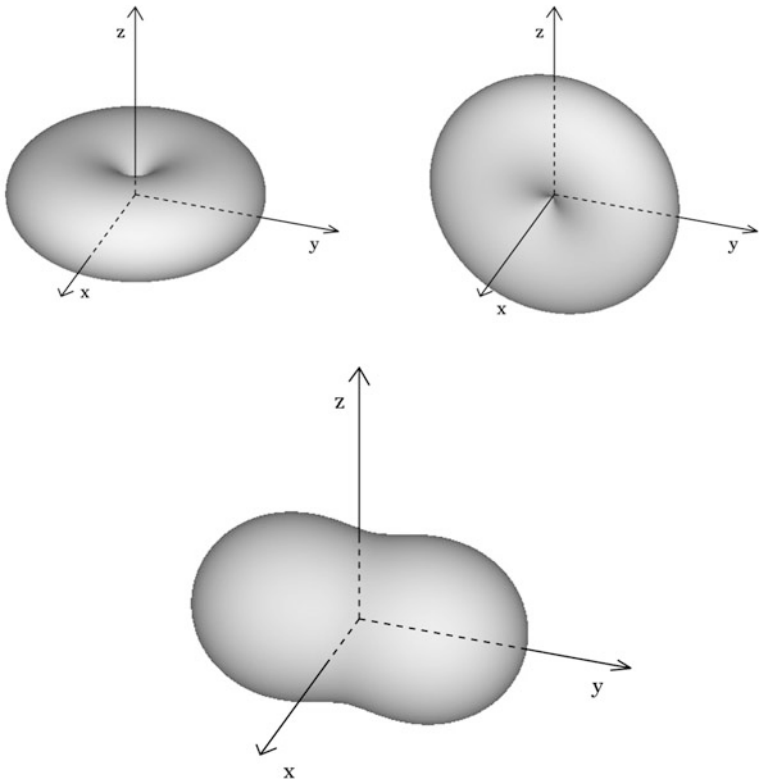


Fig. 5.1 Photons are coming along the y-axis. The *top panels* shows the pattern of the scattered radiation for photons completely linearly polarized along the z-axis (*left*) and along the x-axis (*right*). The sum of the two torii corresponds to the pattern for unpolarized radiation (*bottom panel*). This explains why we have a "peanut" shape, elongated along the velocity vector of the incoming photons. Courtesy of Davide Lazzati

In this case we see that the cross section depends only on the scattering angle θ. The pattern of the scattered radiation is then the superposition of two orthogonal "tori" (one for each polarization direction), as illustrated in Fig. 5.1. When scattering completely linearly polarized radiation, only one "torus" survives. Instead, when scattering unpolarized radiation, some polarization is introduced, because of the difference between the two "tori" patterns. Both terms of the RHS of Eq. 5.6 refer to completely polarized scattered waves (but in two perpendicular planes). The difference between these two terms is then associated to the introduced polarization, which is then

$$\Pi = \frac{1 - \cos^2\theta}{1 + \cos^2\theta} \tag{5.7}$$

The above discussion helps to understand why the scattering process introduces some polarization, which is maximum (100 %) if the angle between the incoming

and the scattered photons is 90°, and zero for 0° and 180°, where the two torii give the same, but orthogonal, contributions.

The total cross section, integrated over the solid angle, is the same as that for polarized incident radiation (Eq. 5.4) since the electron at rest has no preferred defined direction. This is the Thomson cross section:

$$\sigma_{\mathrm{T}} = \int \left(\frac{d\sigma}{d\Omega}\right)_{\mathrm{unpol}} d\Omega = \frac{2\pi r_0^2}{2} \int \left(1 + \cos^2\theta\right) d\cos\theta = \frac{8\pi}{3} r_0^2$$
$$= 6.65 \times 10^{-25}\ \mathrm{cm}^2 \tag{5.8}$$

5.3 Direct Compton Scattering

In the previous section we considered the scattering process as an interaction between an electron and an *electromagnetic wave*. This required $h\nu \ll m_e c^2$. In the general case the quantum nature of the radiation must be taken into account. We consider then the scattering process as a collision between the electron and the *photon*, and apply the conservation of energy and momentum to derive the energy of the scattered photon. It is convenient to measure energies in units of $m_e c^2$ and momenta in units of $m_e c$.

Consider an electron at rest and an incoming photon of energy x_0, which becomes x_1 after scattering. Let θ be the angle between the incoming and outgoing photon directions. This defines the scattering plane. Momentum conservation dictates that also the momentum vector of the electron, after the scattering, lies in the same plane. Conservation of energy and conservation of momentum along the x and y axis gives:

$$x_1 = \frac{x_0}{1 + x_0(1 - \cos\theta)} \tag{5.9}$$

Note that, for $x_0 \gg 1$ and $\cos\theta \neq 1$, $x_1 \to (1 - \cos\theta)^{-1}$. In this case the scattered photon carries information about the scattering angle, rather than about the initial energy. As an example, for $\theta = \pi$ and $x_0 \gg 1$, the final energy is $x_1 = 0.5$ (corresponding to 255 keV) independently of the exact value of the initial photon energy. See Fig. 5.4. Note that for $x_0 \ll 1$ the scattered energy $x_1 \simeq x_0$, as assumed in the classical Thomson scattering. The energy shift implied by Eq. 5.9 is due to the recoil of the electron originally at rest, and becomes significant only when x_0 becomes comparable with 1 (or more). When the energy of the incoming photon is comparable to the electron rest mass, another quantum effect appears, namely the energy dependence of the cross section.

5.4 The Klein–Nishina Cross Section

The Thomson cross section is the classical limit of the more general Klein–Nishina cross section (here we use x as the initial photon energy, instead of x_0, for simplic-

ity):

$$\frac{d\sigma_{\rm KN}}{d\Omega} = \frac{3}{16\pi}\sigma_{\rm T}\left(\frac{x_1}{x}\right)^2\left(\frac{x}{x_1} + \frac{x_1}{x} - \sin^2\theta\right) \tag{5.10}$$

This is a compact form, but there appears dependent quantities, as $\sin\theta$ is related to x and x_1. By inserting Eq. 5.9, we arrive to

$$\frac{d\sigma_{\rm KN}}{d\Omega} = \frac{3}{16\pi}\frac{\sigma_{\rm T}}{[1+x(1-\cos\theta)]^2}\left[x(1-\cos\theta) + \frac{1}{1+x(1-\cos\theta)} + \cos^2\theta\right] \tag{5.11}$$

In this form, only independent quantities appear (i.e. there is no x_1). Note that the cross section becomes smaller for increasing x and that it coincides with $d\sigma_{\rm T}/d\Omega$ for $\theta = 0$ (for this angle $x_1 = x$ independently of x). This however corresponds to a vanishingly small number of interactions, since $d\Omega \to 0$ for $\theta \to 0$.

Integrating Eq. 5.11 over the solid angle, we obtain the total Klein–Nishina cross section:

$$\sigma_{\rm KN} = \frac{3}{4}\sigma_{\rm T}\left\{\frac{1+x}{x^3}\left[\frac{2x(1+x)}{1+2x} - \ln(1+2x)\right] + \frac{1}{2x}\ln(1+2x) - \frac{1+3x}{(1+2x)^2}\right\} \tag{5.12}$$

Asymptotic limits are:

$$\begin{aligned} \sigma_{\rm KN} &\simeq \sigma_{\rm T}\left(1 - 2x + \frac{26x^2}{5} + \cdots\right); \quad && x \ll 1 \\ \sigma_{\rm KN} &\simeq \frac{3}{8}\frac{\sigma_{\rm T}}{x}\left[\ln(2x) + \frac{1}{2}\right]; && x \gg 1 \end{aligned} \tag{5.13}$$

Figure 5.2 shows the total Klein–Nishina cross section as a function of the energy x of the incoming photon, while Fig. 5.3 shows the behavior of the differential cross section.

The direct Compton process implies a transfer of energy from the photons to the electrons. It can then be thought as a heating mechanism. In the next subsection we discuss the opposite process, called *inverse Compton scattering*, in which hot electrons can transfer energy to low frequency photons.

We have so far neglected the momentum exchange between radiation and the electron. One can see, even classically, that there must be a net force acting along the direction of the wave if one considers the action of the magnetic field of the wave. In fact the Lorentz force $e\mathbf{v} \times \mathbf{B}$ is *always* directed along the direction of the wave (here $\mathbf{v}$ is the velocity along the $\mathbf{E}$ field). This explains the fact that light can exert a pressure, even classically.

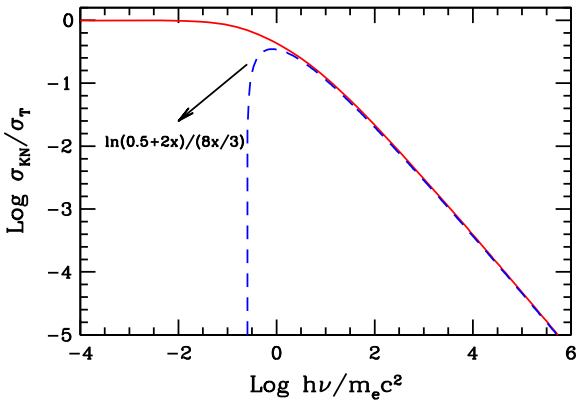


Fig. 5.2 The total Klein–Nishina cross section as a function of energy. The *dashed line* is the approximation at high energies as given in Eq. 5.13

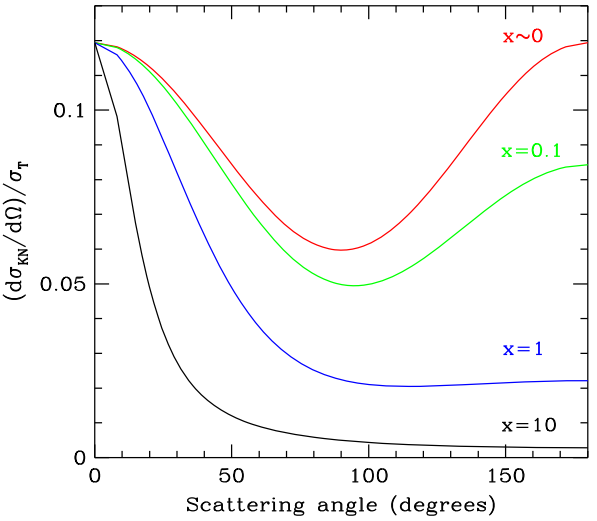


Fig. 5.3 The differential Klein–Nishina cross section (in units of σ_T), for different incoming photon energies. Note how the scattering becomes preferentially forward as the energy of the photon increases

5.4.1 Another Limit

We have mentioned that, in order for the magnetic Lorentz force to be negligible, the electron must have a transverse (perpendicular to the incoming wave direction) velocity $\ll c$. Considering a wave of frequency ω and electric field $E = E_0 \sin(\omega t)$, this implies that:

$$\frac{v_\perp}{c} = \int_0^{T/2} \frac{eE_0}{cm_e} \sin(\omega t) dt = \frac{2eE_0}{m_e c\omega} \ll 1 \tag{5.14}$$

This means that the scattering process can be described by the Thomson cross section if the wave have a sufficiently low amplitude and a not too small frequency (i.e. for very small frequencies the electric field of the wave accelerates the electron for a long time, and then to large velocities).

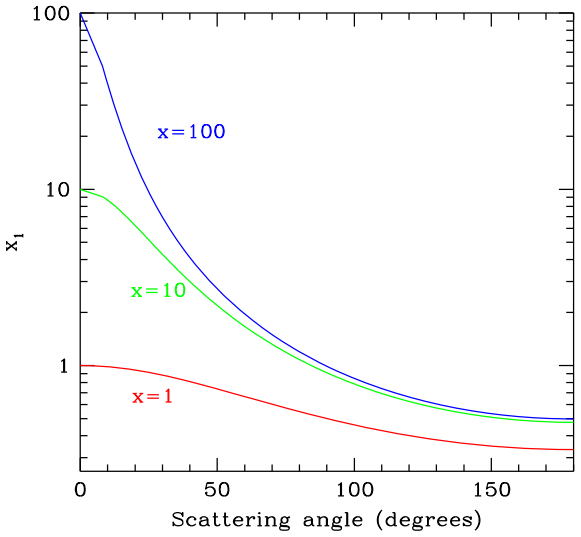


Fig. 5.4 Scattered photons energies as a function of the scattering angle, for different incoming photon energies. Note that, for $x \gg 1$ and for large scattering angle, the scattered photon energies becomes $x_1 \sim 1/2$, independent of the initial photon energy x

5.4.2 Pause

Now pause, and ask if there are some ways to apply what we have done up to now to real astrophysical objects.

- The Eddington luminosity is derived with the Thomson cross section, with the thought that it describes the smallest probability of interaction between matter and radiation. But the Klein–Nishina cross section can be even smaller, as long as the source of radiation emits at high energy. What are the consequences? If you have forgotten the definition of the Eddington luminosity, here it is:

$$L_{\rm Edd} = \frac{4\pi G M m_{\rm p} c}{\sigma_{\rm T}} = 1.3 \times 10^{38} \frac{M}{M_\odot} \ {\rm erg\,s^{-1}} \tag{5.15}$$

- In Nova Muscae, some years ago a (transient) annihilation line was detected, together with another feature (line-like) at 200 keV. What can this feature be?
- It seems that high energy radiation can suffer less scattering and therefore can propagate more freely through the universe. Is that true? Can you think to other processes that can kill high energy photons in space?
- Suppose to have an astrophysical source of radiation very powerful above say—100 MeV. Assume that at some distance there is a very efficient "reflector" (i.e. free electrons) and that you can see the scattered radiation. Can you guess the spectrum you receive? Does it contain some sort of "pile-up" or not? Will this depend upon the scattering angle?

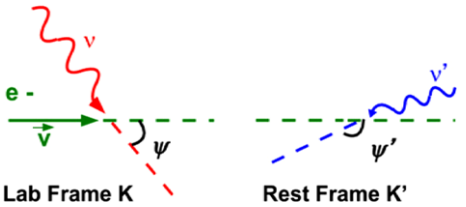


Fig. 5.5 In the lab frame an electron is moving with velocity **v**. Its velocity makes an angle ψ with an incoming photon of frequency ν. In the frame where the electron is at rest, the photon is coming from the front, with frequency ν', making an angle ψ' with the direction of the velocity

5.5 Inverse Compton Scattering

When the electron is not at rest, but has an energy greater that the typical photon energy, there can be a transfer of energy from the electron to the photon. This process is called *inverse* Compton to distinguish it from the *direct* Compton scattering, in which the electron is at rest, and it is the photon to give part of its energy to the electron.

We have two regimes, that are called the *Thomson* and the *Klein–Nishina* regimes. The difference between them is the following: we go in the frame where the electron is at rest, and in that frame we calculate the energy of the incoming photon. If the latter is smaller than $m_e c^2$ we are in the Thomson regime. In this case the recoil of the electron, even if it always exists, is small, and can be neglected. In the opposite case (photon energies larger than $m_e c^2$), we are in the Klein–Nishina one, and we cannot neglect the recoil. As we shall see, in both regimes the typical photon *gains* energy, even if there will always be some arrangements of angles for which the scattered photon looses part of its energy.

5.5.1 Thomson Regime

Perhaps, a better name should be "inverse Thomson" scattering, as will appear clear shortly.

5.5.2 Typical Frequencies

In the frame K' comoving with the electron, the incoming photon energy is

$$x' = x\gamma(1 - \beta\cos\psi) \tag{5.16}$$

where ψ is the angle between the electron velocity and the photon direction (see Fig. 5.5).

At first sight this is different from $x' = x\delta$ derived in Chap. 3. But notice that (i) in this case the angle ψ is measured in the lab frame; (ii) it is not the same angle

going into the definition of δ (i.e. in δ we use the angle between the line of sight and the velocity of the emitter, i.e. $\theta' = \pi - \psi'$). Going to the rest frame of the electrons we should use (recalling Eq. 3.16 for the transformation of angles):

$$\cos\psi = \frac{\beta + \cos\psi'}{1 + \beta\cos\psi'} \tag{5.17}$$

Substituting this into Eq. 5.16 we have

$$x' = \frac{x}{\gamma(1 + \beta\cos\psi')} \tag{5.18}$$

Finally, consider that $\cos\theta' = \cos(\pi - \psi') = -\cos\psi'$, validating $x' = x\delta$.

If $x' \ll 1$, we are in the Thomson regime. In the rest frame of the electron the scattered photon will have the same energy x'_1 as before the scattering, independent of the scattering angle. Then

$$x'_1 = x' \tag{5.19}$$

This photon will be scattered at an angle ψ'_1 with respect to the electron velocity. The pattern of the scattered radiation will follow the pattern of the cross section (i.e. a peanut). *Think to the scattering in the comoving frame as a re-isotropization process: even if the incoming photons are all coming from the same direction, after the scattering they are distributed quasi-isotropically*. Going back to K the observer sees

$$x_1 = x'_1\gamma\left(1 + \beta\cos\psi'_1\right) \tag{5.20}$$

Recalling again Eq. 3.16, for the transformation of angles:

$$\cos\psi'_1 = \frac{\cos\psi_1 - \beta}{1 - \beta\cos\psi_1} \tag{5.21}$$

we arrive to the final formula:

$$x_1 = x\frac{1 - \beta\cos\psi}{1 - \beta\cos\psi_1} \tag{5.22}$$

Now all quantities are calculated in the lab-frame.

Let us see the minimum and maximum energies. See Fig. 5.6. The maximum is when $\psi = \pi$ (head on collision), and when $\psi_1 = 0$ (the photon is scattered along the electron velocity vector). In these head-on collisions:

$$x_1 = x\frac{1 + \beta}{1 - \beta} = \gamma^2(1 + \beta)^2 x \to 4\gamma^2 x; \quad \text{head-on} \tag{5.23}$$

where the last step is valid if $\gamma \gg 1$. The other extreme is for $\psi_1 = \pi$ and $\psi = 0$. In this case the incoming photon "comes from behind" and bounces back. In these "tail-on" collisions:

$$x_1 = x\frac{1 - \beta}{1 + \beta} = \frac{x}{\gamma^2(1 + \beta)^2} \to \frac{x}{4\gamma^2}; \quad \text{tail-on} \tag{5.24}$$

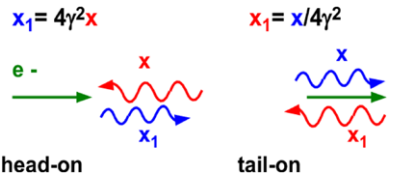


Fig. 5.6 Maximum and minimum scattered frequencies. The maximum occurs for head-on collisions, the minimum for tail-on ones. These two frequencies are one the inverse of the other

where again the last step is valid if $\gamma \gg 1$. Another typical angle is $\sin\psi_1 = 1/\gamma$, corresponding to $\cos\psi_1 = \beta$. This corresponds to the aperture angle of the beaming cone. For this angle:

$$x_1 = \frac{1-\beta\cos\psi}{1-\beta^2}x = \gamma^2(1-\beta\cos\psi)x; \quad \text{beaming cone} \tag{5.25}$$

which becomes $x_1 = x/(1+\beta)$ for $\psi = 0$, $x_1 = \gamma^2 x$ for $\psi = \pi/2$ and $x_1 = \gamma^2(1+\beta)x$ for $\psi = \pi$.

For an isotropic distribution of incident photons and for $\gamma \gg 1$ the average photon energy after scattering is (see Eq. 5.47):

$$\langle x_1\rangle = \frac{4}{3}\gamma^2 x \tag{5.26}$$

Total Loss Rate

We can simply calculate the rate of scatterings per electron considering all quantities in the lab-frame. Let $n(\epsilon)$ be the density of photons of energy $\epsilon = h\nu$, v the electron velocity and ψ the angle between the electron velocity and the incoming photon. For mono-directional photon distributions, we have:

$$\frac{dN}{dt} = \int \sigma_{\rm T} v_{\rm rel} n(\epsilon) d\epsilon \tag{5.27}$$

$v_{\rm rel} = c - v\cos\psi$ is the relative velocity between the electron and the incoming photons. We then have

$$\frac{dN}{dt} = \int \sigma_{\rm T} c(1-\beta\cos\psi) n(\epsilon) d\epsilon \tag{5.28}$$

Note that the rate of scatterings in the lab frame, when the electron and/or photon are anisotropically distributed, can be described by an effective cross section $\sigma_{\rm eff} \equiv \int \sigma_{\rm T}(1-\beta\cos\psi)d\Omega/4\pi$. For photons and electrons moving in the same direction the scattering rate (hence, the effective optical depth) can be greatly reduced.

The power contained in the scattered radiation is then

$$\frac{dE_\gamma}{dt} = \frac{\epsilon_1 dN}{dt} = \sigma_T c \int \frac{(1-\beta\cos\psi)^2}{1-\beta\cos\psi_1}\epsilon n(\epsilon)d\epsilon \tag{5.29}$$

Independently of the incoming photon angular distribution, the average value of $1-\beta\cos\psi_1$ can be calculated recalling that, in the rest frame of the electron, the scattering has a backward–forward symmetry, and therefore $\langle\cos\psi_1'\rangle = \pi/2$. The average value of $\cos\psi_1$ is then β, leading to $\langle 1-\beta\cos\psi_1\rangle = 1/\gamma^2$. We therefore obtain

$$\frac{dE_\gamma}{dt} = \sigma_T c\gamma^2 \int (1-\beta\cos\psi)^2 \epsilon n(\epsilon)d\epsilon \tag{5.30}$$

If the incoming photons are isotropically distributed, we can average out $(1-\beta\cos\psi)^2$ over the solid angle, obtaining $1+\beta^2/3$. The power produced is then

$$\frac{dE_\gamma}{dt} = \sigma_T c\gamma^2 \left(1+\frac{\beta^2}{3}\right) U_r \tag{5.31}$$

where

$$U_r = \int \epsilon n(\epsilon)d\epsilon \tag{5.32}$$

is the energy density of the radiation before scattering. Equation 5.31 gives the power contained in the scattered radiation. To calculate the energy loss rate of the electron, we have to subtract the initial power of the radiation eventually scattered

$$P_c(\gamma) \equiv \frac{dE_e}{dt} = \frac{dE_\gamma}{dt} - \sigma_T c U_r = \frac{4}{3}\sigma_T c\gamma^2\beta^2 U_r \tag{5.33}$$

A simple way to remember Eq. 5.33 is:

$$\begin{aligned} P_c(\gamma) &= \left(\frac{\#\text{ of collisions}}{\text{sec}}\right)(\text{average phot. energy after scatt.}) \\ &= \left(\sigma_T c \frac{U_r}{\langle h\nu\rangle}\right)\left(\frac{4}{3}\langle h\nu\rangle\gamma^2\right) \end{aligned} \tag{5.34}$$

Note the similarity with the synchrotron energy loss. The two energy loss rates are identical, once the radiation energy density is replaced by the magnetic energy density U_B. Therefore, if relativistic electrons are in a region with some radiation and magnetic energy densities, they will emit by both the synchrotron and the Inverse Compton scattering processes. The ratio of the two luminosities will be

$$\frac{L_{syn}}{L_{IC}} = \frac{P_{syn}}{P_c} = \frac{U_B}{U_r} \tag{5.35}$$

where we have set $dE_{IC}/dt = dE_e/dt$. This is true unless one of the two processes is inhibited for some reason. For instance:

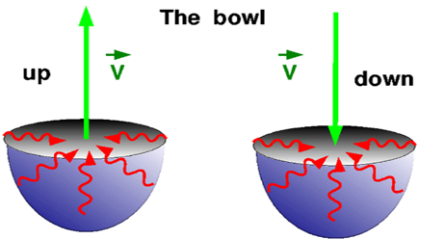


Fig. 5.7 In the center of a semi-sphere (the "bowl") we have relativistic electrons going down and going up, all with the same γ. Since the seed photon distribution is anisotropic, so is the scattered radiation and power. The losses of the electron going down are 7 times larger than those of the electron going up (if $\gamma \gg 1$). Since almost all the radiation is produced along the velocity vector of the electrons, also the downward radiation is 7 times more powerful than the upward radiation

- At (relatively) low energies, electrons could emit *and absorb* synchrotron radiation, so the synchrotron cooling is compensated by the heating due to the absorption process.
- At high energies, electrons could scatter in the Klein–Nishina regime: in this case, since the cross section is smaller, they will do less scatterings, and cool less.

But let us go back to Eq. 5.30, that is the starting point when dealing with *anisotropic* seed photon distributions. Think for instance to an accretion disk as the producer of the seed photons for scattering, and some cloud of relativistic electrons above the disk. If the cloud is not that distant, and it is small with respect to the disk size, then this case is completely equal to the case of having a little cloud of relativistic electrons located at the center of a semi-sphere. That is, we have the "bowl" case illustrated in Fig. 5.7. Just for fun, let us calculate the total power emitted by an electron going "up" and by its brother (i.e. it has the same γ) going down. Using Eq. 5.30 we have:

$$\frac{P_{\rm down}}{P_{\rm up}} = \frac{\int_{-1}^{0}(1-\beta\mu)^2 d\mu}{\int_{0}^{1}(1-\beta\mu)^2 d\mu} = \frac{1+\beta+\beta^2/3}{1-\beta+\beta^2/3} \rightarrow 7 \tag{5.36}$$

where $\mu \equiv \cos\psi$ and the last step assumes $\beta \rightarrow 1$. Since almost all the radiation is produced along the velocity vector of the electrons, also the downward radiation is more powerful than the upward radiation (i.e. 7 times more powerful for $\gamma \gg 1$). What happens if the cloud of electrons is located at some height above the bowl? Will the $P_{\rm down}/P_{\rm up}$ be more or less?

5.5.3 Cooling Time and Compactness

The cooling time due to the inverse Compton process is

$$t_{\rm IC} = \frac{E}{dE_e/dt} = \frac{3\gamma m_e c^2}{4\sigma_{\rm T} c \gamma^2 \beta^2 U_{\rm r}} \sim \frac{3 m_e c^2}{4\sigma_{\rm T} c \gamma U_{\rm r}}; \quad \gamma\epsilon \ll m_{\rm e}c^2 \tag{5.37}$$

This equation offers the opportunity to introduce an important quantity, namely *the compactness* of an astrophysical source, that is essentially the luminosity L over the size R ratio. Consider in fact how U_r and L are related:

$$U_\mathrm{r} = \frac{L}{4\pi R^2 c} \tag{5.38}$$

Although this relation is almost universally used, there are subtleties. It is surely valid if we measured U_r *outside* the source, at a distance R from its center. In this case $4\pi R^2 c$ is simply the volume of the shell crossed by the source radiation in one second. But if we are *inside* a homogeneous, spherical transparent source, a better way to calculate U_r is to think to the average time needed to the typical photon to exit the source. This is $t_\mathrm{esc} = 3R/(4c)$. It is less than R/c because the typical photon is not born at the center (there is more volume close to the surface). If $V = (4\pi/3)R^3$ is the volume, we can write:

$$U_\mathrm{r} = \frac{L}{V} t_\mathrm{esc} = \frac{3L}{4\pi R^3} \frac{3R}{4c} = \frac{9L}{16\pi R^2 c} \tag{5.39}$$

This is greater than Eq. 5.38 by a factor $9/4$. Anyway, let us be conventional and insert Eq. 5.38 in Eq. 5.37:

$$t_\mathrm{IC} = \frac{3\pi m_e c^2 R^2}{\sigma_\mathrm{T} \gamma L} \rightarrow \frac{t_\mathrm{IC}}{R/c} = \frac{3\pi}{\gamma} \frac{m_e c^3 R}{\sigma_\mathrm{T} L} \equiv \frac{3\pi}{\gamma} \frac{1}{\ell} \tag{5.40}$$

where the dimensionless compactness ℓ is defined as

$$\ell = \frac{\sigma_\mathrm{T} L}{m_\mathrm{e} c^3 R} \tag{5.41}$$

For ℓ close or larger than unity, we have that even low energy electrons cool by the Inverse Compton process in less than a light crossing time R/c.

There is another reason why ℓ is important, related to the fact that it directly measures the optical depth (hence the probability to occur) of the photon–photon collisions that lead to the creation of electron–positron pairs. The compactness is one of the most important physical parameters when studying high energy compact sources (X-ray binaries, AGNs and Gamma Ray Bursts).

5.5.4 Single Particle Spectrum

As we did for the synchrotron spectrum, we will not repeat the exact derivation of the single particle spectrum, but we try to explain why the typical frequency of the scattered photon is a factor γ^2 larger than the frequency of the incoming photon. Here are the steps to consider:

1. Assume that the relativistic electron travels in a region where there is a radiation energy density $U_{\rm r}$ made by photons which we will take, for simplicity, monochromatic, therefore all having a dimensionless frequency $x = h\nu/m_{\rm e}c^2$.
2. In the frame where the electron is at rest, half of the photons appear to come from the front, within an angle $1/\gamma$.
3. The typical frequency of these photons is $x' \sim \gamma x$ (it is twice that for photons coming exactly head on).
4. Assuming that we are in the Thomson regime means that (i) $x' < 1$; (ii) the cross section is the Thomson one; (iii) the frequency of the scattered photon is the same of the incoming one, i.e. $x'_1 = x' \sim \gamma x$, and (iv) the pattern of the scattered photons follows the angular dependence of the cross section, therefore the "peanut".
5. Independently of the initial photon direction, and therefore independently of the frequencies seen by the electrons, all photons after scatterings are isotropized. This means that all observers (at any angle ψ'_1) in this frame see the same spectrum, and the same typical frequency. Half of the photons are in the semi-sphere with $\psi'_1 \leq \pi/2$.
6. Now we go back to the lab-frame. Those photons that had $\psi'_1 \leq \pi/2$ now have $\psi_1 \leq 1/\gamma$. Their typical frequency if another factor γ greater than what they had in the rest frame, therefore

$$x_1 \sim \gamma^2 x \tag{5.42}$$

This is the typical Inverse Compton frequency.

The exact derivation can be found e.g. in [3] and [1]. We report here the final result, valid for a monochromatic and isotropic seed photons distribution, characterized by a specific intensity

$$\frac{I(x)}{x} = \frac{I_0}{x}\delta(x - x_0) \tag{5.43}$$

Note that $I(x)/x$ is the analog of the normal intensity, but it is associated with the number of photons. If we have n electrons per cubic centimeter we have:

$$\epsilon_{\rm IC}(x_1) = \frac{\sigma_{\rm T} n I_0 (1+\beta)}{4\gamma^2\beta^2 x_0} F_{\rm IC}(x_1) \tag{5.44}$$

The function $F_{\rm IC}$ contains all the frequency dependence:

$$\begin{aligned} F_{\rm IC}(x_1) &= \frac{x_1}{x_0}\left[\frac{x_1}{x_0} - \frac{1}{(1+\beta)^2\gamma^2}\right]; \quad \frac{1}{(1+\beta)^2\gamma^2} < \frac{x_1}{x_0} < 1 \\ F_{\rm IC}(x_1) &= \frac{x_1}{x_0}\left[1 - \frac{x_1}{x_0}\frac{1}{(1+\beta)^2\gamma^2}\right]; \quad 1 < \frac{x_1}{x_0} < (1+\beta)^2\gamma^2 \end{aligned} \tag{5.45}$$

The first line corresponds to *downscattering*: the scattered photon has *less* energy than the incoming one. Note that in this case $F_{\rm IC}(x_1) \propto x_1^2$. The second line corresponds to *upscattering*: in this case $F_{\rm IC}(x_1) \propto x_1$ except for frequencies close to the

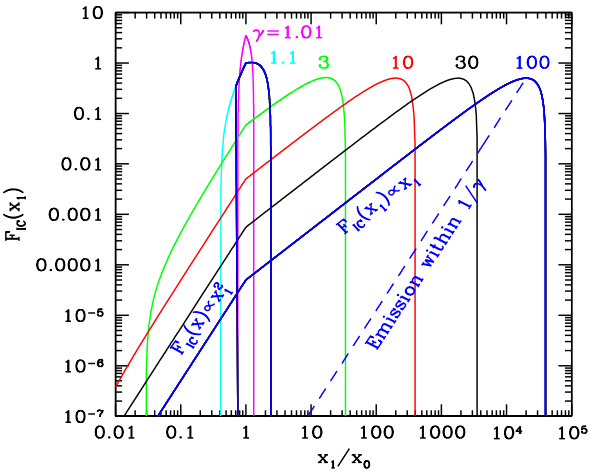


Fig. 5.8 Spectrum emitted by the Inverse Compton process by electrons of different γ (as labeled) scattering an isotropic monochromatic radiation field of dimensionless frequency x_0. The *dashed line* corresponds to the spectrum emitted within the $1/\gamma$ beaming cone: it always contains the 75 % of the total power, for any γ. For $x_1 < x_0$ we have *downscattering*, i.e. the photons loose energy in the process. Note also the power law segments arising when $\gamma \gg 1$: $F_{\rm IC}(x_1) \propto x_1^2$ for the downscattering tail, and $F_{IC}(x_1) \propto x_1$ for the upscattering segment

maximum ones. The function $F_{\rm IC}(x_1)$ is shown in Fig. 5.8 for different values of γ. The figure shows also the spectrum of the photons contained in the beaming cone $1/\gamma$: the corresponding power is always 75 % of the total.

The average frequency of $F_{\rm IC}(x_1)$ is

$$\langle x_1 \rangle = 2\gamma^2 x_0; \quad \text{energy spectrum} \tag{5.46}$$

This is the average frequency *of the energy spectrum*. We sometimes want to know the average energy *of the photons*, i.e. we have to calculate the average frequency of *the photon spectrum* $F_{\rm IC}(x_1)/x_1$. This is:

$$\langle x_1 \rangle = \frac{4}{3}\gamma^2 x_0; \quad \text{photon spectrum} \tag{5.47}$$

5.6 Emission from Many Electrons

We have seen that the emission spectrum from a single particle is peaked, and the typical frequency is boosted by a factor γ^2. This is equal to the synchrotron case. Therefore we can derive the Inverse Compton emissivity as we did for the synchrotron one. Again, assume a power-law energy distribution for the relativistic electrons:

$$N(\gamma) = K\gamma^{-p} = N(E)\frac{dE}{d\gamma}; \quad \gamma_{\rm min} < \gamma < \gamma_{\rm max} \tag{5.48}$$

and assume that it describes an isotropic distribution of electrons. For simplicity, let us assume that the seed photons are isotropic and monochromatic, with frequency ν_0 (we now pass to real frequencies, since we are getting closer to the real world...). Since there is a strong link between the scattered frequency ν_c and the electron energy that produced it, we can set:

$$\nu_c = \frac{4}{3}\gamma^2\nu_0 \rightarrow \gamma = \left(\frac{3\nu_c}{4\nu_0}\right)^{1/2} \rightarrow \left|\frac{d\gamma}{d\nu}\right| = \frac{\nu_c^{-1/2}}{2}\left(\frac{3}{4\nu_o}\right)^{1/2} \tag{5.49}$$

Now, repeating the argument we used for synchrotron emission, we can state that the power lost by the electron of energy $\gamma m_e c^2$ within $m_e c^2 d\gamma$ goes into the radiation of frequency ν within $d\nu$. Since we will derive an emissivity (i.e. erg cm^{-3} s^{-1} sterad^{-1} Hz^{-1}) we must remember the 4π term (if the emission is isotropic). We can set:

$$\epsilon_c(\nu_c)d\nu_c = \frac{1}{4\pi}P_c(\gamma)N(\gamma)d\gamma \tag{5.50}$$

This leads to:

$$\epsilon_c(\nu_c) = \frac{1}{4\pi}\frac{(4/3)^\alpha}{2}\sigma_T c K \frac{U_r}{\nu_0}\left(\frac{\nu_c}{\nu_0}\right)^{-\alpha} \tag{5.51}$$

Again, a power law, as in the case of synchrotron emission by a power law energy distribution. Again the same link between α and p:

$$\alpha = \frac{p-1}{2} \tag{5.52}$$

Of course, this is not a coincidence: it is because both the Inverse Compton and the synchrotron single electron spectra are peaked at a typical frequency that is a factor γ^2 greater than the starting one.

Equation 5.51 becomes a little more clear if

- we express $\epsilon_c(\nu_c)$ as a function of the photon energy $h\nu_c$. Therefore $\epsilon_c(h\nu_c) = \epsilon_c(\nu_c)/h$;
- we multiply and divide by the source radius R;
- we consider a proxy for the scattering optical depth of the relativistic electrons setting $\tau_c \equiv \sigma_T K R$.

Then we obtain:

$$\epsilon_c(h\nu_c) = \frac{1}{4\pi}\frac{(4/3)^\alpha}{2}\frac{\tau_c}{R/c}\frac{U_r}{h\nu_0}\left(\frac{\nu_c}{\nu_0}\right)^{-\alpha} \tag{5.53}$$

In this way: τ_c (for $\tau_c < 1$) is the fraction of the seed photons $U_r/h\nu_0$ undergoing scattering in a time R/c, and $\nu_c/\nu_0 \sim \gamma^2$ is the average gain in energy of the scattered photons.

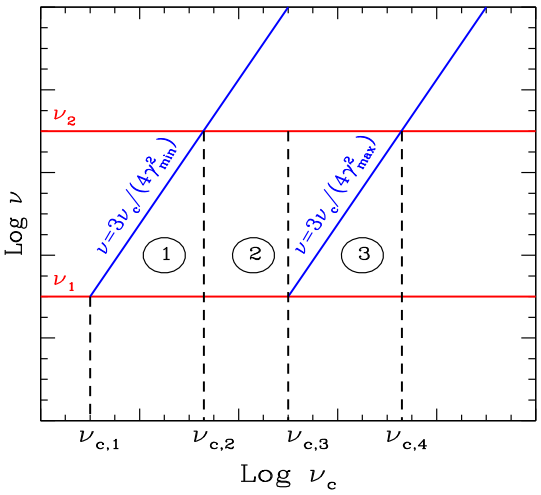


Fig. 5.9 The ν–ν_c plane. The *two diagonal lines* delimit the regions of the seed photons that can be used to give a given frequency ν_c

5.6.1 Non-monochromatic Seed Photons

It is time to consider the more realistic case in which the seed photons are not monochromatic, but are distributed in frequency. This means that we have to integrate Eq. 5.51 over the incoming photon frequencies. For clarity, let us drop the subscript 0 in ν_0. We have

$$\epsilon_c(\nu_c) = \frac{1}{4\pi}\frac{(4/3)^\alpha}{2}\frac{\tau_c}{R/c}\nu_c^{-\alpha}\int_{\nu_{min}}^{\nu_{max}}\frac{U_r(\nu)}{\nu}\nu^\alpha d\nu \tag{5.54}$$

where $U_r(\nu)$ [erg cm^{-3} Hz^{-1}] is the specific radiation energy density at the frequency ν. The only difficulty of this integral is to find the correct limit of the integration, that, in general, *depend on* ν_c. Note also another interesting thing. We have just derived that if the same electron population produces Inverse Compton and synchrotron emission, than the slopes of the two spectra are the same. Therefore, when $U_r(\nu)$ is made by synchrotron photons, then $U_r(\nu) \propto \nu^{-\alpha}$. The result of the integral, in this case, will be $\ln(\nu_{max}/\nu_{min})$.

Figure 5.9 helps to understand what are the right ν_{max} and ν_{min} to use. On the y-axis we have the frequencies of the seed photon distribution, which extend between ν_1 and ν_2. On the x-axis we have the scattered frequencies, which extend between $\nu_{c,1} = (4/3)\gamma^2_{min}\nu_1$ and $\nu_{c,4} = (4/3)\gamma^2_{max}\nu_1$. The diagonal lines are the functions

$$\nu = \frac{3\nu_c}{4\gamma^2_{min}}; \qquad \nu = \frac{3\nu_c}{4\gamma^2_{max}} \tag{5.55}$$

that tell us what are the appropriate ν that can give ν_c once we change γ.

There are three zones:

1. In zone (1), between $\nu_{c,1}$ and $\nu_{c,2} = (4/3)\gamma_{min}^2 \nu_2$ the appropriate limits of integration are:

$$\nu_{min} = \nu_1; \qquad \nu_{max} = \frac{3\nu_c}{4\gamma_{min}^2} \tag{5.56}$$

2. In zone (2), between $\nu_{c,2}$ and $\nu_{c,3} = (4/3)\gamma_{max}^2 \nu_1$ the limits are:

$$\nu_{min} = \nu_1; \qquad \nu_{max} = \nu_2 \tag{5.57}$$

3. In zone (3), between $\nu_{c,3}$ and $\nu_{c,4} = (4/3)\gamma_{max}^2 \nu_2$ the limits are:

$$\nu_{min} = \frac{3\nu_c}{4\gamma_{max}^2}; \qquad \nu_{max} = \nu_2 \tag{5.58}$$

We see that only in zone (2) the limits of integration coincide with the extension in frequency of the seed photon distribution, and are therefore constant. Therefore $\epsilon_c(\nu_c)$ will be a power law of slope α only in the corresponding frequency limits. Note also that for a broad range in $[\nu_1; \nu_2]$ or a narrow range in $[\gamma_{min}; \gamma_{max}]$ we do not have a power law, since there is no ν_c for which the limits of integrations are both constants.

5.7 Thermal Comptonization

With this term we mean the process of *multiple* scattering of a photon due to a *thermal* or *quasi-thermal* distribution of electrons. By *quasi-thermal* we mean a particle distribution that is peaked, even if it is not a perfect Maxwellian. Since the resulting spectrum, by definition, is due to the superposition of many spectra, each corresponding to a single scattering, the details of the particle distribution will be lost in the final spectrum, as long as the distribution is peaked. The "bible" for an extensive discussion about this process is [2].

There is one fundamental parameter measuring the importance of the Inverse Compton process in general, and of multiple scatterings in particular: *the Comptonization parameter*, usually denoted with the letter y. Its definition is:

$$y = [\text{average \# of scatt.}] \times [\text{average fractional energy gain for scatt.}] \tag{5.59}$$

If $y > 1$ the Comptonization process is important, because the Comptonized spectrum has more energy than the spectrum of the seed photons.

5.7.1 Average Number of Scatterings

This can be calculated thinking that the photon, before leaving the source, experience a sort of random walk inside the source. Let us call

$$\tau_{\mathrm{T}} = \sigma_{\mathrm{T}} n R \tag{5.60}$$

the Thomson scattering optical depth, where n is the electron density and R the size of the source. When $\tau_{\mathrm{T}} < 1$ most of the photons leave the source directly, without any scattering. When $\tau_{\mathrm{T}} > 1$ then the mean free path is $d = R/\tau_{\mathrm{T}}$ and the photon will experience, on average, τ_{T}^2 scatterings before leaving the source. Therefore the total path traveled by the photon, from the time of its birth to the time it leaves the source is:

$$c\Delta t = \tau_{\mathrm{T}}^2 \frac{R}{\tau_{\mathrm{T}}} = \tau_{\mathrm{T}} R \tag{5.61}$$

and Δt is the corresponding elapsed time.

5.7.2 Average Gain per Scattering

Relativistic Case

If the scattering electrons are relativistic, we have already seen that the photon energy is amplified by the factor $(4/3)\gamma^2$ (on average). Therefore the problem is to find what is $\langle \gamma^2 \rangle$ in the case of a relativistic Maxwellian, that has the form

$$N(\gamma) \propto \gamma^2 e^{-\gamma/\Theta}; \quad \Theta \equiv \frac{kT}{m_{\mathrm{e}} c^2} \tag{5.62}$$

Setting $x_0 = h\nu_0/(m_{\mathrm{e}}c^2)$ we have that the average energy of the photon of initial frequency x_0 after a single scattering with electrons belonging to this Maxwellian is:

$$\begin{aligned} \langle x_1 \rangle &= \frac{4}{3}\langle \gamma^2 \rangle x_0 = \frac{4}{3} x_0 \frac{\int_1^\infty \gamma^2 \gamma^2 e^{-\gamma/\Theta} d\gamma}{\int_1^\infty \gamma^2 e^{-\gamma/\Theta} d\gamma} \\ &= \frac{4}{3} x_0 \Theta^2 \frac{\Gamma(5)}{\Gamma(3)} \\ &= \frac{4}{3} x_0 \Theta^2 \frac{4!}{2!} = 16\Theta^2 x_0 \end{aligned} \tag{5.63}$$

Non-relativistic Case

In this case the average gain is proportional to the electron energy, not to its square. The derivation is not immediate, but we must use a trick. Also, we have to account

that in any Maxwellian, but especially when the temperature is not large, there will be electrons that have *less* energy than the incoming photons. In this case it is the photon that gives energy to the electron: correspondingly, the scattered photon will have less energy than the incoming one. Averaging out over a Maxwellian distribution, we will have:

$$\frac{\Delta x}{x} = \frac{x_1 - x_0}{x_0} = \alpha\Theta - x \tag{5.64}$$

Where $\alpha\Theta$ is what the photon gains and the $-x$ term corresponds to the downscattering of the photon (i.e. direct Compton). We do not know yet the value for the constant α. To determine it we use the following argument. We know (from general and robust arguments) what happens when photons and electrons are in equilibrium under the only process of scattering, and neglecting absorption (i.e. when the *number of photon is conserved*). What happens is that the photons follow the so-called *Wien distribution* given by:

$$F_{\mathrm{W}}(x) \propto x^3 e^{-x/\Theta} \rightarrow N_{\mathrm{W}}(x) = \frac{F_{\mathrm{W}}(x)}{x} \propto x^2 e^{-x/\Theta} \tag{5.65}$$

where F correspond to the radiation spectrum, N to the photon spectrum, and Θ is the dimensionless electron temperature. When a Wien distribution is established we must have $\langle \Delta x \rangle = 0$, since we are at equilibrium, So we require that, on average, gains equal losses:

$$\langle \Delta x \rangle = 0 \rightarrow \alpha\Theta\langle x \rangle - \langle x^2 \rangle = 0 \tag{5.66}$$

Calculating $\langle x \rangle$ and $\langle x^2 \rangle$ for a photon Wien distribution, we have:

$$\begin{aligned} \langle x \rangle &= \frac{\int_0^\infty x^3 e^{-x/\Theta} dx}{\int_0^\infty x^2 e^{-x/\Theta} dx} = \frac{\Gamma(4)}{\Gamma(3)}\Theta = \frac{3!}{2!}\Theta = 3\Theta \\ \langle x^2 \rangle &= \frac{\int_0^\infty x^4 e^{-x/\Theta} dx}{\int_0^\infty x^2 e^{-x/\Theta} dx} = \frac{\Gamma(5)}{\Gamma(3)}\Theta^2 = \frac{4!}{2!}\Theta^2 = 12\Theta^2 \end{aligned} \tag{5.67}$$

This implies that $\alpha = 4$ not only at equilibrium, but always, and we finally have

$$\frac{\Delta x}{x} = 4\Theta - x \tag{5.68}$$

Combining the relativistic and the non-relativistic cases, we have an expression valid for all temperatures:

$$\frac{\Delta x}{x} = 16\Theta^2 + 4\Theta - x \tag{5.69}$$

going back to the y parameter we can write:

$$y = \max\left(\tau_{\mathrm{T}}, \tau_{\mathrm{T}}^2\right) \times \left[16\Theta^2 + 4\Theta - x\right] \tag{5.70}$$

Going to the differential form, and neglecting downscattering, we have

$$\frac{dx}{x} = \left[16\Theta^2 + 4\Theta\right] dK \rightarrow x_\mathrm{f} = x_0 e^{(16\Theta^2+4\Theta)K} \rightarrow x_\mathrm{f} = x_0 e^y \tag{5.71}$$

where now K is the number of scatterings. If we subtract the initial photon energy, and consider that the above equation is valid for all the x_0 of the initial seed photon distribution, of luminosity L_0, we have

$$\frac{L_\mathrm{f} - L_0}{L_0} = e^y - 1 \tag{5.72}$$

Then the importance of y is self evident, and also the fact that it marks the importance of the Comptonization process when it is larger than 1.

5.7.3 Comptonization Spectra: Basics

We will illustrate why even a thermal (Maxwellian) distribution of electrons can produce a power law spectrum. The basic reason is that the total produced spectrum is the superposition of many orders of Compton scattering spectra: when they are not too much separated in frequency (i.e. for not too large temperatures) the sum is a smooth power law. We can distinguish 4 regimes, according to the values of τ_T and y. As usual, we set $x \equiv h\nu/(m_\mathrm{e}c^2)$ and $\Theta \equiv kT/(m_\mathrm{e}c^2)$.

The Case $\tau_\mathrm{T} < 1$

Neglect downscattering for simplicity. The fractional energy gain is $\Delta x/x = 16\Theta^2 + 4\Theta$, so the amplification A of the photon frequency at each scattering is

$$A \equiv \frac{x_1}{x} = 16\Theta^2 + 4\Theta + 1 \sim \frac{y}{\tau_\mathrm{T}} \tag{5.73}$$

We can then construct Table 5.1.

A look to Fig. 5.10 should convince you that the sum of all the scattering orders gives a power law, and should also make clear how to find the spectral slope. Remember that we are in a log–log plot, so the spectral index is simply $\Delta y/\Delta x$. We can find it considering two successive scattering orders: the typical (logarithm of) frequency is enhanced by $\log A$, and the fraction of photons doing the scattering is $-\log \tau_\mathrm{T}$. Remember also that we use $F(x) \propto x^{-\alpha}$ as the definition of energy spectral index.

Therefore

$$\alpha = -\frac{\log \tau_\mathrm{T}}{\log A} \sim -\frac{\log \tau_\mathrm{T}}{\log y - \log \tau_\mathrm{T}} \tag{5.74}$$

Table 5.1 When $\tau_T < 1$, a fraction $e^{-\tau_T}$ of the seed photons escape without doing any scattering, and a fraction $1 - e^{-\tau_T} \to \tau$ undergoes at least one scattering. We can then repeat these fractions for all scattering orders. Even if a tiny fraction of photons does several scatterings, they can carry a lot of energy

# scatt.	Fraction of escaping photons	$\langle x \rangle$
0	$e^{-\tau_T} \to 1 - \tau_T$	x_0
1	$\sim\tau_T$	$x_0 A$
2	$\sim\tau_T^2$	$x_0 A^2$
3	$\sim\tau_T^3$	$x_0 A^3$
4	$\sim\tau_T^4$	$x_0 A^4$
⋮	⋮	⋮
n	$\sim\tau_T^n$	$x_0 A^n$

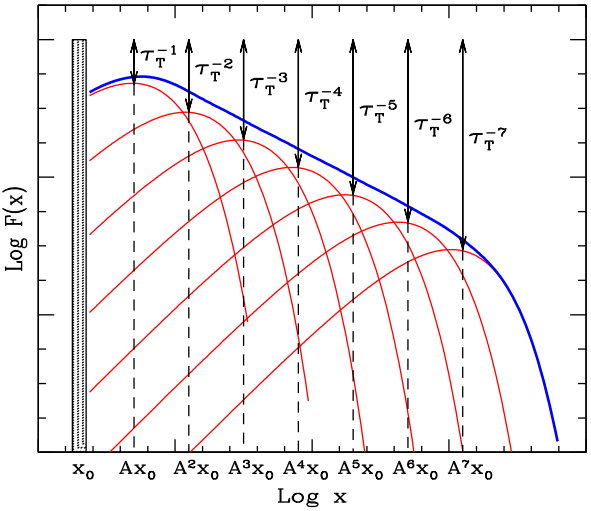


Fig. 5.10 Multiple Compton scatterings when $\tau_T < 1$. A fraction τ_T of the photons of the previous scattering order undergoes another scattering, and amplifying the frequency by the gain factor A, until the typical photon frequency equals the electron temperature Θ. Then further scatterings leave the photon frequency unchanged

When $y \sim 1$, its logarithm is close to zero, and we have $\alpha \sim 1$. When $y > 1$, then $\alpha < 1$ (i.e. *flat, or hard*), and vice-versa, when $y < 1$, then its logarithm will be negative, as the logarithm of τ_T, and $\alpha > 1$ (i.e. *steep, or soft*).

Attention! when $\tau_T \ll 1$ and A is large (i.e. big frequency jumps between one scattering and the next), then the superposition of all scattering orders (by the way, there are fewer, in this case) will not guarantee a perfect power-law. In the total spectrum we can see the "bumps" corresponding to individual scattering orders.

The Case $\tau_T \gtrsim 1$

This is the most difficult case, as we should solve a famous equation, the equation of Kompaneet. The result is still a power law, whose spectral index is approximately

given by

$$\alpha = -\frac{3}{2} + \sqrt{\frac{9}{4} + \frac{4}{y}} \tag{5.75}$$

The Case $\tau_{\mathrm{T}} \gg 1$: Saturation

In this case the interaction between photons and matters is so intense that they go to equilibrium, and they will have the same temperature. But instead of a black-body, the resulting photon spectrum has a Wien shape. This is because the photons are conserved (if other scattering processes such as induced Compton or two-photon scattering are important, then one recovers a black-body, because these processes *do not* conserve photons). The Wien spectrum has the slope:

$$I(x) \propto x^3 e^{-x/\Theta} \tag{5.76}$$

At low frequencies this is *harder* than a black-body.

The Case $\tau_{\mathrm{T}} > 1$, $y > 1$: Quasi-saturation

Suppose that in a source characterized by a large τ_{T} the source of soft photons is spread throughout the source. In this case the photons produced close to the surface, in a skin of optical depth $\tau_{\mathrm{T}} = 1$, leave the source without doing any scattering (note that having the source of seed photons concentrated at the center is a different case). The remaining fraction, $1 - 1/\tau_{\mathrm{T}}$, i.e. *almost* all photons, remains inside. This can be said for each scattering order. This is illustrated in Fig. 5.11, where τ_{T} corresponds to the ratio between the flux of photon inside the source at a given frequency and the flux of photons that escape. If I start with 100 photons, only 1—say—escape, and the other 99 remain inside, and do the first scattering. After it, only one escape, and the other 98 remain inside, and so on, until the typical photon and electron energies are equal, and the photon therefore stays around with the same final frequency until it is its turn to escape. This "accumulation" of photons at $x \sim 3\Theta$ gives the Wien bump. Note that since at any scattering order only a fixed number of photons escape, always the same, then the spectrum in this region will always have $\alpha = 0$. This is a "saturated" index, i.e. one obtains always zero even when changing τ_{T} or Θ. What indeed changes, by increasing τ_{T}, is that (i) the flux characterized by x^0 decreases, (ii) the Wien peak will start to dominate earlier (at lower frequencies), while nothing happens to the flux of the Wien peak (it stays there). Increasing still τ_{T} we fall in the previous case (equilibrium, meaning only the Wien spectrum without the x^0 part).

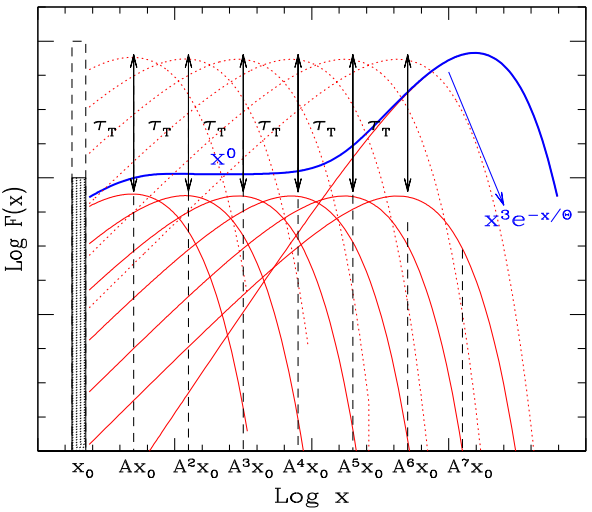


Fig. 5.11 Multiple Compton scatterings when $\tau_T > 1$ and $y \gg 1$. For the first scattering orders, *nearly all* photons are scattered: only a fraction $1/\tau_T$ can escape. Therefore the number of photons escaping at each scattering order is the same. This is the reason of the flat part, where $F(x) \propto x^0$. When the photon frequency is of the order of Θ, photons and electrons are in equilibrium, and even if only a small fraction of photons can escape at each scattering order, they do not change frequency any longer, and therefore they form the *Wien bump*, with the slope $F(x) \propto x^3 e^{-x/\Theta}$. If we increase τ_T, the flux with slope x^0 decreases, while the Wien bump stays the same

References

1. Blumenthal, G.R., Gould, R.J.: Bremsstrahlung, synchrotron radiation, and Compton scattering of high-energy electrons traversing dilute gases. Rev. Mod. Phys. **42**, 237 (1970)
2. Pozdnyakov, L.A., Sobol, I.M., Sunyaev, R.A.: Comptonization and the shaping of the X-ray source spectra: Monte Carlo calculations. Astrophys. Space Phys. Rev. **2**, 189–331 (1983)
3. Rybicki, G.B., Lightman, A.P.: Radiative Processes in Astrophysics. Wiley, New York (1979)

Chapter 6
Synchrotron Self-Compton

Consider a population of relativistic electrons in a magnetized region. They will produce synchrotron radiation, and therefore they will fill the region with photons. These synchrotron photons will have some probability to interact again with the electrons, by the Inverse Compton process. Since the electron "work twice" (first making synchrotron radiation, then scattering it at higher energies) this particular kind of process is called synchrotron self-Compton, or SSC for short.

6.1 SSC Emissivity

The importance of the scattering will of course be high if the densities of electrons and photons are large. If the electron distribution is a power law [$N(\gamma) = K\gamma^{-p}$], then we expect that the SSC flux will be $\propto K^2$, i.e. *quadratic* in the electron density.

We should remember Eq. 5.54, and, instead of a generic $U_{\rm r}(\nu)$, we should substitute the appropriate expression for the specific synchrotron radiation energy density. We will then set:

$$U_{\rm s}(\nu) = \frac{3R}{4c}\frac{L_{\rm s}(\nu)}{V} = 4\pi\frac{3R}{4c}j_{\rm s}(\nu) \tag{6.1}$$

where $3R/(4c)$ is the average photon source-crossing time, and V is the volume of the source. Now a simple trick: we write the specific synchrotron emissivity as

$$j_{\rm s}(\nu) = j_{\rm s,0}\nu^{-\alpha} \tag{6.2}$$

Remember: the α appearing here *is the same* index in Eq. 5.54. Substituting the above equations into Eq. 5.54 we have

$$j_{\rm ssc}(\nu_{\rm c}) = \frac{(4/3)^{\alpha-1}}{2}\tau_{\rm c}j_{\rm s,0}\nu_{\rm c}^{-\alpha}\int_{\nu_{\rm min}}^{\nu_{\rm max}}\frac{d\nu}{\nu} \tag{6.3}$$

As you can see, $j_{\rm s,0}\nu_{\rm c}^{-\alpha} = j_{\rm s}(\nu_{\rm c})$ is nothing else than the specific synchrotron emissivity calculated at the (Compton) frequency $\nu_{\rm c}$. Furthermore, the integral gives

G. Ghisellini, *Radiative Processes in High Energy Astrophysics*,
Lecture Notes in Physics 873, DOI 10.1007/978-3-319-00612-3_6,
© Springer International Publishing Switzerland 2013

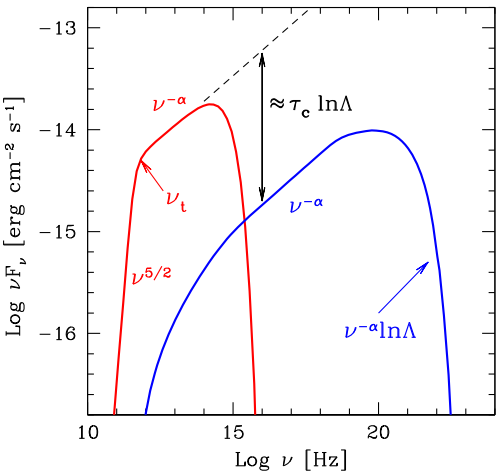


Fig. 6.1 Typical example of SSC spectrum, shown in the νF_ν vs ν representation. The spectral indices instead correspond to the $F_\nu \propto \nu^{-\alpha}$ convention

a logarithmic term, that we will call $\ln \Lambda$. We finally have:

$$j_{\rm ssc}(\nu_{\rm c}) = \frac{(4/3)^{\alpha-1}}{2} \tau_{\rm c} j_{\rm s}(\nu_{\rm c}) \ln \Lambda \tag{6.4}$$

In this form the ratio between the synchrotron and the SSC flux is clear, it is $[(4/3)^{\alpha-1}/2]\tau_{\rm c} \ln \Lambda \sim \tau_{\rm c} \ln \Lambda$. It is also clear that since $\tau_{\rm c} \equiv \sigma_{\rm T} RK$ and $j_{\rm s}(\nu_{\rm c}) \propto KB^{1+\alpha}$, then, as we have guessed, the SSC emissivity $j_{\rm ssc}(\nu_{\rm c}) \propto K^2$ (i.e. electrons work twice). Figure 6.1 summarizes the main results.

6.2 Diagnostic

If we are confident that the spectrum of a particular source is indeed given by the SSC process, then we can use our theory to estimate a number of physical parameters. We have already stated (see Eq. 4.32) that observations of the synchrotron spectrum in its self-absorbed part can yield the value of the magnetic field if we also know the angular radius of the source (if it is resolved). Observations in the thin part can then give us the product $RK \equiv \tau_{\rm c}/\sigma_{\rm T}$ (see Eq. 4.28). But $\tau_{\rm c}$ is exactly what we need to predict the high energy flux produced by the SSC process. Note that if the source is resolved (i.e. we know θ_s) we can get these information even without knowing the distance of the source. To summarize:

$$\begin{aligned} F^{\rm syn}_{\rm thick}(\nu) &\propto \theta_s^2 \frac{\nu^{5/2}}{B^{1/2}} \rightarrow \text{get } B \\ F^{\rm syn}_{\rm thin}(\nu) &\propto \theta_s^2 RK B^{1+\alpha} \nu^{-\alpha} \rightarrow \text{get } \tau_{\rm c} = RK/\sigma_{\rm T} \end{aligned} \tag{6.5}$$

There is an even simpler case, which for reasons outlined below, is the most common case employed when studying radio-loud AGNs. In fact, if you imagine to observe

the source at the self absorption frequency $\nu_{\rm t}$, then you are both observing the thick and the thin flux at the same time. Then, let us call the flux at $\nu_{\rm t}$ simply $F_{\rm t}$. We can then re-write the equation above:

$$\begin{aligned} B &\propto \frac{\theta_s^4 \nu_{\rm t}^5}{F_{\rm t}^2} \\ \tau_{\rm c} &\propto \frac{F_{\rm t} \nu_{\rm t}^{\alpha}}{\theta_s^2 B^{1+\alpha}} \\ F_{\rm ssc}(\nu_{\rm c}) &\propto \tau_{\rm c} F_{\rm syn}(\nu_{\rm c}) \propto \tau_{\rm c}^2 B^{1+\alpha} \nu_{\rm c}^{-\alpha} \\ &\propto F_{\rm t}^{2(2+\alpha)} \nu_{\rm t}^{-(5+3\alpha)} \theta_s^{-2(3+2\alpha)} \nu_{\rm c}^{-\alpha} \end{aligned} \tag{6.6}$$

Once again: on the basis of a few observations of only the synchrotron flux, we can calculate what should be the SSC flux at the frequency $\nu_{\rm c}$. Note the rather strong dependencies, particularly for θ_s, in the sense that the more compact the source is, the larger the SSC flux.

If it happens that we do observe the source at high frequencies, where we expect that the SSC flux dominates, then we can check if our model works. Does it? For the strongest radio-loud sources, almost never. The disagreement between the predicted and the observed flux is really severe, we are talking of several orders of magnitude. Then either we are completely wrong about the model, or we miss some fundamental ingredient. We go for the second option, since, after all, we do not find any mistake in our theory.

The missing ingredient is relativistic bulk motion. If the source is moving towards us at relativistic velocities, we observe an enhanced flux and blueshifted frequencies. Not accounting for it, our estimates of the magnetic field and particles densities are wrong, in the sense that the B field is smaller than the real one, and the particle densities are much greater (for smaller B we need more particles to produce the same synchrotron flux). So we repeat the entire procedure, but this time assuming that $F(\nu) = \delta^{3+\alpha} F'(\nu)$, where $\delta = 1/[\Gamma(1 - \beta\cos\theta)]$ is the Doppler factor and $F'(\nu)$ is the flux received by a comoving observer at the same frequency ν. Then

$$\begin{aligned} F_{\rm thick}^{\rm syn}(\nu) &\propto \theta_s^2 \frac{\nu^{5/2}}{B^{1/2}} \delta^{1/2} \\ F_{\rm thin}^{\rm syn}(\nu) &\propto \theta_s^2 R K B^{1+\alpha} \nu^{-\alpha} \delta^{3+\alpha} \end{aligned} \tag{6.7}$$

The predicted SSC flux then becomes

$$F_{\rm ssc}(\nu_{\rm c}) \propto F_{\rm t}^{2(2+\alpha)} \nu_{\rm t}^{-(5+3\alpha)} \theta_s^{-2(3+2\alpha)} \nu_{\rm c}^{-\alpha} \delta^{-2(2+\alpha)} \tag{6.8}$$

If we now compare the predicted with the observe SSC flux, we can estimate δ. And indeed this is one of the most powerful δ-estimators, even if it is not the only one.

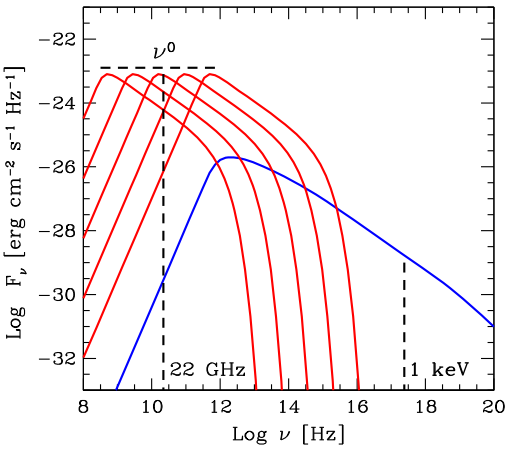


Fig. 6.2 Typical example of the composite spectrum of a flat spectrum quasars (FSRQ) shown in the F_ν vs ν representation, to better see the flat spectrum in the radio. The reason of the flat spectrum is that different parts of the jet contributes at different frequencies, but in a coherent way. The *blue line* is the SSC spectrum. Suppose to observe, with the VLBI, at 22 GHz: in this framework we will always observe the jet component peaking at this frequency. So you automatically observe at the self-absorption frequency of that component (for which you measure the angular size)

6.3 Why It Works

We have insisted on the importance of observing the synchrotron flux both in the self-absorbed and in the thin regime, to get B and τ_c. But the self-absorbed part of the synchrotron spectrum, the one $\propto \nu^{5/2}$ is very rarely observed in general, and never in radio-loud AGNs. So, where is the trick? It is the following. In radio-loud AGN the synchrotron emission, at radio frequencies, comes partly from the radio lobes (extended structures, hundreds of kpc in size, very relaxed, unbeamed, and usually self-absorbing at very small frequencies) and from the jet. The emission from the latter is beamed, and it is the superposition of the fluxes produced in several regions: the most compact ones (closer to the central engine) self-absorb at high radio frequencies (say, at 100 GHz), and the bigger they are, the smaller their self-absorbed frequency. But what is extraordinary about these jets is that the peak flux of each component (i.e. the flux at the self-absorption frequency) is approximately constant (in the past, this phenomenon was called *cosmic conspiracy*). Therefore, when we sum up all the components, we have a flat radio spectrum, as illustrated by Fig. 6.2.

Of course the emission components of the jet, to behave in such a coherent way, must have an electron density and a magnetic field that decrease with the distance from the central engine in an appropriate way. There is a family of solutions, but the most appealing is certainly $B(R) \propto R^{-1}$ and $K(R) \propto R^{-2}$. It is appealing because it corresponds to conservation of the total number of particles, conservation of the bulk power carried by them (if Γ does not change) and conservation of the Poynting flux (i.e. the power carried by the magnetic field).

To our aims, the fact that the jet has many radio emission sites self-absorbing at different frequency is of great help. In fact suppose to observe a jet with the VLBI, at one frequency, say 22 GHz. There is a great chance to observe the emission zone which is contributing the most to that frequency, i.e. the one which is self-absorbing at 22 GHz. At the same time you measure the size. Then, suppose to know the X-ray flux of the source. It will be the X-ray flux not only of that component you see with the VLBI, but an integrated flux from all the inner jet (with X-ray instruments the maximum angular resolution is about 1 arcsec, as in optical). But nevertheless you know that your radio blob cannot exceed the measured, total, X-ray flux. Therefore you can put a limit on δ (including constants):

$$\delta > (0.08\alpha + 0.14)(1+z)\left(\frac{F_{\rm t}}{\rm Jy}\right)\left(\frac{F_x}{\rm Jy}\right)^{-\frac{1}{2(2+\alpha)}}\left(\frac{\nu_x}{1\ {\rm keV}}\right)^{-\frac{\alpha}{2(2+\alpha)}} \times \left(\frac{\nu_{\rm t}}{5\ {\rm GHz}}\right)^{-\frac{5+3\alpha}{2(2+\alpha)}}\left(\frac{2\theta_s}{\rm m.a.s.}\right)^{-\frac{3+2\alpha}{2+\alpha}}\left[\ln\left(\frac{\nu_{\rm s,max}}{\nu_{\rm t}}\right)\right]^{\frac{1}{2(2+\alpha)}} \tag{6.9}$$

For some sources you would find $\delta > 10$ or 20, i.e. rather large values.

Chapter 7
Pairs

In the presence of energetic particles and photons one has to wonder about the possibility that there are collisions between them. One result of these collisions is the production of $e^{\pm}$. If we have a photon–photon collision, then the original photons might disappear, so that this process becomes an important absorption process.

The importance of this process came initially from the realization that the virial temperature of protons, in the vicinity of black holes, can be very large. As an estimate, the kinetic energy of a proton at 3 Schwarzschild radii is

$$E_{\rm kin} = \frac{GMm_{\rm p}}{R} \simeq 150\left(\frac{3R_{\rm S}}{R}\right) \,{\rm MeV} \tag{7.1}$$

therefore particles can be very energetic in accreting systems. Be aware, on the other hand, that protons can efficiently give their energy to electrons, that will emit this energy. This would keep the protons much cooler than the above value.

The other key ingredient, realized in the '60s', is that Active Galactic Nuclei (AGNs) vary quickly (with a variability timescale $t_{\rm var}$). By the causality argument they cannot be larger than $R \sim ct_{\rm var}$. Therefore their emitting regions must be small, and yet produce a huge luminosities. Densities are thus very large, and the collisions between particles, between particles and photons, and between photons must be probable. The discovery that blazars (AGNs with jets pointing at us) are very efficient γ-ray producers is now a proof that high energy particles indeed exist in these objects, that can in turn produce pairs. And finally, also Gamma Ray Bursts (GRBs) are emitting γ-rays.

The importance of electron–positron pair production in the nuclei of AGNs was realized quite early [1] and at the beginning of the '70s' two seminal papers appeared (one by Bysnovaty-Kogan et al. [2], the other by Bonometto and Rees [3]): the first concerned thermal plasmas, the second was about pairs in non-thermal plasmas. Thereafter the field was sleepy for about one decade, when the paper by Lightman [4] and Svensson [5, 6] resurrected the interests of the scientific community.

At those time it was believed that pair processes were fundamental for the formation of the spectrum of *all* AGNs, galactic binaries and GRBs. Now we know

G. Ghisellini, *Radiative Processes in High Energy Astrophysics*,
Lecture Notes in Physics 873, DOI 10.1007/978-3-319-00612-3_7,
© Springer International Publishing Switzerland 2013

that they do not play such a key role for AGNs and binaries, but they still could for GRBs. Nevertheless the entire subject is worth studying, because, at the very least, it allows to pose robust and important limits on the physics of all compact objects.

We will divide the study into thermal and non-thermal plasmas. We will see two fundamental results of pairs in thermal plasmas, and will see in more detail what happens when the particles have a relativistic (and not-Maxwellian) energy distribution.

7.1 Thermal Pairs

Consider particles characterized by a Maxwellian distribution and a temperature T. Since we are dealing with the production of $e^{\pm}$, it is convenient to measure all energies in units of $m_e c^2$ (=511 keV). Let us define:

$$\Theta = \frac{kT}{m_e c^2}, \qquad x = \frac{h\nu}{m_e c^2} \tag{7.2}$$

Furthermore, define:

$$\begin{aligned} n_{\pm} &= \text{number density of positrons } (+) \text{ and electrons } (-) \\ n_{\gamma} &= \text{number density of photons} \\ \dot{n}_{\pm} &= \text{production rate of pairs} \\ \dot{n}_{\rm A} &= \text{rate of annihilation of pairs} \end{aligned} \tag{7.3}$$

To these processes we should add the possibility that the leptons escape the source, with a rate

$$\dot{n}_{\rm esc} = \text{rate of escape of leptons} \tag{7.4}$$

The process that can produce $e^{\pm}$ are:

$$\begin{aligned} \gamma\gamma \to e^+e^-: &\qquad \dot{n}_+ = r_e^2 c n_{\gamma\gamma}^2 F_{\gamma\gamma} \\ \gamma p \to e^+e^- p: &\qquad \dot{n}_+ = \alpha_{\rm F} r_e^2 c n_{\gamma} n_{\rm p} F_{\gamma {\rm p}} \\ \gamma e \to e^+e^- e: &\qquad \dot{n}_+ = \alpha_{\rm F} r_e^2 c n_{\gamma} n_{\rm e} F_{\gamma {\rm e}} \\ ee \to e^+e^- ee: &\qquad \dot{n}_+ = \alpha_{\rm F}^2 r_e^2 c (n_+ + n_-)^2 F_{\rm ee} \\ ep \to e^+e^- ep: &\qquad \dot{n}_+ = \alpha_{\rm F}^2 r_e^2 c (n_+ + n_-) n_{\rm p} F_{\rm ep} \end{aligned} \tag{7.5}$$

while the processes that annihilate pairs or that correspond to the escape of pairs and electrons are:

$$\begin{aligned} e^+e^- \to \gamma\gamma: &\qquad \dot{n}_{\rm A} = 2 r_e^2 c n_+ n_- F_{\rm A} \\ \text{Escape:} &\qquad \dot{n}_{\rm esc} = r_e^2 c (n_+ + n_-)^2 F_{\rm esc} \end{aligned} \tag{7.6}$$

Table 7.1 Summary of the F-factors for the main rates of pair production mechanism. Only photon–photon and particle–particle processes are considered

	$\Theta \ll 1$	$\Theta \gg 1$	Comment
$F_{\gamma\gamma}$	$\frac{\pi^2 e^{-2/\Theta}}{8\Theta^3}$	$\frac{\pi \ln\Theta}{2\Theta^2}$	Wien
$F_{\gamma\gamma}$	...	$\frac{2}{3}(\frac{\Theta}{2})^{2\alpha}$	power law ($\alpha > -1$)
F_{ee}	...	$\frac{112}{27\pi}\ln^3(2\Theta)$	
F_{ep}	...	$\frac{\ln^3(2\Theta)}{\pi}$	
F_A	π	$\frac{\pi \ln\Theta}{2\Theta^2}$	
$F_{\rm esc}$	$\frac{8\pi}{3\tau_{\rm T}}\beta_{\rm esc}$	$\frac{8\pi}{3\tau_{\rm T}}\beta_{\rm esc}$	

The F-factors are averages of the energy dependent part of the cross sections over the Maxwellian distribution. They are dimensionless. The geometrical part of the cross section is always of the form of $\alpha_{\rm F}^a r_{\rm e}^2$: $\alpha_{\rm F} = 1/137$ is the fine structure constant, and $r_{\rm e}$ is the classical electron radius. For photon–photon interaction, $a = 0$, for particle–photon $a = 1$, for particle–particle $a = 2$. Consider that pair production processes *have an energy threshold*: there must be enough energy to produce a pair. But, when dealing with a Maxwellian distribution, one has particles (even if a few) at all energies, so the process can occur even if $\Theta \ll 1$. A brief summary of the F-factors is presented in Table 7.1.

When dealing with processes involving photons, we have to know their spectral distribution. This is why in Table 7.1 there are the rates for a Wien distribution [$L(x) \propto x^3 \exp(-x/\Theta)$], and for a power law [$L(x) \propto x^{-\alpha}$].

7.1.1 First Important Result

We impose that the source is stationary. This implies a detailed balance between the created and the destroyed pairs:

$$\dot{n}_+ = \dot{n}_{\rm A} \tag{7.7}$$

For simplicity, we neglected escape as a way to get rid of pairs (but in reality there will always be some escape). To solve the above equation, we have to know the F-terms, that are functions of Θ. Now the important point: *for particle–particle pair production processes, the F-terms are increasing functions of the temperature*. On the contrary, the pair *annihilation rate decreases* with the temperature. Compare this behavior with the "Klein–Nishina" decline of the scattering cross section.

Therefore, if the temperature is high enough, there is the possibility that we produce more pairs than what we can destroy. The source then becomes non-steady. As a result, if we want a steady source, we require that the temperature cannot be

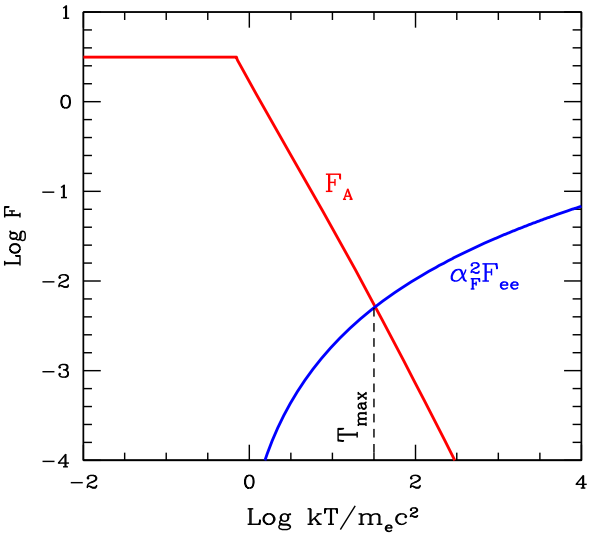


Fig. 7.1 To illustrate pair balance: the annihilation rate can balance pair production at low temperatures, but as $\Theta \equiv kT/m_e c^2$ becomes large, the particle–particle processes increase their rate. Above T_{max}, annihilation cannot keep up with pair production, pair balance is impossible, and the number of pairs increases. Having more particles to share the available energy it is very likely that the temperature then decreases, making the system to return to pair balance

greater than a critical value. This value is:

$$\Theta = 24 \rightarrow kT_{\max} = 12 \text{ MeV} \tag{7.8}$$

To see this, consider a plasma that is pair-dominated (i.e. neglect the original electrons associated with protons). Let us set $n_e = n_+ + n_-$. Neglect also all the particle–photon processes. Stationarity demands:

$$\alpha_F^2 n_e^2 F_{ee} + n_\gamma^2 F_{\gamma\gamma} = 2n_e^2 F_A \rightarrow \left(\frac{n_\gamma}{n_e}\right)^2 = \frac{2F_A - \alpha_F^2 F_{ee}}{F_{\gamma\gamma}} \geq 0 \tag{7.9}$$

Figure 7.1 shows how the two functions F_A and $\alpha_F^2 F_{ee}$ behave. We require that $F_A > \alpha_F^2 F_{ee}$, since otherwise the annihilation rate cannot keep the pace with the production rate, the number of particles increases, and if they are at the same temperature, then they continue to produce even more pairs... (and this would quickly make an explosion).

But in reality what happens is that the energy stored in the system is limited: if the number of particles increases, then *they will share the available energy among themselves*. There will be less energy per particle → the temperature will decrease. This is the second important result, that we will see now in more detail.

7.1.2 Second Important Result

Usually, when we increase the energy of a system, the temperature increases. But when kT approaches $m_e c^2$, the pair production processes start to be important. *New particles are created*: the energy per particle decreases → kT decreases.

Example: Wien Plasmas

The name "Wien plasma" indicates a plasma in which the photons and particles are in equilibrium, *reached through scattering*. We must have $\tau_T \equiv \sigma_T n_e R > 1$. The spectrum of the radiation *is not* a black body, because we do not have absorption and re-emission, but only scattering. In these conditions, whatever the process of photon production (i.e. bremsstrahlung) the spectrum of the radiation is

$$\dot{n}_\gamma(\epsilon) \propto \epsilon^2 \exp(-\epsilon/kT) \rightarrow \dot{n}_\gamma(x) \propto x^2 \exp(-x/\Theta) \tag{7.10}$$

where $\epsilon = h\nu$. $\dot{n}_\gamma(\epsilon)$ is the photon production rate. To convert it in a density of photons, we use a very simplified equation of radiative transport:

$$n_\gamma(x) = \dot{n}_\gamma(x) \frac{R}{c}(1 + \tau_T) \tag{7.11}$$

where R is the size of the region.

Pause and observe the above equation: when $\tau_T \ll 1$, the difference between n_γ and $\dot{n}_\gamma$ is the light crossing time of the photon inside the source. It is the time needed for a photon created in the center to escape. When $\tau_T \gg 1$, we have that the "transit time" is longer by a factor τ_T. This corresponds to have done τ_T^2 scatterings (remember the random walk) before escaping. The distance traveled between two consecutive scatterings is the mean free path, namely R/τ_T. Hence the time needed to escape is $\tau_T^2 R/(\tau_T c) = \tau_T R/c$. With this link between the production rate and the density of photons, we can write the luminosity

$$\begin{aligned} L &= \frac{4}{3}\pi R^3 \int \epsilon \dot{n}_\gamma(\epsilon)\, d\epsilon \\ &= \frac{4\pi R^3}{3R/c} \int \epsilon \frac{n_\gamma(\epsilon)}{1 + \tau_T}\, d\epsilon \end{aligned} \tag{7.12}$$

When $\tau_T \gg 1$, we can set $\tau_T + 1 \sim \tau_T = \sigma_T R n_e$. In this case

$$L = \frac{4\pi R c}{3\sigma_T} \langle \epsilon \rangle \frac{n_\gamma}{n_e} \tag{7.13}$$

where $\langle \epsilon \rangle$ is the mean energy of the photons. Note these remarkable facts:

1. L depends on the ratio n_γ/n_e. For pair plasmas (i.e. when pairs outnumber original electrons), this ratio is fixed by the F terms.
2. For a Wien spectrum, $\langle \epsilon \rangle = 3kT$ (and then $\langle x \rangle = 3\Theta$).
3. For large luminosities, the dominating pair production process is photon–photon.

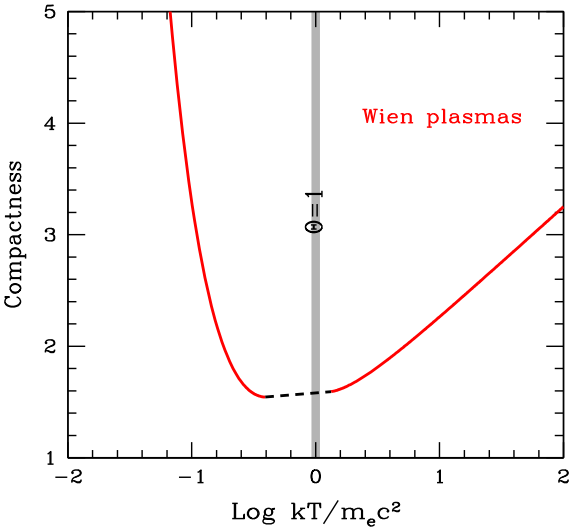


Fig. 7.2 Wien plasmas: assuming that the pairs outnumber original electrons, there is a fixed relation between the compactness and the temperature. Large compactnesses (and then luminosities, for a given size), are possible only if the temperature is small

4. Therefore n_γ/n_e is fixed by $(F_\mathrm{A}/F_{\gamma\gamma})^{1/2}$. From Table 7.1, assuming $\Theta \ll 1$, and assuming pair balance (i.e. $\dot{n}_+ = \dot{n}_\mathrm{A}$), we have

$$\frac{n_\gamma}{n_\mathrm{e}} = \left(\frac{F_\mathrm{A}}{F_{\gamma\gamma}}\right)^{1/2} = \left(\frac{8\pi\Theta^3}{\pi^2 e^{-2/\Theta}}\right)^{1/2}$$
$$\frac{n_\gamma}{n_\mathrm{e}} = 2\sqrt{2/\pi}\,\Theta^{3/2} e^{1/\Theta} \tag{7.14}$$

We can see how the luminosity of a pair dominated, steady Wien source depends on the temperature:

$$L = \frac{4}{3}\pi\frac{Rc}{\sigma_\mathrm{T}} 3\Theta m_e c^2 2\sqrt{2/\pi}\,\Theta^{3/2} e^{1/\Theta} \quad \Rightarrow \quad L \propto \Theta^{5/2} e^{1/\Theta} \tag{7.15}$$

For a given R, *high luminosities are possible only for low temperatures*! Introducing the compactness

$$\ell \equiv \frac{\sigma_\mathrm{T} L}{R m_\mathrm{e} c^3} \tag{7.16}$$

the luminosity–temperature relation has a simple form:

$$\ell_\mathrm{Wien} = 16\pi\sqrt{2/\pi}\,\Theta^{5/2} e^{1/\Theta}, \quad \Theta \ll 1 \tag{7.17}$$

Figure 7.2 shows ℓ_Wien as a function of Θ. Note the minimum for $\theta \sim 1$. The dashed line corresponds to the region where the asymptotic approximations are invalid.

7.2 Non-thermal Pairs

In non-thermal plasmas the density of the particles is small, and the particle energies can be large. If so, the production rate is usually large, corresponding to a large density of very energetic photons even if the plasma is rarefied. In these conditions the main pair production process is photon–photon.

The threshold energy for pair production is ($x \equiv h\nu/m_e c^2$):

$$x_1 x_2 \geq \frac{2}{1-\cos\theta} \tag{7.18}$$

where θ is the angle between the two photons: $\theta = 2\pi$ means head on collisions. In this case the threshold is $x_1 x_2 \geq 1$. For tail on encounters ($\theta = 0$) the process cannot occur.

Naively, one would have thought that the threshold condition were $x_1 + x_2 > 2$, namely that the *sum* of the photon energies is larger than $2m_e c^2$. But the threshold condition *must be calculated* in a reference frame where the energies of the two photons are equal. To illustrate this point, consider the simple case of a head on collision, with $x_1 \neq x_2$. Let us go in a frame where $x_1' = x_2'$. To do that, let us go in a reference frame having a Lorentz factor Γ such that the two energies become equal. In this frame the angle would still be 2π (head on collisions), and the two energies will be $x_1' = x_1/(2\Gamma)$ and $x_2' = 2\Gamma x_2$. In this frame we require that

$$\begin{aligned} &x_1' + x_2' \geq 2 \quad \text{and} \quad x_1' = x_2' \quad \Rightarrow \quad 2\Gamma = \left(\frac{x_1}{x_2}\right)^{1/2} \\ &\frac{x_1}{2\Gamma} + 2\Gamma x_2 \geq 2 \quad \Rightarrow \quad x_1 x_2 \geq 1 \end{aligned} \tag{7.19}$$

The cross section resembles the Klein–Nishina cross section, and it has a peak for $x_1 x_2 \sim 2$ where its value is

$$\sigma_{\gamma\gamma} \sim \frac{\sigma_T}{5}, \qquad (x_1 x_2 \sim 2) \tag{7.20}$$

The cross section is of course zero below threshold, and decreases after the peak. See Fig. 7.3. This means that a γ-ray photon with energy x can interact with all photons with energy $x_T > 1/x$, but it will interact preferentially with those photons near its threshold, i.e. $x_T = 1/x$ (here the subscript "T" stands for "target"). See Fig. 7.4.

7.2.1 Optical Depth and Compactness

We want to calculate the optical depth $\tau_{\gamma\gamma}$ for a source of a given luminosity. Assume that this luminosity is at high frequencies. A photon with energy ~0.5–1 MeV will interact with photons of the same energy (i.e. 0.5–1 MeV) to produce pairs (photons of 5 MeV will have $x = 10$ and will interact mainly with photons of energy $x_T \sim 1/10$, i.e. 50 keV).

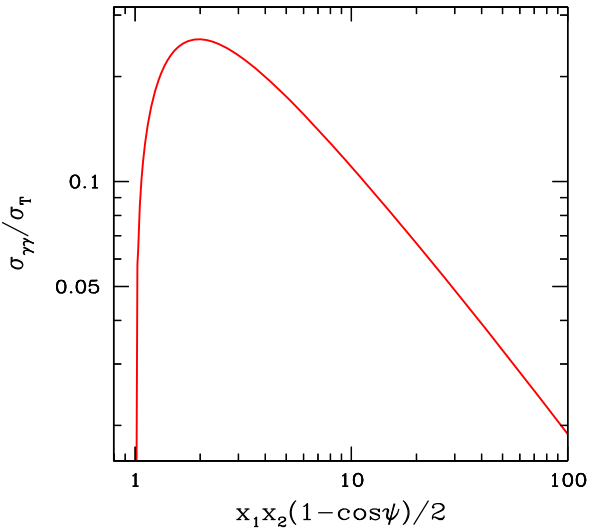


Fig. 7.3 The photon–photon cross section, as a function of $x_1x_2(1-\cos\psi)$, where ψ is the angle between the direction of the two photons (i.e. $\psi = 180°$ corresponds to head on collisions). The cross section is in units of the Thomson cross section σ_T

Like all the optical depths, $\tau_{\gamma\gamma}$ depends on the cross section, the density of the targets, and the size for which the process can occur. The density of targets is

$$n_\gamma(1\ \mathrm{MeV}) \simeq \frac{U_{\rm rad}(1\ \mathrm{MeV}) \times 1\ \mathrm{MeV}}{1\ \mathrm{MeV}} \simeq \frac{L_X}{4\pi R^2 c m_e c^2}$$

$$\Rightarrow \quad \tau_{\gamma\gamma}(1\ \mathrm{MeV}) \simeq \frac{\sigma_T}{5} R \frac{L_X}{4\pi R^2 m_e c^3} = \frac{\sigma_T}{20\pi} \frac{L_X}{R m_e c^3} \tag{7.21}$$

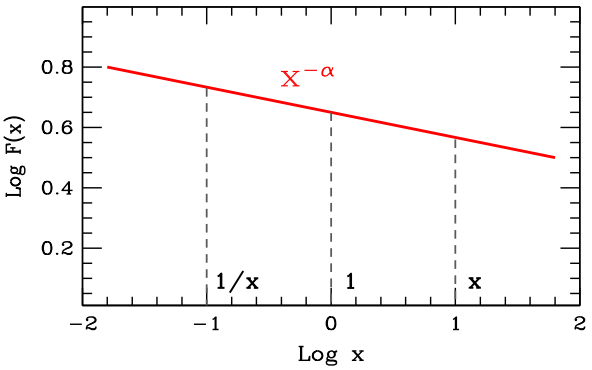


Fig. 7.4 Photons of energy $x > 1$ can interact with photons of energy $x_T > 1/x$ to produce pairs. Since the cross section is decreasing when increasing the energy of the targets, and since for a power law spectrum with $\alpha > 0$ the number of photons is also decreasing when increasing their energy, we can approximate the number of target photons as $(1/x) \cdot n(1/x)$. Note the "x–$1/x$" symmetry when we plot $F(x)$ in a logarithmic scale

Therefore $\tau_{\gamma\gamma}$ depends (apart from the numerical factor) upon the so-called *compactness* parameter ℓ, defined as:

$$\ell \equiv \frac{L}{R m_e c^3} \tag{7.22}$$

and we have:

$$\tau_{\gamma\gamma}(1\ \mathrm{MeV}) \simeq \frac{\ell}{60} \tag{7.23}$$

If we measure L in Eddington units, and R in Schwarzschild radii, we have

$$\ell = \frac{2\pi}{3}\frac{m_p}{m_e}\frac{L}{L_{\mathrm{Edd}}}\frac{R_S}{R} \quad \Rightarrow \quad \ell_{\mathrm{Edd}} = \ell_{\max} \simeq 10^4 \tag{7.24}$$

7.2.2 Photon–Photon Absorption

Let us assume that a compact source produces a spectrum with a power law shape: $F(x) \propto x^{-\alpha}$, where α is the energy spectral index. Assume also that this spectrum extends above the threshold for pair production. We want to calculate the optical depth for the γ–$\gamma \to e^{\pm}$ process.

Consider a γ-ray photon with $x > 1$. First we need to know the number density of the targets. These are all photons of energy $x_T > 1/x$. On the other hand, we know that the cross section decreases when increasing the energy of the targets. In most cases, furthermore, we deal with spectral indices $\alpha > 0$, meaning that also the number of photons decreases with energy (but be aware that this "rule" has an important exception, since several Gamma Ray Bursts have very flat spectra).

We then adopt the following important simplification:

$$\begin{aligned}
\tau_{\gamma\gamma} &= R\int_{1/x}^{\infty} \sigma_{\gamma\gamma} n(x)\, dx \\
&\sim \frac{\sigma_T}{5} R \frac{1}{x} n\left(\frac{1}{x}\right) \\
&\propto \frac{1}{x}\frac{F(1/x)}{x} \propto \frac{1}{x}\left(\frac{1}{x}\right)^{-\alpha-1} \\
&\propto x^{\alpha}
\end{aligned} \tag{7.25}$$

Therefore $\tau_{\gamma\gamma}$ increases increasing x: there are more targets (if $\alpha > 0$). Consider also that the spectral index α *is the spectral index of the targets*: the same calculation would hold if we had a broken power law, with the break at—say—$x = 1$. Let us calculate the resulting spectrum, recalling the simplest equation of radiative transfer through a slab (a slab, instead of a sphere, is here used for simplicity):

$$I(x) = \frac{j(x)R}{\alpha(x)R}\left[1 - e^{-\tau_{\gamma\gamma}(x)}\right] \tag{7.26}$$

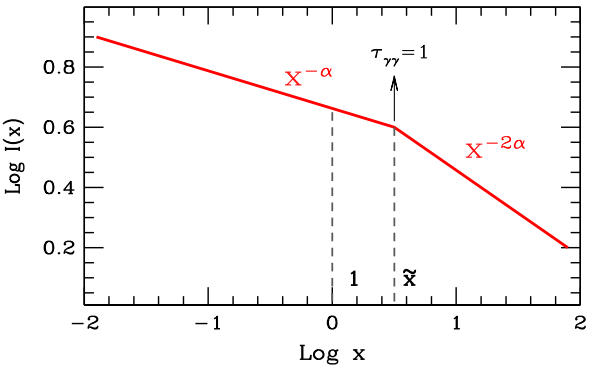


Fig. 7.5 The expected spectrum after photon–photon absorption, but without reprocessing. The initial spectrum is a single power law of index α. Absorption produces a break at the energy $\tilde{x}$, where the optical depth $\tau_{\gamma\gamma}$ is unity. After the break, the spectrum becomes $\propto x^{-2\alpha}$

where $I(x)$ is the monochromatic intensity; $j(x)$ is the emissivity and $\alpha(x)$ is the absorption coefficient. The little trick that we have used here is to multiply both the numerator and the denominator by R, the size of the source, because in this way $\alpha(x)R = \tau_{\gamma\gamma}(x)$, and this allows to write:

$$I(x) = j(x)R\left[\frac{1 - e^{-\tau_{\gamma\gamma}(x)}}{\tau_{\gamma\gamma}(x)}\right] \tag{7.27}$$

Written in this way, it is easy to see the behavior when $\tau_{\gamma\gamma}(x)$ is much smaller or much larger than unity:

$$\begin{aligned} \tau_{\gamma\gamma}(x) \ll 1 \quad &\Rightarrow \quad I(x) = j(x)R \propto x^{-\alpha} \\ \tau_{\gamma\gamma}(x) \gg 1 \quad &\Rightarrow \quad I(x) = \frac{j(x)R}{\tau_{\gamma\gamma}(x)} \propto x^{-2\alpha} \end{aligned} \tag{7.28}$$

There is a well defined break in the spectrum, occurring at the energy $\tilde{x}$ for which $\tau_{\gamma\gamma}(\tilde{x}) \sim 1$, as illustrated in Fig. 7.5...

BUT

this is not the end of the story.

In fact the produced pairs emit, and contribute to the spectrum (if they remain into the source). In general, each pair of electron and positron will share the energy of the photon creating them: (i.e. the electron and positron will have $\gamma m_e c^2 \sim h\nu/2$, i.e. $\gamma = x/2$). Therefore the radiation they can produce will be at energies smaller than x. Depending on the energies, the secondary photons can themselves pair-produce. Alternatively, the secondary photons can be used as targets, enhancing the rate of the process, and the number of pairs that the source can produce. Therefore the pair production process is

highly non-linear

photons that produce pairs that produce photons that produce pairs...

7.2.3 An Illustrative Case: Saturated Pair Production

If the source is compact, meaning that the compactness parameter $\ell > 1$, the photon density is huge. This means that the cooling timescale for inverse Compton scattering is very short, shorter than the light crossing time [remember that ℓ measures not only the importance of the γ–$\gamma \to e^{\pm}$ process, but also the ratio $t_{\rm cool}/(R/c)$, see Eq. 4.38]. Therefore, since all leptons cool in a short time, to have a steady source we have to replenish the "dead leptons" with new ones. In general, we have two ways to do that.

The first is to have "heating". With this word we mean that, besides cooling, leptons are also heated by some mechanism. Then there is a competition between energy losses and energy gains. Since the cooling rate for inverse Compton is $\propto \gamma^2$, it is very likely that cooling "wins" at high energies, and heating at low energies. There will be a specific energy where heating and cooling balance. All leptons will quickly move (in the energy space) towards this energy. In the absence of diffusion (in the energy space) the leptons will form a monoenergetic distribution. Diffusion will broaden this, and we may have the formation of a Maxwellian particle distribution even if the particles do not directly exchange energy between them.

The second way to "refill" the source with fresh energy is to continuously inject new energetic particles throughout the source. A shock does exactly that: at the shock front the particles are accelerated in a time that must be shorter than the cooling time. Particles are therefore continuously injected downstream, where they cool. Proton–proton collisions is another example (but also photon–photon collisions producing pairs can do). There can be differences among these processes: for instance, we expect a stratification in the downstream region of a shock, with the most energetic particles closer to the shock front, while we might expect a more homogeneous distribution of particles following the injection through proton–proton or photon–photon. We will neglect these differences in the following, and assume, for simplicity, that the injection and cooling mechanisms are homogeneous.

Let us assume that we inject $Q(\gamma)$ leptons per second and per cm^3:

$$Q(\gamma) = \left[\frac{\text{number of particles}}{\text{cm}^3\,\text{s}}\right] \to \text{injection} \tag{7.29}$$

This *is not* the quantity we need to calculate the spectrum. We want the *density*:

$$N(\gamma) = \left[\frac{\text{number of particles}}{\text{cm}^3}\right] \to \text{density} \tag{7.30}$$

The injection rate and the density are linked by the continuity equation.

The Continuity Equation

In its simplest form it reads:

$$\frac{\partial N(\gamma)}{\partial t} = \frac{\partial}{\partial \gamma}\left[\dot{\gamma} N(\gamma)\right] + Q(\gamma) \tag{7.31}$$

It describes how $N(\gamma)$ evolves in time. If we want a steady source, we require $\partial N(\gamma)/\partial t = 0$. This allows to obtain the solution:

$$N(\gamma) = \frac{\int_{\gamma}^{\gamma_{\max}} Q(\gamma')\, d\gamma'}{\dot{\gamma}} \tag{7.32}$$

To go further let us assume that:

(1) the injection rate is a power law in energy: $Q(\gamma) = Q_0 \gamma^{-s}$;
(2) the cooling rate is quadratic with energy: $\dot{\gamma} \propto \gamma^2$;
(3) all particles cool down to $\gamma = 1$, and then "disappear" (i.e. we neglect the accumulation of "dead leptons").

We have 2 cases:

$$\begin{aligned} &(1) \quad s < 1 \quad \Rightarrow \quad N(\gamma) \propto \gamma^{-2} \\ &(2) \quad s > 1 \quad \Rightarrow \quad N(\gamma) \propto \gamma^{-(s+1)} \end{aligned} \tag{7.33}$$

If we inject a monoenergetic $Q(\gamma) = Q_0\, \delta(\gamma - \gamma_{\max})$ we have $N(\gamma) \propto \gamma^{-2}$.

We have learnt that if $N(\gamma)$ is a power law, the emitted spectrum will also be a power law, with a well defined link between the slope p of $N(\gamma)$ and the radiation spectrum α. We have $\alpha = (p-1)/2$.

Now we have all the ingredients to see the effects of the *reprocessing of pairs* on the emitted spectrum. To fix the ideas, consider a region of radius R close to an accretion disk emitting UV radiation. Assume to continuously inject, throughout this region, relativistic leptons. Just to make it simpler, consider a monoenergetic injection at some $\gamma = \gamma_{\max}$. Assume that the inverse Compton process is the dominant one. Let us see what happens in a few steps:

(1) After cooling, the particle density $N(\gamma) \propto \gamma^{-2}$, and the inverse Compton spectrum will have $L(x) \propto x^{-0.5}$. Assume that the maximum photon energy ($x_{\max}$) is well above the threshold for pair production, and that the compactness is very large for all photons with $x > 1$. In these condition, all high energy photons get absorbed and produce pairs (*saturated pair cascade*).
(2) The generation of pairs means that, besides $Q(\gamma)$, there is another injection term. Call it $P_1(\gamma)$. We know the slope of $P_1(\gamma)$. In fact it will be the same of the photon spectrum, whose *energy* index is $\alpha = 0.5$, and therefore its *photon* index is $\alpha + 1 = 1.5$.

$$\begin{aligned} &P_1(\gamma) = 2\dot{n}_{\gamma}(2\gamma) \propto \frac{L(x)}{x}, \quad x > 1 \\ &P_1(\gamma) \propto \gamma^{-\alpha-1} = \gamma^{-1.5} \end{aligned} \tag{7.34}$$

(3) This new injection term originates a corresponding density of the first generation of pairs:

$$N_1(\gamma) \propto \frac{\int_{\gamma}^{\gamma_{\max}} P_1(\gamma')\, d\gamma'}{\gamma^2} \propto \gamma^{-2.5} \tag{7.35}$$

And consequently the radiation spectrum due to this first generation of pairs will have a spectral index

$$\alpha_1 = \frac{2.5-1}{2} = 0.75 \tag{7.36}$$

(4) The cycle repeats. If pairs have enough energy to emit above threshold, their photons will get absorbed, and generate the second generation of pairs.

$$\begin{aligned} P_2(\gamma) &\propto \gamma^{-\alpha_1-1} = \gamma^{-1.75} \\ N_2(\gamma) &\propto \frac{\int_\gamma^{\gamma_{\max}} P_2(\gamma')\, d\gamma'}{\gamma^2} \propto \gamma^{-2.75} \\ \alpha_2 &= \frac{2.75-1}{2} = 0.875 \end{aligned} \tag{7.37}$$

(5) If these second-generation pairs have enough energy to produce photons above threshold, we will have a third generation of pairs, and so on. A very interesting result of this exercise is that the final spectral index tends towards unity.

$$\alpha_{i+1} = \frac{\alpha_i}{2} + \frac{1}{2} \tag{7.38}$$

where i stands for the ith generation of pairs. The equation above is valid even if we start with a steep spectrum ($\alpha > 1$). But in this case the reprocessed energy will be a minor fraction of the total: most of the power is emitted at low frequencies. So, even if we correctly derive the slope of the reprocessed spectrum, this will be energetically unimportant.

If the initial spectrum is flat (i.e. $\alpha < 1$), instead, the reprocessing due to pairs can be very important, and will have the effect to soften the overall spectrum, redistributing photons at lower frequencies.

7.2.4 Importance in Astrophysics

The pair production processes were intensively studied in the '80s', especially in the field of Active Galactic Nuclei (AGNs). Researchers, at that time, hoped that the reprocessing due to pairs could explain the "universality" of the X-ray spectrum of AGNs, that has $\alpha_x \sim 0.7$. This would have implied a non-thermal origin of the spectrum, required to extend much above threshold. In other words, it was though that the typical AGN spectrum would resemble the one shown in Fig. 7.6. It was then predicted that all AGNs, i.e. also the radio-quiet ones, emit in the γ-rays, with a relatively steep power law shape. The first results obtained at high energies, coming from the *Compton Gamma Ray Observatory, CGRO* satellite showed instead an exponential cutoff at a few hundreds keV, and no signs of γ-rays in radio-quiet

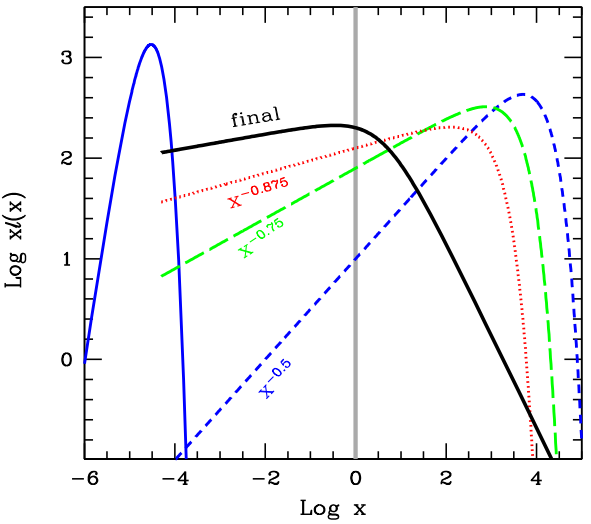


Fig. 7.6 Reprocessing due to pairs. A source produces a soft photon distribution (here it is a *black body*, *blue solid line*). The relativistic primary leptons injected throughout the source produce, by inverse Compton, a primary high energy spectrum $\propto x^{-0.5}$ (*blue short-dashed line*). All photons above threshold get absorbed and transformed in pairs. They emit, and the spectrum of this first generation of pairs is $\propto x^{-0.75}$ (*green long-dashed line*). Again, the photons above threshold are absorbed and create the second generation of pairs, whose spectrum $\propto x^{-0.875}$ (*dotted red line*). The process can continue, and the limiting spectrum has a spectral index close to unity. The *thick black solid line* shows how the final spectrum would look like: it is a broken power law with indices $\sim$1 and $\sim$2 below and above $x \sim 1$

AGNs. It was then concluded that (1) the X-ray spectra of radio-quiet AGNs have a thermal origin (i.e. Comptonization) and (2) that pairs have no or little role in the formation of this spectrum.

On the other hand, the main surprise of *CGRO* was the discovery that radio-loud AGNs are strong γ-ray emitters, as a class (i.e. we believe that *all* of them do). The properties of the observed spectra tell us that, again, photon–photon absorption inside the source rarely occurs (we do see a lot of γ-rays...). The absence of this effect poses a problem, because the high energy flux of these sources is varying quickly, requiring very compact sources, and the observed large luminosities imply very large values of the compactness parameter. The process *should* indeed occur, and yet it does not. The solution of this puzzle is relativistic motion, shortening variability timescales, blue-shifting the observed frequencies, and enhancing the apparent luminosities. Indeed, requiring that the sources are optically thin for photon–photon absorption, we can derive a limit on the bulk Lorentz factor of the emitting sources.

Another interesting field where pairs can be important is Gamma Ray Bursts (GRBs). Again, these sources emit high energy radiation that varies quickly. Since we now know that they are cosmological, the implied powers are huge, as well as the estimated photon densities. As in radio-loud AGNs, we can estimate a limit to

their bulk Lorentz factor requiring that they are optically thin to the photon–photon absorption process.

At this point you may ask if pairs are indeed produced in some class of sources... The answer is yes, even if the reprocessing features outlined above do not have (yet) a clear application to specific sources. At the beginning of the '90s', it was possible to detect TeV photons from the ground, through optical Cherenkov telescopes. Soon, low power blazars (i.e. BL Lac objects) were found to strongly emit at these frequencies. Some of them are distant enough that the interaction of TeV photons with the cosmic IR background photons is not negligible. We do see signs of the corresponding absorption. The importance of the latter depends, of course, of the density of the target photons, i.e. the level of the cosmic IR background. Since the latter is not precisely known, one can use the absorption features of the observed spectrum to estimate the background itself.

References

1. Jelley, J.V.: Absorption of high-energy gamma-rays within quasars and other radio sources. Nature **211**, 472 (1966)
2. Bisnovatyi-Kogan, G.S., Zeldovich, Ya.B., Syunyaev, R.A.: Physical processes in a low-density relativistic plasma. Sov. Astron. **15**, 17 (1971)
3. Bonometto, S., Rees, M.J.: On possible observable effects of electron pair-production in QSOs. Mon. Not. R. Astron. Soc. **152**, 21 (1971)
4. Lightman, A.P.: Relativistic thermal plasmas – pair processes and equilibria. Astrophys. J. **253**, 842 (1982)
5. Svensson, R.: The pair annihilation process in relativistic plasmas. Astrophys. J. **258**, 321 (1982)
6. Svensson, R.: Electron-positron pair equilibria in relativistic plasmas. Astrophys. J. **258**, 335 (1982)

Chapter 8
Active Galactic Nuclei

8.1 Introduction

Up to the seventeenth century, the unaided eye was the only receiver that humanity could use to observe the Universe. Evolution was able to apt this "instrument" to be sensitive to the light of the star we happen to be orbiting, the Sun. The invention of the telescope amplified the sensitivity of the eye and its angular resolution, letting humanity discover, less than a century ago, that other galaxies exist, far beyond out Milky way, and that these galaxies are moving apart: the Universe expands. However, all we could discover using the eye and its extension, the optical telescope, concerned a tiny, very tiny, part of the entire electromagnetic spectrum. As soon as technology enabled humanity to open new windows, we discovered other phenomena, other objects, and could push our knowledge farther out in space and in time.

The opening of the radio window made the sixties the golden decade for astronomy, with the discovery of the microwave background and of pulsars. The third great discovery made in that decade was that of quasars. The term "quasar" originally stood for "quasi-stellar radio source", and refers to the fact that when an optical telescope is pointed towards the direction of some radio source, which can be as extended as minutes of arc in radio maps, the resulting optical plate shows a source which looks like a star, i.e. a not extended, a "pointlike" object. This apparently innocuous point is instead a gigantic energy plant, able to produce much more power that an entire galaxy like our own, in a volume which is ridiculously small, if compared with the dimension of the Galaxy, and comparable with our Solar System. *The process that powers the stars, thermonuclear reactions, is not enough to power quasars.* For this reason we believe that at the core of these sources there is a massive black hole, with a mass between a million and a billion the mass of the Sun. Matter around the hole is attracted by the black hole gravity, it is compressed, heated, and then radiates. This was realized quite soon [10, 12, 15, 16].

Another major advance came with the opening of the X-ray window, first (in the sixties) with rocket experiments pioneered by Riccardo Giacconi, Bruno Rossi and others, and then with the first X-ray satellites, in the early seventies. The Uhuru, Ariel 5, HEAO–1 and then *Einstein* satellites made clear that all kinds of quasars

G. Ghisellini, *Radiative Processes in High Energy Astrophysics*,
Lecture Notes in Physics 873, DOI 10.1007/978-3-319-00612-3_8,
© Springer International Publishing Switzerland 2013

were strong X-ray emitters: at the same time, people started to believe that quasars were the major contributors to the cosmic diffuse X-ray background, already discovered in 1962 [6].[1]

A third qualitative "jump" was the improvements of the interferometric technique in the radio band, in the early seventies. Radio telescopes in different continents, looking at the same source, can resolve details as close as a few tenths of a millisecond of arc. This enabled us to discover that some radio emitting quasars have spots of radio emission which are observed to move. Given the huge distances, this motion corresponds to velocities that exceed the speed of light. Far from challenging special relativity, this "superluminal" motion, as it is now called, was even predicted before it was observed, by Martin Rees in 1966,[2] and corresponds to real fast motion (but slower than the velocity of light!) at an angle close to our line of sight.

8.2 The Discovery

8.2.1 Maarten Schmidt Discovers the Redshift of 3C 273

From Maarten Schmidt [14]:

> "The puzzle was suddenly resolved in the afternoon of February 5, 1963, while I was writing a brief article about the optical spectrum of 3C 273. Cyril Hazard had written up the occultation results for publication in Nature and suggested that the optical observations be published in an adjacent article. While writing the manuscript, I took another look at the spectra. I noticed that four of the six lines in the photographic spectra showed a pattern of decreasing strength and decreasing spacing from red to blue. For some reason, I decided to construct an energy–level diagram based on these lines. I must have made an error in the process which seemed to contradict the regular spacing pattern. Slightly irritated by that, I decided to check the regular spacing of the lines by taking the ratio of their wavelengths to that of the nearest line of the Balmer series. The first ratio, that of the 5630 line to H–β, was 1.16. The second ratio was also 1.16. When the third ratio was 1.16 again, it was clear that I was looking at a Balmer spectrum redshifted by 0.16.
>
> ...
>
> I was stunned by this development: stars of magnitude 13 are not supposed to show large redshift! When I saw Jesse Greenstein minutes later in the hallway and told him what had happened, he produced a list of wavelengths of emission lines from a just completed manuscript about the spectrum of 3C 48. Being prepared to look for large redshift, it took us only minutes to derive a redshift of 0.37.
>
> ...

[1] Giacconi was awarded the Nobel Prize in Physics in 2002.

[2] Martin Rees was born in 1942. He was 24 in 1966.

The interpretation of such large redshifts was an extraordinary challenge. Greenstein and I soon found that an explanation in terms of gravitational redshift was essentially impossible on the basis of spectroscopic arguments. We recognized that the alternative explanation in terms of cosmological redshifts, large distances, and enormous luminosities and energies was very speculative but could find no strong arguments against it. The results for 3C 273 and 3C 48 were published six weeks later in four consecutive articles in *Nature* (Hazard, et al. [9]; Schmidt [13]; Oke [11]; Greenstein [8]).”

8.3 Basic Components

The first quasars that were discovered were radio-loud, but we now know that these radio-loud AGNs are only roughly the 10 % of all AGNs. The majority are *radio-quiet*.

The basic structure of AGNs includes:

- A black hole, with $10^6\ M_\odot < M < 10^{10}\ M_\odot$. It is probably spinning at some level, even if we do not have secure measurements of the spin value.
- An accretion disk. Matter with even a small amount of angular momentum, attracted by the black hole gravity, spirals in and forms a disk. This is a major source of power.
- An X-ray corona, sandwiching the accretion disk. It is supposed to be a hot layer, or an ensemble of clumpy regions particularly active in the inner parts of the disk.
- An obscuring torus located at several parsec from the black hole, intercepting some fraction of the radiation produced by the disk and re-emitting it in the infrared. Figure 8.2 shows the contribution of the accretion disk, the corona and the molecular torus to the overall spectral distribution of a radio-quiet AGN.
- A region of many small clouds at a distance of $\sim 10^{17}$–10^{18} cm from the hole (i.e. less than a parsec) moving rapidly ($\sim 3000\ \mathrm{km\,s^{-1}}$). They intercept $\sim$10 % of the ionizing radiation of the disk, and re-emit it in the form of lines. Doppler shifts broaden the observed lines. This is why this region is called *Broad Line Region* (*BLR*).
- At larger distance ($\sim$100 pc) there is another region where less dense clouds are moving, less rapidly. This is called *Narrow Line Region* (*NLR*).
- About 10 % of AGNs, besides accreting matter, are able to expel it in two oppositely directed jets. Their direction likely traces the rotational axis of a spinning black hole. The material inside these jets is moving at relativistic speeds. Therefore the jet emission is highly beamed, and their appearance depends on the viewing angle. AGNs whose jets are pointing at us are called *blazars*. AGNs whose jets are pointing elsewhere are called *radio-galaxies*.

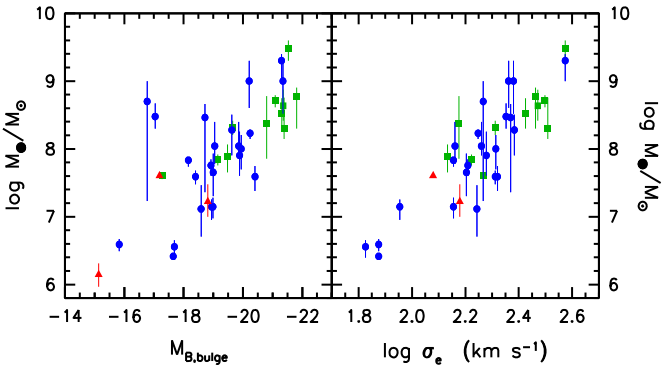


Fig. 8.1 The mass of the supermassive black hole correlates with the luminosity of the bulge of the host galaxy and with the velocity dispersion of the stars of the central regions of the host galaxy. From http://chandra.as.utexas.edu/~kormendy/bhsearch.html

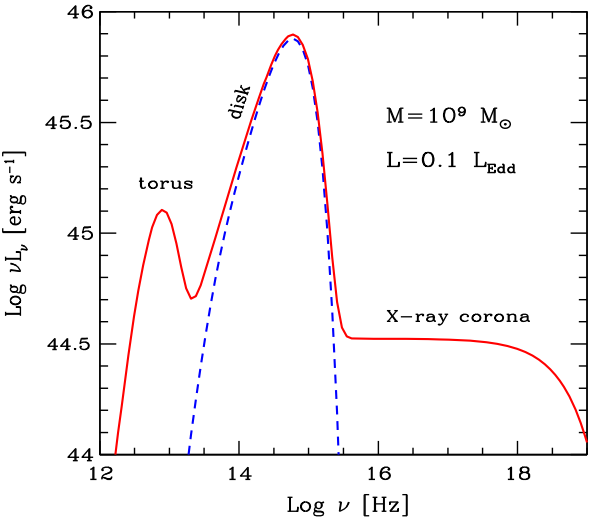


Fig. 8.2 Spectrum from a standard accretion disk, the infrared torus and the X-ray emitting corona

8.4 The Supermassive Black Hole

The black hole in the center of AGNs has a mass that "knows" of the mass of the host galaxy. In fact there is a correlation between the black hole mass and the luminosity of the bulge, due to the stars (see Fig. 8.1, left panel). The black hole mass correlates even more with the velocity dispersion of these stars (see Fig. 8.1, right panel). The correlation with the bulge luminosity is linear: $M_{\rm BH} \sim 2 \times 10^{-3} M_{\rm bulge}$, while the correlation with the velocity dispersion σ is between $M_{\rm BH} \propto \sigma^4$ and $M_{\rm BH} \propto \sigma^5$.

8.5 Accretion Disk: Luminosities and Spectra

The luminosity of the accretion disk depends on the amount of the mass accretion rate $\dot{M}$. It is usually measured in solar masses per year. The process has a very large efficiency η, defined as the fraction of rest mass energy that is converted into radiation, before being swallowed by the black hole. We have

$$L_{\rm disk} = \eta \dot{M} c^2 \tag{8.1}$$

The efficiency η depends on the details of the accretion mode, but it is of the order of $\eta \sim 0.1$. To produce a disk luminosity of $L_{\rm disk} = 10^{46} L_{46}$ erg s^{-1} we then require

$$\dot{M} = \frac{L_{\rm disk}}{\eta c^2} \sim 1.75 L_{46}\ M_\odot\ {\rm yr}^{-1} \tag{8.2}$$

There is a limit on the disk luminosity. This is called *Eddington luminosity*. It corresponds to radiation pressure balancing gravity. Radiation pressure acts on electrons, gravity acts both on electrons and their companions protons, that are heavier.

$$\sigma_{\rm T} \frac{L_{\rm Edd}}{4\pi R^2 c} = \frac{GMm_{\rm p}}{R^2} \longrightarrow L_{\rm Edd} \equiv \frac{4\pi c G M m_{\rm p}}{\sigma_{\rm T}} = 1.3 \times 10^{38} \frac{M}{M_\odot}\ {\rm erg\ s}^{-1} \tag{8.3}$$

The Eddington luminosity depends only on the black hole mass. If the accretion rate for some reason produces a luminosity $L_{\rm disk} > L_{\rm Edd}$, then the accreting mass feels a radiation pressure that contrasts gravity, and the accretion stops, making $L_{\rm disk}$ to decrease below $L_{\rm Edd}$. We have a *self-regulating* process.

Ask yourself:

- What *implicit* assumptions have we made to derive $L_{\rm Edd}$?
- Did we neglect some other forces?
- Why is there $\sigma_{\rm T}$?
- What happens if we have electron–positron pairs?
- Can you envisage cases in which the Eddington limit can be avoided?

8.5.1 Spectrum

Accreting matter, by spiraling inside, has to dissipate angular momentum and potential energy. The potential energy of a proton at distance R (much larger than the Schwarzschild radius $R_{\rm S} \equiv 2GM/c^2$) is

$$E_{\rm g} = \frac{GMm_{\rm p}}{R} \tag{8.4}$$

namely, it increases (or decreases, if you take it negative) as R decreases. More energy has to be dissipated close to the black hole than far from it. Besides, the surface $2 \times 2\pi R dR$ (there are two faces of the disk...) of the ring at a distance R and width dR becomes smaller and smaller as you move close to the black hole. More

energy has to be dissipated from a smaller surface. Assuming that the produced disk radiation is a blackbody, this inevitably implies that the temperature must increase as R decreases. If all rings of the disk emit black-body radiation, the temperature profile is:

$$T = \left[\frac{3R_S L_{\rm disk}}{16\pi\eta\sigma_{\rm SB}R^3}\right]^{1/4}\left[1-\left(\frac{3R_S}{R}\right)^{1/2}\right]^{1/4}$$
$$\propto R^{-3/4}, \quad \text{for } R \gg 3R_S \tag{8.5}$$

where $\sigma_{\rm SB}$ is the Stefan–Boltzmann constant. The term in the second square brackets allows for the fact that not all the orbits are stable around a black hole, but only those beyond the marginally stable orbit: for a Schwarzschild black hole this orbit is at $3R_S$. Matter at $R < 3R_S$ falls directly onto the hole in a short time. If we measure R in units of the Schwarzschild radius R_S, $x \equiv R/R_s$ we have:

$$T = \left[\frac{3\dot{M}c^6}{64\pi\sigma_{\rm SB}x^3G^2M^2}\right]^{1/4}\left[1-\left(\frac{3}{x}\right)^{1/2}\right]^{1/4}$$
$$\propto \frac{\dot{M}^{1/4}}{M^{1/2}}x^{-3/4}, \quad \text{for } x \gg 3 \tag{8.6}$$

We can now have an idea of the emitted spectrum. It will be the sum of black-bodies peaking at different temperatures: each ring of width dR emits a luminosity dL:

$$dL = 2\times 2\pi\sigma_{\rm SB}RT^4dR \longrightarrow \frac{dL}{dR} = 2\times 2\pi\sigma_{\rm SB}T^{-4/3}T^4 \tag{8.7}$$

We can then set:

$$\frac{dL}{dT} = \frac{dL}{dR}\frac{dR}{dT} \propto \sigma_{\rm SB}T^{-4/3}T^4\frac{dR}{dT} \propto T^{1/3} \tag{8.8}$$

where we have used $R \propto T^{-4/3}$ and then $(dR/dT) \propto T^{-7/3}$. This is valid as long as $R \gg 3R_S$. Since there is a one to one correspondence between the temperature and the peak frequency of the black-body, we have that

$$L_{\rm disk}(\nu) \propto \nu^{1/3}; \qquad h\nu \ll kT_{\rm max} \tag{8.9}$$

up to a frequency corresponding to the maximum temperature. Beyond that the emission is not a superposition of black-bodies anymore, and only the region at the maximum temperature contributes. Therefore, at large frequencies, we will see an exponential drop. At the opposite side (small frequencies) we see only the black-body produced by the outer radius of the disk $R_{\rm out}$, and correspondingly, we see the Raleigh–Jeans emission of that radius. Therefore we can approximate the disk spectrum as:

$$\begin{aligned} L_{\rm disk} &\propto \nu^2, && h\nu < kT(R_{\rm out}) \\ &\propto \nu^{1/3}e^{-h\nu/kT_{\rm max}}, && h\nu > kT(R_{\rm out}) \end{aligned} \tag{8.10}$$

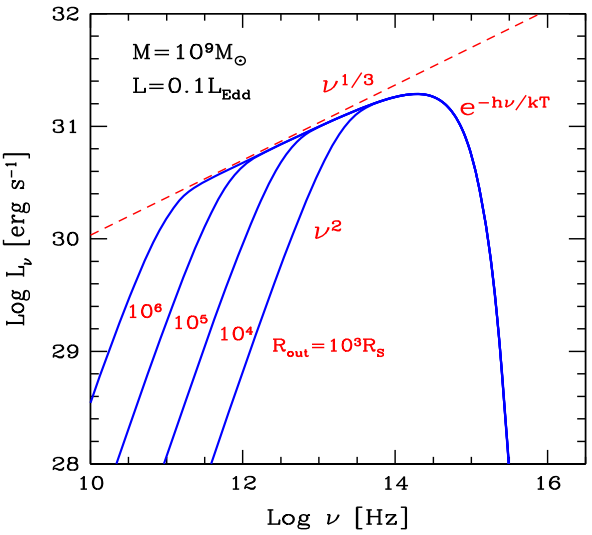


Fig. 8.3 The spectrum from a standard accretion disk, emitting black-body radiation from all its surface, with a temperature profile given by Eq. 8.5. The disk extends from $R_{\rm in} = 3R_{\rm S}$ to different values of $R_{\rm out}$, as labeled. Note that the $\nu^{1/3}$ slope is present only for very large values of $R_{\rm out}$

The peak is determined by $T_{\rm max}$. We can estimate it by assuming that most of the luminosity is produced within—say—$10R_{\rm S}$:

$$L_{\rm disk} \approx 2 \times \pi 10^2 R_{\rm S}^2 \sigma_{\rm SB} T_{\rm max}^4$$
$$\longrightarrow T_{\rm max} \sim \left(\frac{L_{\rm disk}}{200\pi R_{\rm S}^2 \sigma_{\rm SB}} \right)^{1/4} \sim 4.2 \times 10^4 \left(\frac{L_{46}}{M_9^2} \right)^{1/4} {\rm K} \qquad (8.11)$$

where M_9 is the black hole mass in units of $10^9\ M_\odot$. This temperature corresponds to a frequency

$$\nu_{\rm peak} \sim \frac{kT_{\rm max}}{h} \sim 8.8 \times 10^{14} \left(\frac{L_{46}}{M_9^2} \right)^{1/4} {\rm Hz} \qquad (8.12)$$

i.e. in the near ultraviolet. For disks emitting at the same Eddington ratio (i.e. $L_{\rm disk}/L_{\rm Edd} = {\rm const}$), we have $\nu_{\rm peak} \propto M^{-1/4}$. Figure 8.3 shows the spectrum calculated numerically according to the assumed temperature distribution of Eq. 8.5, for different values of the outer radius of the disk $R_{\rm out}$. Note that the $\nu^{1/3}$ behavior can be seen only if $R_{\rm out}$ is very large.

8.6 Emission Lines

A distinctive characteristic of AGNs is the presence, in their optical spectra, of emission lines. They comes in two flavors: *the broad and the narrow.*

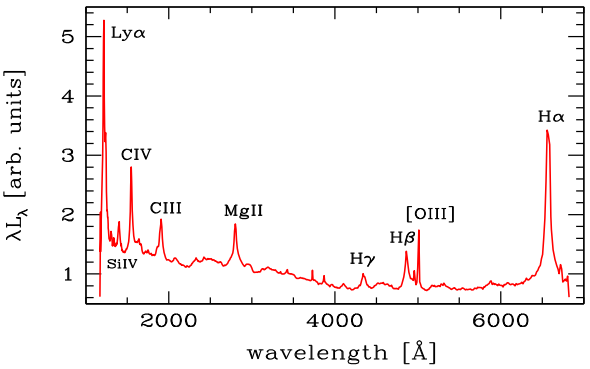


Fig. 8.4 Template of the optical/UV spectra for optically-selected quasars in the Sloan Digital Sky Survey. Notice the presence of *broad lines* and also of the forbidden [OIII] *narrow line*. Courtesy of Giorgio Calderone

8.6.1 Broad Emission Lines

Figure 8.4 shows an atlas (i.e. the average spectrum of many sources) of the optical-UV spectrum of typical AGNs. Typical lines are labeled. The most prominent are the Hydrogen Lyα (transitions from $n = 2$ to $n = 1$), the lines from partially ionized Carbon, Magnesium, Oxygen and then the Hydrogen Hα (transitions from $n = 3$ to $n = 2$). If you look carefully, you should notice that most of these lines are broad, while the [OIII] line is narrow. The square brackets indicate that this is a "forbidden" line. So why do we see it? The reason to call this line "forbidden" is that when the density is larger than some critical value, the de-excitation of the excited state is made by collisions, occurring faster than the radiative ones. In our labs the densities are always larger than the critical ones, so in the lab we do not see the line. This gives some hints of the density where the narrow lines are made.

The most used way to quantify the width of a line is to measure it at a flux level which is half of the peak flux. In this case we speak of Full Width at Half Maximum (FWHM). Full width means that it is the entire width, not only one half as in the case of a σ of a Gaussian. The units can be Å or $\mathrm{km\,s^{-1}}$. In fact the width can be related immediately with a Doppler shift, and thus to a velocity.

The typical values for the broad emission lines are:

- **FWHM**: from 1000 to 10,000 $\mathrm{km\,s^{-1}}$. They are too large to be due to thermal motions. In fact, with a temperature of $T \sim 10^4$ K, we have that thermal broadening implies:

$$v \sim \left(\frac{kT}{m_\mathrm{p}}\right)^{1/2} \sim 10^6\ \mathrm{cm\,s^{-1}} = 10\ \mathrm{km\,s^{-1}} \tag{8.13}$$

  Therefore we need bulk motions (in different directions with respect to our line of sight) of the material emitting the lines.
- **Density**: between 10^9 and 10^{11} $\mathrm{cm^{-3}}$. This comes from the presence or absence of specific lines.
- **Temperature**: around 10^4 K. Again, this comes from the presence or absence of specific lines.

- **Covering factor**: around 0.1. A simple estimate comes from the luminosity of all the broad lines with respect to the continuum.
- **Distance**: depends on the luminosity of the ionizing continuum. Recent studies use the technique of "reverberation mapping": taking spectra of a source regularly, one can see the time delay between a variation of the continuum and the variations of the lines. From these studies one gets a size:

$$R_{\rm BLR} \sim 10^{17} L_{\rm ion,45}^{1/2} \sim 10^{17} L_{\rm disk,45}^{1/2} \ {\rm cm} \tag{8.14}$$

  Where we have assumed that most of the disk radiation can ionize the atoms in the BLR. Please note that this is only approximately true.

  One useful quantity when studying lines is the "ionization parameter ξ". ξ can be defined as the ratio of the densities of the ionizing photons and the electrons:

$$\xi = \frac{1}{n_{\rm e}} \int_{\nu_{\rm i}}^{\infty} \frac{L(\nu)}{4\pi R^2 ch\nu} d\nu = \frac{n_{\gamma,{\rm i}}}{n_{\rm e}} \propto \frac{\text{Ionization rate}}{\text{Recombination rate}} \tag{8.15}$$

So, what is then the Broad Line Region? We do not know exactly yet. It can be an ensemble of clouds in Keplerian motions around the black hole, or material that is infalling, or outflowing, with a range of velocities. Broad lines could also be produced within the accretion disk itself, but in this case we should see "double horned" lines, because for a typical inclination of the disk, the opposite sides of the disk produce redshifted and blueshifted lines. They are seen sometimes, but not often. It has been proposed also that broad line clouds are stars with bloated envelopes, coming close to the black hole. But a large number of them is required, possibly too large. If broad lines are due to individual clouds, we must have many of them, because each one contributes for only 10 km s^{-1} to the broadening, and if they were a few, we should see a not completely smooth profile of the line. Estimates range from 10^5 to billions. But the total required mass is tens of solar masses, a very small quantity.

8.6.2 Narrow Emission Lines

The main properties of the narrow emission lines are:

- **FWHM**: around 300–500 km s^{-1}. These lines are "narrow", but in any case much larger than thermal broadening.
- **Density**: around 10^3 cm^{-3}. This comes from the presence of forbidden lines, requiring small densities.
- **Temperature**: around 10^4 K. This comes from the presence/absence of specific lines.
- **Covering factor**: around 0.01. This comes from the entire NLR luminosity divided by the continuum luminosity.
- **Distance**: around 100 parsec. They can be resolved in nearby objects. Sometimes they appear contained in a double cone.

Since the NLR is located at greater distances than the BLR, they are unaffected by the possible presence, in a region close to the accretion disk, of absorbing material. This is a crucial fact, as we will soon see.

8.7 The X-Ray Corona

From Eq. 8.5 it is clear that the standard accretion disk is relatively "cold", in the sense that even the inner regions cannot reach ∼keV temperatures (1 keV $\sim 10^7$ K). On the other hand, AGNs are powerful X-ray emitters, and their X-ray spectrum extends out to hundreds of keV. We must assume that there is an additional component, besides the accretion disk, responsible for this emission. Observed in the energy range 0.1–10 keV, with low spectral resolution, the X-ray spectrum can be approximated by a power law: $F_X(\nu) \sim \nu^{-\alpha_X}$, with $\alpha_X \sim 0.7$–0.9. At first sight, it seems a *non-thermal* spectrum, because it is characterized by a power law. But then more accurate observations were made, that revealed three important features:

- **Cut-off power law**—When high energy observations in the 10–200 keV were available, a cut-off was observed, of an exponential type. The spectrum was thus a power law ending with an exponential cut:

$$F_X(\nu) \propto \nu^{-\alpha_X} e^{-\nu/\nu_c} \tag{8.16}$$

  where ν_c is somewhat different for different objects, and it is in the range 40–300 keV.
- **6.4 keV Fe line**—When spectral resolution was improved in the soft X-rays (soft means 0.1–10 keV), an emission line appeared at ~ 6.4 keV (see Fig. 8.5). This is the Kα line from cold Iron. It is a *fluorescent* line. It means that a photon of enough energy interacts with one electron of the inner shell of the Iron atom, and ionizes it. There is then a "vacant place", triggering a $n = 2 \rightarrow n = 1$ transition. The energy of this transition depends on the ionization state of the Iron. If it is partially ionized, the energy of the jump is more. So the energy of the line tells us about the ionization state of the Iron. For almost completely ionized Iron, we should observe a line at 6.7 keV (and sometimes we do). A line at 6.4 keV means that it is not largely ionized, and therefore it is relatively cold (i.e. less than 10^6 K).
- **Compton hump**—At the same time, the improved spectral resolution revealed that the slope of the spectrum was more complex than a simple power law. There is the presence of a hump, peaking at roughly 30 keV, superposed to the power law. So the previously determined slope of the power law was not correct, because it included the hump. Depurating from this extra component, the spectral index of the power law becomes $\alpha_X \sim 0.9$–1. The right panel of Fig. 8.5 illustrates this point. The nature of this 30 keV "hump" was soon interpreted as the emission coming from an *irradiated disk*, and was baptized "Compton hump" or "Compton reflection".

We will now discuss in somewhat more details these three components: (i) the power law; (ii) the Compton reflection, and (iii) the Iron line.

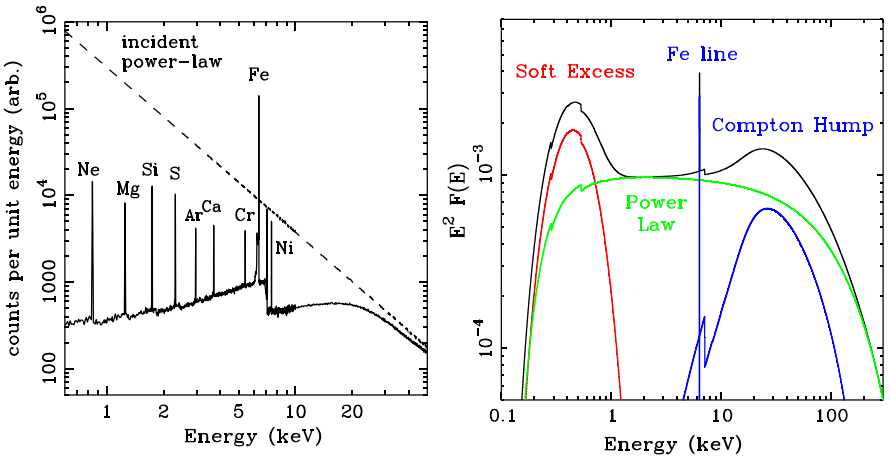


Fig. 8.5 *Left*: The "Compton reflection hump", together with the produced emission lines. *Right*: X-ray spectrum and its components: a power law continuum, a soft excess, and a "Compton reflection", together with the Iron Kα line. From Fabian & Miniutti [4]

8.7.1 The Power Law: Thermal Comptonization

We have seen in the previous chapters that a power law does not necessarily imply a non-thermal emission. Bremsstrahlung and thermal Comptonization are made by thermal electrons, but their shape is a power law (ending in an exponential cut). Following this idea we will now postulate that there is a region above and below the disk, where the electrons are hot, much hotter than the disk. It is something similar to the corona of our Sun, and therefore this region is called X-ray corona. It cannot be located far from the black hole for several reasons:

1. Its luminosity is smaller than, but comparable to the luminosity of the accretion disk. If its power depends on the release of the gravitational energy, it must be close to the black hole (i.e. remember $E_g \propto 1/R$).
2. The X-ray flux varies rapidly.
3. It must illuminate the disk and produce the ionization flux for the production of the fluorescent Iron line. As we shall see, the Iron line is sometimes very broad, as a result of Doppler broadening due to the high Keplerian velocities in the inner regions of the disk. So also the "illuminator" must be close.

Can we derive some more information from the spectral shape? We can exclude bremsstrahlung as the main radiation process because it is too inefficient, meaning that we would require too many electrons to produce what we see. Variability tells us that the emitting volume is small, so the electron density would be large, and the Thomson optical depth would be much larger than unity. In these conditions, Compton scatterings would be more important. Therefore let us assume that the spectrum is due to thermal Comptonization. The temperature can be inferred from

the exponential cut:

$$\Theta \equiv \frac{kT}{m_e c^2} \sim \frac{h\nu_c}{m_e c^2} = 0.2 \frac{h\nu_c}{100\,\mathrm{keV}} \tag{8.17}$$

For each scattering, the energy gain $A = x_1/x$ of the photon is

$$A = 16\Theta^2 + 4\Theta + 1 \sim 1.9 \quad (\text{for } \Theta = 0.2) \tag{8.18}$$

If $\tau_T < 1$, to be checked a posteriori, we have a relation between the spectral shape, the amplification factor A and the optical depth:

$$\alpha_X = -\frac{\log \tau_T}{\log A} \longrightarrow \log \tau_T = -\alpha_X \log A \longrightarrow \tau_T = A^{-\alpha_X} = 0.5 \tag{8.19}$$

where the last equality assumes $\alpha_X = 1$ and $A \sim 2$. The Comptonization parameter y must be of the order of unity, because $A \sim y/\tau_T$. What derived here are typical values. There are sources where we need $\tau_T > 2$: for these sources the simple equation we have used to relate α_X, τ_T and A is not valid, and another relation must be used.

Why the corona is so hot, even if the disk is cold? What are the mechanisms able to extract energy from the accreting matter and to deposit it in the corona? We do not know exactly, even if we suspect that the magnetic field plays a crucial role.

8.7.2 Compton Reflection

If the corona emits isotropically, half of its flux will be intercepted by the disk. We have seen that the disk in AGNs should be relatively cold, in the sense that most of its material is not ionized. X-ray photons will interact with the material in the disk in the following ways:

1. at low energies ($h\nu < 10$ keV) they will be photoelectrically absorbed by the metals present in the disk;
2. at intermediate energies ($10 < h\nu < 40$ keV) they will be Thomson scattered and part of them will be scattered in the upward direction;
3. at large energies ($h\nu > 40$ keV) the scattering will not be in the Thomson regime, but Klein–Nishina effects will start to be important: the scattering is preferentially forward directed (and therefore the scattered photons will penetrate more deeply into the disk) and the photon energy will be reduced. The decrease of the energy means that photoelectric absorption, initially negligible, is again important, and the photon will be absorbed.

The result is that some of the incoming radiation will be scattered back, with a modified shape. This *Compton reflection* component will be peaked at ∼30 keV, where photoelectric absorption and Klein–Nishina effects are not important. See Fig. 8.5 to see the shape of this component, and how it modifies the original power law spectrum.

If the disk is hot, and partially ionized, the amount of free electrons will increase the importance of Thomson scattering, and the "left shoulder" of the Compton reflection increases. Increasing the ionization state of the disk implies that the Compton reflection is not peaked any longer, but it retains, at low energies, the slope of the original power law.

8.7.3 The Iron Line

Among the metals in the disk irradiated by the hot corona, Iron is the one producing the most prominent emission line. This is due to a combination of two factors: it is one of the most abundant elements (but not the most abundant), and it is the one "suffering" less from the Auger effect. This is, in very simple terms, a non-radiative transition: the energy of the $n = 2 \rightarrow n = 1$ transition is used to expel an electron from the atom instead of producing a photon. See the left panel of Fig. 8.5 to see the relative strength of the emission lines. The energy, luminosity, width, and profile of the Iron line are a powerful diagnostic of the condition of the inner parts of the accretion disk.

The energy of the Kα Fe line (from 6.4 to 6.7 keV) tells about the ionization state of the Iron, and thus the temperature of the disk.

The luminosity of the line tells about the amount of Iron, and thus about the abundance of metals of the disk. The ratio about the line to continuum luminosity tells about the geometry of the emitting region and possible anisotropy of the continuum.

The width of the line tells about the velocities of the irradiated material forming the line.

The profile (symmetric, double horned, skewed) tells about Doppler boosting and gravitational redshift.

The studies of Iron lines in AGNs received a lot of attention in the recent past. The most intriguing observation concerns the finding of *relativistically broadened lines*. Figure 8.6 shows in a schematic way what happens. Suppose to see an accretion disk from an intermediate angle (i.e. neither face on or edge on). If the emitting material is moving with a non relativistic velocity (Newtonian case, upper panel) we see a symmetric double peaked line, because the parts of the disk that are approaching us emit a line that we observe blue-shifted, while the parts of the disk moving away from us emit a line that we observe redshifted. The symmetry refers to the fact that the blue and red lines have equal fluxes. But if the material is orbiting very close to the black hole, the Doppler enhancement of the flux becomes important, and the blue peak will have more flux than the red one (second panel from the top). If the emission takes place *very* close to the black hole (within a few Schwarzschild radii) also the gravitational redshift is important: then all frequencies are redshifted by an amount that is larger as the emitting regions are closer to the black hole (third panel). Furthermore, we have to account for gravitational light bending, changing the emission pattern and thus the received flux.

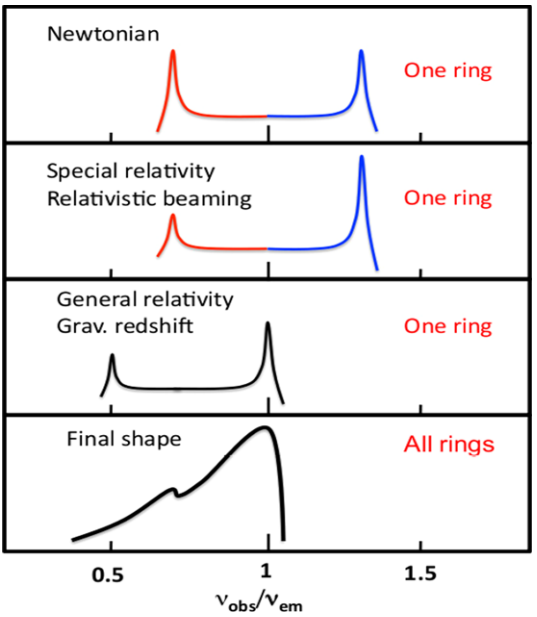


Fig. 8.6 Schematic profile of an intrinsically narrow emission line, modified by the interplay of Doppler/gravitational energy shifts, relativistic beaming, and gravitational light bending occurring in the accretion disc. *Upper panel*: the symmetric double—peaked profile from an annulus of a non-relativistic Newtonian disc. *Second panel*: the transverse Doppler shifts make the profiles redder; the relativistic beaming enhances the *blue peak* with respect to the *red*. *Third panel*: the gravitational redshift shifts the overall profile to the *red side* and reduces the *blue peak* strength. *Bottom panel*: The integration over all annuli gives rise to a broad, skewed line profile. See also Fabian & Miniutti [4]

All these effects have opened the way to *the possibility to test general relativity in the strong field case*.

Besides this, there is another, crucial effect, related to *the spin of the black hole.* This is conceptually simple: for a Kerr black hole fastly rotating the innermost stable orbit is not $3R_S$ (i.e. 6 gravitation radii $= 6R_g$), but it moves closer to the hole, becoming equal to one gravitational radius for a maximally rotating hole. The closer to the hole the emitting material is, the larger the velocities, and the stronger the gravitational effects. So the broadening of the line becomes larger, as it is illustrated in Fig. 8.7. *We can tell the spin of the black hole* by observing the profile of the Iron line.

8.8 The Torus and the Seyfert Unification Scheme

Seyfert galaxies are spiral galaxies with a bright core, that host an Active Galactic Nucleus. They come in two flavors: the Type 1 and the Type 2. Type 1 Seyferts have

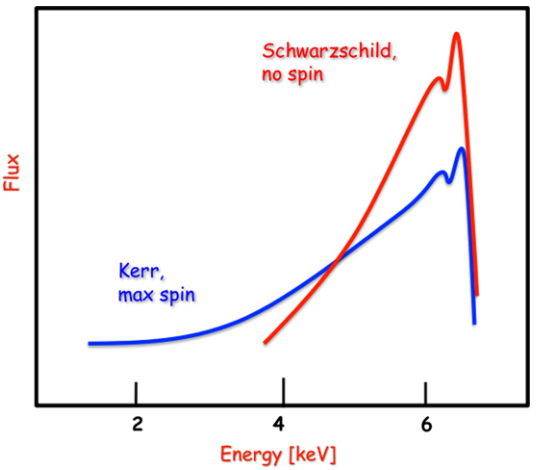


Fig. 8.7 How to distinguish a Schwarzschild (no spin) and a Kerr (maximally rotating) black hole. The Kα Fe line is broader in the case of the Kerr hole, since part of it is produced closer to the hole, and therefore it is more Doppler and gravitationally shifted. See also Fabian & Miniutti [4]

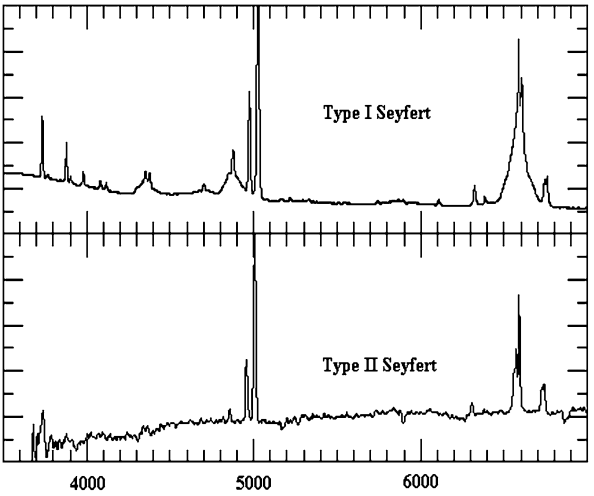


Fig. 8.8 The optical spectrum of a Seyfert Type 1 and Type 2. Note that Type 1 Seyferts have both broad and narrow lines, while Type 2 Seyferts have only narrow lines

both broad and narrow emission lines, while Type 2 have only narrow lines. See Fig. 8.8.

Antonucci & Miller [1] made spectropolarimetry observations of NGC 1068, a nearby and bright Seyfert 2 galaxy. In total light the broad lines were not seen, but in polarized light they emerged. Therefore the broad line clouds are there, but for some reason their emission is overwhelmed by the unpolarized continuum, and in total light their emission is not seen. Antonucci & Miller then argued that this is due to obscuration. Figure 8.9 illustrates the point. If there is a big and dusty torus surrounding the accretion disk, and the observer is looking from the side, the emission from the disk and the BLR is absorbed by the dust in the torus. Instead the narrow lines, coming from an extended region $\sim$100 pc in size, are not intercepted by the torus, and can reach observers located at any viewing angle.

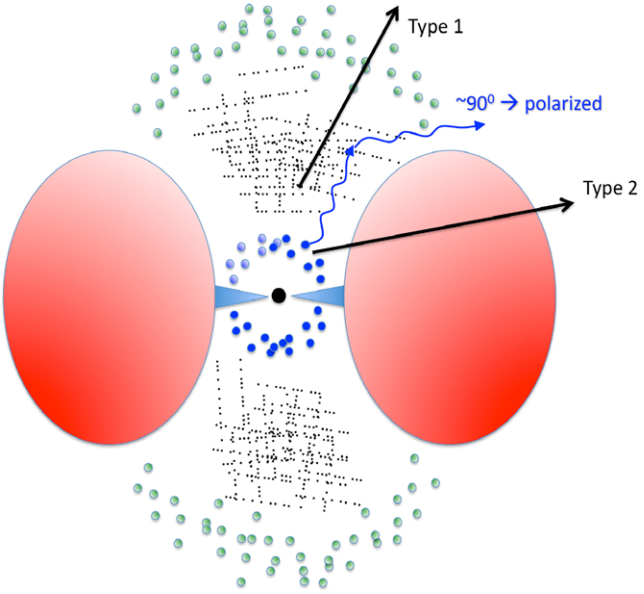


Fig. 8.9 Schematic illustration of the disk+torus system, with the *broad line* clouds that are close to the disk, and the *narrow line* clouds external to the torus. *Narrow lines* are then observable at all viewing angles, while side observers cannot see the disk and the BLR. However, if a populations of free electrons fill the region (*black little dots*), they can scatter the emission line photons into the line of sight. Since the scattering angle is close to 90°, the scattered photons are polarized. Observing in polarized light the broad emission lines emerge

Furthermore, if the "funnel" of the torus is filled with free electrons, they can scatter the emission of the disk and the broad lines also into the direction of side observers. The amount of this scattered radiation can be tiny, but it is polarized (remember: for scattering angles close to 90° the scattering photons are maximally polarized). Observing the polarized light we select these photons and discard the much more intense unpolarized light: as a result the broad lines now appear. *The free electrons act as a periscope.*

This simple idea implies that all Seyferts are intrinsically equal, but their appearance depends on the viewing angle: observers looking face on can see all the components (and thus also the broad lines): they see a Type 1 object. Observers looking from the side see only the narrow lines and the emission of the torus. Being at some distance from the accretion disk, the torus in fact intercepts part of the disk emission and re-emits it in the infrared. We can even predict approximately at which frequencies the torus emission will start to be important. This is because the dust cannot exist at temperatures hotter than ∼2000 K. Taking this temperature as reference, we have $\nu \sim 3kT/h \sim 10^{14}$ Hz, which corresponds to a wavelength of 3 μ. If we are correct, then we predict that all the radiation that the torus intercepts from the disk comes out at frequencies smaller than 10^{14} Hz.

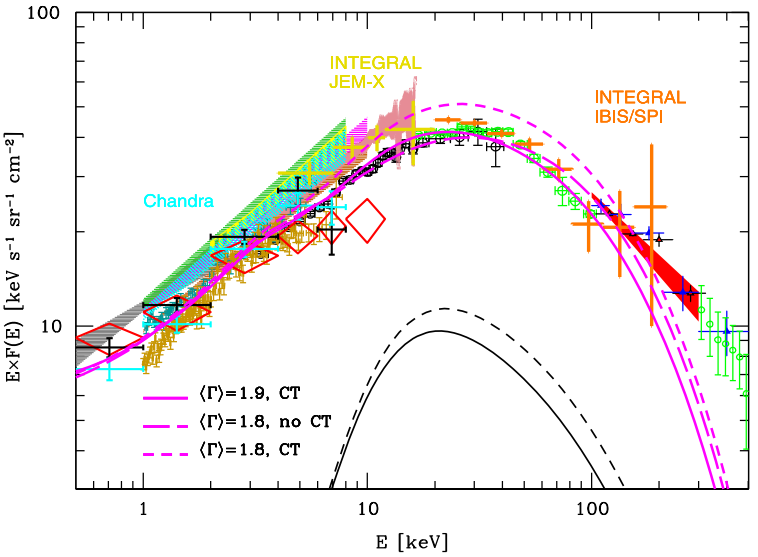


Fig. 8.10 The X-ray background. The lines are synthesis models assuming some prescriptions about the intrinsic slope of the X-ray spectrum and the ratio of "thick to thin" AGNs. From Gilli et al. [7]

8.8.1 The X-Ray Background

Another very important consequence of the presence of the torus concerns the X-ray emission, because also X-rays are absorbed by the torus, especially in the soft energy range (soft X-rays are much more absorbed than hard X-rays). In addition, the walls of the torus will also "reflect" X-rays, producing a "Compton reflection hump", like the disk. The main difference is that the fluorescent Iron line will in this case be extremely narrow (since the typical velocities of the torus material, located far from the black hole, are very small).

The importance of the absorption depends on the metals present along the line of sight. For solar abundances, there is a well defined relation between the amount of metals and the amount of hydrogen. So it is customary to express the amount of absorption in terms of the "column of hydrogen" along the line of sight. It is $N_{\rm H} = n_{\rm H} R$, where R is the size of the absorbing region, and $n_{\rm H}$ is the hydrogen number density. The units of $N_{\rm H}$ are thus cm^{-2}. When $N_{\rm H} > 10^{24}$ cm^{-2} we have that $\tau_{\rm T} = \sigma_{\rm T} N_{\rm H}$ becomes close or larger than unity, and we speak of *Compton thick* sources.

With these properties, a mixture of Type 1 and Type 2 objects can account for the *X-ray background*, namely, the integrated X-ray emission from all sources. It was a mystery for decades, because its spectrum in the 0.5–10 keV energy range is very hard ($\alpha_X \sim 0.4$), unlike most of the known extragalactic X-ray sources (that have $\alpha_X \sim 1$). Figure 8.10 shows a modern collection of data defining the X-ray background from 0.5 to 300 keV.

To explain it, we need a population of very hard X-ray sources and the Type 2 ones have indeed the right properties: since soft X-rays are more absorbed than hard ones, their spectrum is very hard. Since the X-ray continuum is depressed, but the reflection hump (from the torus) is not, they can contribute significantly at $\sim$30 keV, just where the X-ray background peaks.

8.9 The Jet

About 10 % of AGNs, besides accreting matter, are able to expel part of it at relativistic speeds in two oppositely directed jets. These *radio-loud* AGNs were the first to be discovered, due to their relevant radio emission. Radio jets can be spectacular, since they can reach a few Mpc in size, tens of times the radius of their host galaxies. AGNs with relativistic jets were believed to always have giant ellipticals as host galaxies, but now this paradigm is challenged by the observations of Narrow Line Seyfert 1 Galaxies (beware that the term "narrow" here indicates lines that are in any case broad, but "less" broad than usual, namely with FWHM < 2000 km s^{-1}).

The radio emission produced by jets is only a small fraction of the entire electromagnetic power they emit. We now know that most of it is produced in the range mm-optical and in the γ-ray band. In turn, the electro-magnetic output is only a small fraction of the total power carried by the jet. Most of it is carried in the form of bulk kinetic energy of the matter flowing relativistically, and by the moving magnetic field (i.e. Poynting flux); in powerful sources it reaches the large radio structure: the hot spots and the radio lobes. In less powerful sources, however, these structures are absent. We call the powerful sources *FR II* radio-galaxies, and the weaker sources *FR I* radio-galaxies. The name FR comes from Fanaroff & Riley, that classified radio-galaxies in this way.

8.9.1 Flat and Steep Radio AGNs

Since the emitting material is moving with a bulk Lorentz factor Γ, its radiation is beamed. What we see is therefore amplified if the jet points at us, and depressed if the jet points elsewhere. The large structures (hot spots and radio-haloes), instead, are not moving, and their emission is isotropic. The ratio between the jet emission and the radio-lobe emission is thus a strong function of the viewing angle.

Figure 8.11 illustrates this point: the jet is producing a very flat spectrum [i.e. $F(\nu) \propto \nu^0$] up to 10^{12} Hz. The observed intensity is $I_{\rm jet}(\nu) \propto \delta^3 I'_{\rm jet}(\nu')$, and changes a lot changing the viewing angle. The emission coming from the extended, unbeamed, region is characterized by a steeper slope [for instance: $I_{\rm lobe}(\nu) \propto \nu^{-1}$]. Therefore:

- At very low frequencies we expect that the emission is always dominated by the lobe, for all viewing angles.
- Lobe and jet emission are equal at some frequency that is larger as the viewing angle increases.

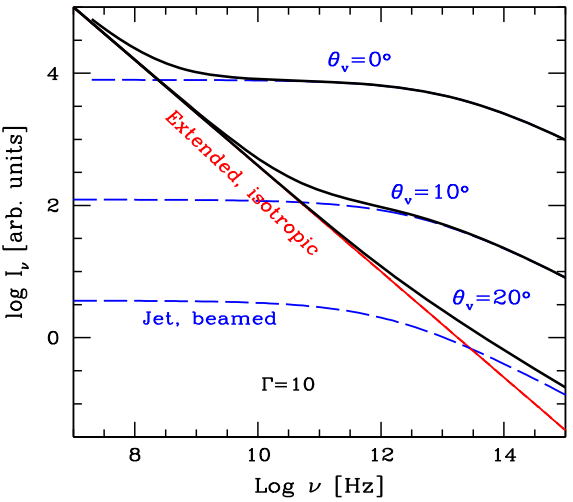


Fig. 8.11 The emission of the jet is beamed, and depends on the viewing angle θ_v. Since it is a superposition of emission from several blobs of different sizes, the spectrum is flat up to the self-absorption frequency of the most compact component (hundreds of GHz). The emission from the radio-lobe is instead isotropic, and is optically thin. Since it is not beamed, it *does not* depend on the viewing angle. The overall appearance of the radio spectrum depends therefore on the viewing angle. Steep radio spectra correspond to large θ_v (and small δ), flat radio spectra to small θ_v (and large δ)

- For misaligned jets the depressing factor due to beaming is so large that we do not see the jet, we see only the lobe emission.
- Aligned sources show a *flat radio spectrum*. Misaligned sources show a *steep radio spectrum*. The slope of the radio spectrum is thus an indication of the viewing angle.
- If we perform a radio survey with some limiting flux, the number of aligned and misaligned sources changes according to the observing frequency: if we use 178 MHz, we preferentially look at the lobe emission, and we can pick up aligned and misaligned sources; if we observe at 30 GHz we pick up preferentially the flat, aligned sources.

To summarize, and simplifying a bit:
flat radio spectrum $\longrightarrow$ **aligned, beamed**
steep radio spectrum $\longrightarrow$ **misaligned, de-beamed**.

8.9.2 Blazars

Sources whose jet is pointing at us are called *blazars*. The sub-classification of blazars is rather complex, reflecting either the way they were discovered (radio or

X-rays) or the location of their synchrotron peak (in νF_ν), or the presence or absence of broad emission lines. Particularly relevant in this respect is the concept of *equivalent width of a line* (EW). It is defined as

$$EW = \int \frac{F_0 - F_\lambda}{F_0} d\lambda \tag{8.20}$$

where F_λ is the total flux (line + continuum) and F_0 is the flux of the continuum. This describes the EW of both absorption and emission lines, but in the case of emission lines the result is negative, so sometimes the absolute value is given. The units of the EW are Å.

The classical subdivision of blazars is

BL Lac objects (BL Lacs)—They have weak or absent lines. Their equivalent width is EW < 5 Å.
Flat Spectrum Radio Quasars (FSRQs)—They have strong emission lines, whose EW > 5 Å.

Since we are considering very variable objects, this subdivision depends on the state of the source when it is observed: this is because the EW is a ratio between the line and (beamed) optical flux, and the latter varies. Now we believe that the absence or weakness of the lines in BL Lacs is not due to a particularly amplified continuum, but it is an intrinsic property. In other words, the luminosity of the lines in BL Lacs is less than in FSRQs.

The Overall Spectrum of Blazars

Figure 8.12 shows the source 3C 454.3, a powerful FSRQ, that was the brightest blazar detected in the γ-ray band for a few years. One can see the extraordinary variability, encompassing 2 orders of magnitude in flux, both in the γ-ray band and in the optical. When the optical flux is in the low state, one can also see the contribution of the accretion disk (see the little upturn of the optical-UV data at 10^{15} Hz). The dashed black line illustrates a model for the disk emission (10^{15} Hz) and the torus emission (at 10^{13} Hz).

Radio sources in general, and blazars in particular, emit over the entire electromagnetic spectrum, from the radio (down to 10^7 Hz) to the TeV band (up to 10^{27} Hz). The main characteristics are:

- The overall spectral energy distribution (SED), once plotted in νF_ν, shows two broad peaks. The location of the peak frequencies varies from object to object, but in general the first peak is between the mm and the soft-X-rays, while the high energy peak is in the MeV–GeV band.
- They are variable, at all frequencies, but especially at high energies. Minimum variability timescales range between weeks and tens of minutes.
- In restricted frequency ranges, their spectrum is a power law.
- The variability is often (even if not always) coordinated and simultaneous in different energy bands (excluding the radio).

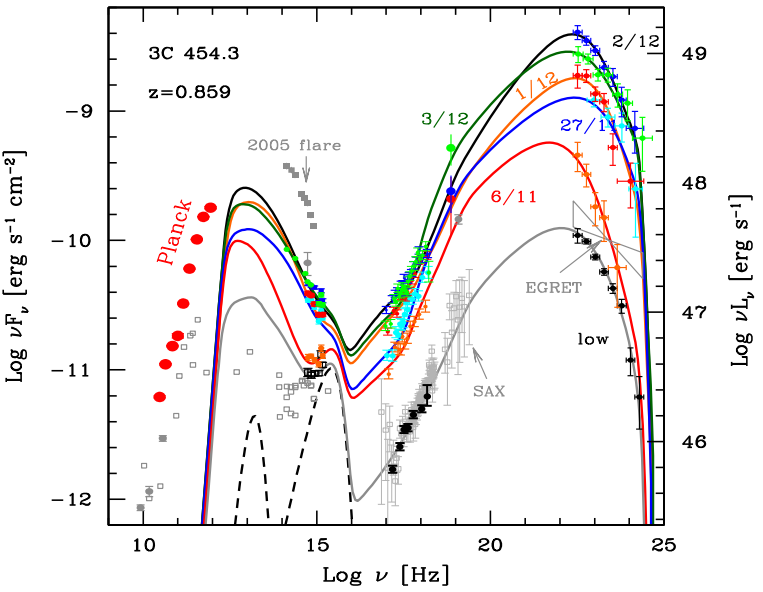


Fig. 8.12 The overall electromagnetic spectrum of 3C 454.3, the most luminous γ-ray source up to now. Note the large amplitude variability, even day-by-day. Dates refer to the year 2009. Lines correspond to fitting models. See Bonnoli et al. [2]

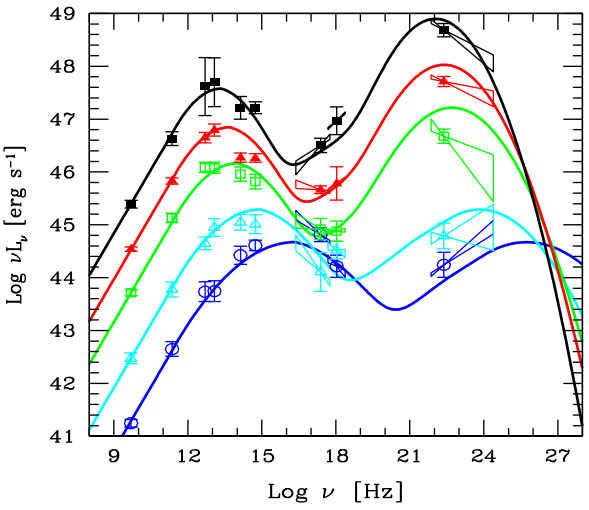


Fig. 8.13 The blazar sequence. As the bolometric luminosity increases, the peak of the two humps shifts to smaller frequencies, and the high energy hump becomes more important. From Fossati et al. [5]; Donato et al. [3]

- They are often polarized, in the radio and in the optical.
- The high energy hump often dominates the power output.

Besides these common features, it seems that blazars form a sequence of SEDs, according to their observed bolometric luminosity. Figure 8.13 illustrates this point. It was constructed taking the average luminosity in selected bands, and consider-

ing ∼100 blazars coming from radio and X-ray complete samples (complete here means: it contains all blazar whose flux is greater than a limiting one). Note that:

- Low power blazars, that are BL Lacs (i.e. no lines), are *bluer* than powerful blazars, that are FSRQs (with lines). Bluer means that the peak frequencies of both peaks are larger.
- The high energy hump increases its relevance as we increase the bolometric luminosity. At low luminosities both humps have the same power, while the most powerful FSRQ have a high energy hump that is $\sim 10\times$ the low energy one.

Interpretation of the SED of Blazars

First Hump It is rather straightforward to interpret the first hump of the SED as synchrotron emission. Since it sometimes varies rapidly and simultaneously (at least in optical-UV-soft-X-rays bands) we believe that it comes from a single region of the jet.

High Energy Hump It is believed (but with no unanimity) that it is produced by the Inverse Compton process, by the same electrons producing the synchrotron. The seed photons could be the synchrotron photons themselves (especially in low power blazars) and/or the emission line photons (when the lines are present, so only in powerful objects...). Remember that in the comoving frame of the jet, the lines are seen blue-shifted (factor Γ) and the arrival time is contracted (another factor Γ) so that in the comoving frame the radiation energy density of the lines is seen enhanced by Γ^2.

Simple Estimates

Suppose to know the luminosity of both peaks of a blazar, call them L_S and L_C, and the location of their peak frequency ν_S and ν_C. You also have information about the minimum variability timescale t_{var}. Assume that the emitting region is only one, and approximate it with a sphere of radius R.

Let us consider two cases. For the first we will assume that the high energy emission is due to the synchrotron self-Compton process (SSC), in the second we will assume that it is due to inverse Compton on the photons of the broad line region. For both cases the size R is given by

$$R \sim c t_{var} \frac{\delta}{1+z} \tag{8.21}$$

SSC In this case the ratio between L_C and L_S is given by:

$$\frac{L_C}{L_S} = \frac{U'_{rad}}{U'_B} = \frac{L_S}{4\pi R^2 c \delta^4} \frac{1}{U'_B} \tag{8.22}$$

where primed quantities refer to the comoving frame. Note the δ^4 factor to pass from the observed to the comoving luminosity. We have assumed that U'_{rad} is en-

tirely due to the synchrotron luminosity, with no contribution from the SSC one. Is that correct? It is, if most of the SSC radiation is at frequencies so large that the corresponding scattering process occurs in the Klein–Nishina regime, and thus can be neglected. From Eq. 8.22 we can derive ($U'_{\rm B} = B'^2/8\pi$):

$$B'\delta^2 = \frac{L_{\rm S}}{R}\left(\frac{2}{cL_{\rm C}}\right)^{1/2} \longrightarrow B'\delta^3 = (1+z)\frac{L_{\rm S}}{ct_{\rm var}}\left(\frac{2}{cL_{\rm C}}\right)^{1/2} \tag{8.23}$$

Now let us use the peak frequencies: the ratio between them is

$$\frac{\nu_{\rm C}}{\nu_{\rm S}} = \gamma^2_{\rm peak} \tag{8.24}$$

Note that this is a *ratio*, therefore there is no δ, no $(1+z)$. The observed synchrotron peak frequency is given by

$$\nu_{\rm S} \sim \frac{4}{3}\nu'_{\rm B}\gamma^2_{\rm peak}\frac{\delta}{1+z} = \frac{4}{3}\frac{eB'}{2\pi m_{\rm e}c}\gamma^2_{\rm peak}\frac{\delta}{1+z} \tag{8.25}$$

Inserting Eq. 8.24 we arrive to

$$B'\delta = \frac{3\pi m_{\rm e}c}{2e}\frac{\nu_{\rm S}^2}{\nu_{\rm C}}(1+z) = \frac{1}{3.7\times10^6}\frac{\nu_{\rm S}^2}{\nu_{\rm C}}(1+z) \tag{8.26}$$

We have two equations (Eq. 8.23 and Eq. 8.26) for the two unknowns B' and δ.

Example SSC Figure 8.14 shows the SED of the BL Lac 0851 + 201 (=0J 287), at $z = 0.306$. For this source we have: $L_{\rm C} \sim L_{\rm S} \sim 10^{46}$ erg s^{-1}. We can guess $\nu_{\rm C} \sim 10^{20}$ Hz extrapolating the X-ray and the γ-ray spectra. Let us take $\nu_{\rm S} \sim 5\times10^{13}$ Hz, and assume that $t_{\rm var} = 10^4$ s.

From Eq. 8.23 we have $B'\delta^3 = 3.5\times10^3$ G and from Eq. 8.26 we derive $B'\delta = 8.8$ G. Therefore $\delta = 20$ and $B' = 0.44$ G. Notice that if $\nu_{\rm C}$ were 10^{21} Hz instead of 10^{20} Hz, than we would have found $\delta = 63$ and $B' = 0.014$ G. These estimates are very sensitive to the $\nu_{\rm C}/\nu_{\rm S}$ ratio. The larger the separation between the two peaks, the larger δ and the smaller B'.

Inverse Compton with Broad Line Photons In this case let us assume that most of the radiation energy density in the comoving frame comes from the BLR. We have

$$U'_{\rm rad} \sim \Gamma^2\frac{L_{\rm BLR}}{4\pi R^2_{\rm BLR}c} \tag{8.27}$$

We may remember that $L_{\rm BLR} \sim 0.1L_{\rm disk}$, and that $R_{\rm BLR} \sim 10^{17}L_{\rm ion,45}$ cm. This assumptions lead to (assuming that $L_{\rm ion} \sim L_{\rm disk}$):

$$U'_{\rm rad} \sim \frac{\Gamma^2}{12\pi} \tag{8.28}$$

a remarkable result, due to the $R_{\rm BLR} \propto L^{1/2}_{\rm disk}$ dependence. As long as the emitting region of the jet is within the BLR, then $U'_{\rm rad}$ depends only from Γ, but not on the

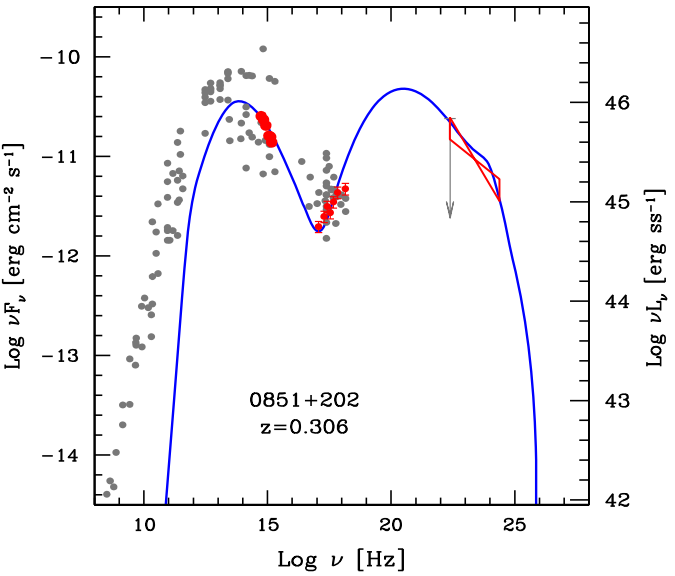


Fig. 8.14 The SED of the BL Lac 0851 + 202, together with a fitting model. *Red points* are simultaneous, *grey points* are archival data

power of the disk or the actual value of the size of the BLR. By making the ratio with $U'_{\rm B}$ we have

$$\frac{L_{\rm C}}{L_{\rm S}} = \frac{U'_{\rm rad}}{U'_{\rm B}} = \frac{2\Gamma^2}{3B'^2} \longrightarrow \frac{B'}{\Gamma} = \left(\frac{2L_{\rm S}}{3L_{\rm C}}\right)^{1/2} \tag{8.29}$$

The synchrotron peak frequency is still given by Eq. 8.25, *if* $\nu_{\rm S}$ *is larger than the self absorption frequency* $\nu_{\rm t}$. The peak frequency of the Compton hump is now given by:

$$\nu_{\rm C} = \frac{4}{3}\gamma^2_{\rm peak}\nu_{{\rm Ly}\alpha}\frac{\delta\Gamma}{1+z} \tag{8.30}$$

where we have taken the frequency of the Lyα line as the characteristic frequency of the seed photons (since the Lyα line is the most intense). The factor $\Gamma\delta$ comes from considering the scattering in the comoving frame, where the typical frequency is $\nu'_{{\rm Ly}\alpha} \sim \Gamma\nu_{{\rm Ly}\alpha}$, and then blueshifting the frequency after the scattering in the comoving frame by the factor δ. Making the ratio $\nu_{\rm C}/\nu_{\rm S}$ we have

$$\frac{\nu_{\rm C}}{\nu_{\rm S}} = \frac{(4/3)\gamma^2_{\rm peak}\nu_{{\rm Ly}\alpha}\delta\Gamma/(1+z)}{(4/3)\gamma^2_{\rm peak}\nu'_{\rm B}\delta/(1+z)} = \frac{\Gamma\nu_{{\rm Ly}\alpha}}{\nu'_{\rm B}} \tag{8.31}$$

From this equation we have:

$$\frac{B'}{\Gamma} \sim 8.8\times10^8\frac{\nu_{\rm S}}{\nu_{\rm C}} \tag{8.32}$$

Unfortunately, Eq. 8.32 and Eq. 8.29 give two relations for the same quantity: B'/Γ. We cannot derive B' and Γ separately. But we can use them to derive a relation between the peak frequencies and the synchrotron and inverse Compton luminosities:

$$\frac{\nu_C}{\nu_S} \sim 10^9 \left(\frac{L_C}{L_S}\right)^{1/2}; \quad \nu_S > \nu_t \tag{8.33}$$

This can be thought as a *consistency check*, to see if our assumption of inverse Compton on the BLR photons is reasonable. Instead, to the aim to derive the parameters, we have to use additional information. One important information comes from the *superluminal motion* of the sources. Usually, it is observed at 5–22 GHz. At these frequencies the flux is due to a region of the jet self-absorbing there. This region *is not* the same as the one producing most of the emission (we know it because of variability: most of the emission is produced in a much more compact region, self-absorbing at $\nu_t \sim$ 100–1000 GHz). Therefore we must make the assumption that both the viewing angle and the bulk Lorentz factor do not change from the two regions. If this is true, and assuming that the viewing angle is $\theta_v \sim 1/\Gamma$, we can set

$$\Gamma \sim \beta_{app} \tag{8.34}$$

and thus solve for B'. Additional information may come from the details of the SED, if we see some signs of the SSC emission: even if not dominating the bolometric luminosity, it may contribute, especially in the X-rays.

Example EC By EC we mean "External Compton", namely that the relevant seed photons for scattering are produced *externally* to the jet, as in the case of the BLR photons. Suppose that we observe a source as the one shown in Fig. 8.15. Assume $\beta_{app} = 10$. From the figure $L_C/L_S = 10$. Assume $\nu_C \sim 10^{22}$ Hz. We do not observe directly the synchrotron peak, but the radio spectrum is flat ($\propto \nu^0$) and the optical emission is steep [i.e. $F(\nu) \propto \nu^{-1.5}$ in the optical, once the contribution from the accretion is subtracted].

From Eq. 8.29 we have $B'/\Gamma = 0.26$. Assuming $\Gamma = \beta_{app}$, we derive $B' = 2.6$ G. From Eq. 8.32 we have $\nu_S = \nu_C(B'/\Gamma)/8.8 \times 10^8 = 3 \times 10^{12}$ Hz. Is that consistent with what we observe? Yes: the radio and optical spectrum indicate a peak (in νF_ν) between the last observable radio frequencies (usually 100 GHz $= 10^{11}$ Hz) and the optical spectrum. The value of $\nu_S = 3 \times 10^{12}$ Hz is larger than the self-absorption frequency of our emitting region.

8.9.3 The Power of the Jet

It is not easy to estimate the total power of the jet. There are a few ways to do it, including studying the energy content of the radio lobes, thought to be the calorimeter of the source, and, more recently, the energy required for the jet to produce an "X-ray cavity" in cluster of galaxies, around the central giant galaxies that are also radio-loud sources.

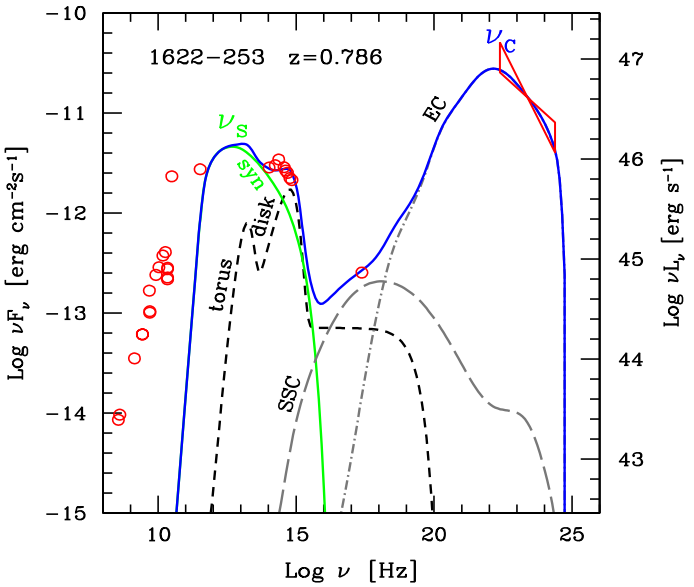


Fig. 8.15 The SED of the blazar 1622–253, together with a fitting model. The peak of the Compton emission $\nu_C = 10^{22}$ Hz, and the ratio $L_C/L_S = 10$. The figure shows also the contribution from the accretion disk, its X-ray corona and the IR torus (*short dashed line*) and SSC (*long dashed*)

The jet power has different components:

- The jet emits, and the produced radiation must be at the expenses of the jet power. Calculating the power (in all directions) in the form of radiation sets a lower limit to the jet power.
- The jet transports matter. If anything, we must have the electrons responsible for the radiation we see. They are relativistic in the comoving frame (lower case γ), and have also a relativistic bulk motion (capital Γ).
- The jet transports also protons. How many? This is controversial, because if the emission is totally produced by electron–positrons, there are no protons. If instead the emitting plasma is a normal electron–proton one, than there is one proton per emitting electron.
- The jet transports a magnetic field. There is a Poynting flux.

All these components can be formally accounted for by writing

$$P_i = \pi R^2 \Gamma^2 \beta c U'_i \tag{8.35}$$

where U'_i is the comoving energy density of the i*th* component: when dealing with the emitting electrons we will have

$$U'_e = m_e c^2 \int \gamma N(\gamma) d\gamma = \langle\gamma\rangle n'_e m_e c^2 \tag{8.36}$$

When dealing with the magnetic field we have

$$U'_{\rm B} = \frac{B'^2}{8\pi} \tag{8.37}$$

and when dealing with the radiation we have

$$U'_{\rm rad} = \frac{L'}{4\pi R^2 c} = \frac{L}{4\pi R^2 c \delta^4} \tag{8.38}$$

For the protons, assuming them cold,

$$U'_{\rm p} = U'_{\rm e} \frac{m_{\rm p}}{m_{\rm e}} \frac{n'_{\rm p}}{\langle\gamma\rangle n'_{\rm e}} \tag{8.39}$$

The logic is the following: we sit at some place along the jet, stationary with respect to the black hole, and cut a cross sectional surface of the jet. We count how many photons, protons, electrons and magnetic field are passing by in one second. One factor Γ accounts for the different mass or energy as seen in the lab frame (i.e. a proton will have a mass $\Gamma m_{\rm p}$) and the other factor Γ comes because the density we see is more than the comoving density (lengths are smaller in the direction of motion). This is a flux of energy, i.e. a power.

It is found that the jet is powerful, often as powerful as the accretion disk, and sometimes more. Furthermore, the jet of powerful blazars *cannot be* dominated by the Poynting flux. This is to be expected, since the synchrotron component in these sources is only a minor fraction of the bolometric luminosity, dominated by the inverse Compton component. This limits the possible values of the magnetic field.

8.9.4 Lobes as Energy Reservoirs

It is also found that the energy dissipated into radiation is only a minor fraction of the jet power, at least in powerful FSRQs. Most of the power goes to energize the lobes. There, we have a relaxed region, in the sense that the dimensions are huge, and the magnetic field must be small (i.e. $B \sim 10^{-5}$ G). Large dimensions also means that the radiation energy density is small. Therefore the radiative cooling timescales are very long. Particles have not enough time to emit their energy, that instead goes to increase the dimension of the region. Extended radio lobes are therefore a reservoir of the energy that the jet has provided through the years. If we could measure the energy content of the lobe and its lifetime, than we could measure (E/t): the *average* power of the jet.

Lobes emit in the radio, through synchrotron radiation. They are so big that we can easily resolve them. So we know their size. To produce synchrotron radiation, there must be some magnetic field and relativistic particles. For a given observed synchrotron luminosity, we could have relatively large magnetic fields and fewer

particles, or, on the contrary, less magnetic field and more particles. These solutions are not energetically equivalent, as we shall see. When the energy content in the magnetic field and particles balance, then we have the minimum total energy. To see this, consider a lobe of size $R_{\rm lobe}$ emitting $L_{\rm lobe}$ by synchrotron:

$$\begin{aligned} L_{\rm lobe} &= \frac{4\pi}{3} R_{\rm lobe}^3 m_{\rm e} c^2 \int N(\gamma) \dot{\gamma}_{\rm S} d\gamma \\ &= \frac{4\pi}{3} R_{\rm lobe}^3 \frac{4}{3} \sigma_{\rm T} c \frac{B^2}{8\pi} \langle \gamma^2 \rangle n_{\rm e} \end{aligned} \tag{8.40}$$

This gives $n_{\rm e}$:

$$n_{\rm e} = \frac{9 L_{\rm lobe}}{2 R_{\rm lobe}^3 \sigma_{\rm T} c B^2 \langle \gamma^2 \rangle} \tag{8.41}$$

The energy contained in the magnetic field is

$$E_{\rm B} = \frac{4\pi}{3} R_{\rm lobe}^3 \frac{B^2}{8\pi} \tag{8.42}$$

The energy contained in the particles depends if we have cold or hot protons. We do not know. We can parametrize our ignorance saying that the proton energy is k times the energy contained in the relativistic electrons. Therefore the particle energy in the lobe is

$$\begin{aligned} E_{\rm e,p} &= \frac{4\pi}{3} R_{\rm lobe}^3 \langle \gamma \rangle n_{\rm e} m_{\rm e} c^2 (1+k) \\ &= 6\pi \frac{\langle \gamma \rangle m_{\rm e} c^2}{\langle \gamma^2 \rangle} \frac{L_{\rm lobe}}{\sigma_{\rm T} c B^2} (1+k) \end{aligned} \tag{8.43}$$

Note the dependence on B^2: $E_{\rm B} \propto B^2$, while $E_{\rm e,p} \propto 1/B^2$.

Due to these scalings, the total energy $E_{\rm tot} = E_{\rm B} + E_{\rm e,p}$ *will have a minimum* for $E_{\rm B} = E_{\rm e,p}$. This condition of minimum energy also corresponds to *equipartition*. Figure 8.16 shows an example, for which the *equipartition magnetic field* is $B_{\rm eq} \sim 10^{-5}$ G: with this field we minimize the total energy requirement. In the specific case illustrated in Fig. 8.16, the minimum energy contained in the lobe is $E_{\rm tot} \sim 10^{60}$ erg. If we knew its lifetime, we could calculate the average jet power. Assuming 10 million years $\sim 3 \times 10^{14}$ s, we have $\langle P_{\rm jet} \rangle \sim 3 \times 10^{45}$ erg s^{-1}. In this case the lobe synchrotron luminosity is only a tiny fraction (i.e. $\sim 3 \times 10^{-3}$) of the jet power. This estimates neglects adiabatic losses, likely to be important. Suppose to include them: how they modify the estimate on the average jet power?

8.10 Open Issues

Research in the AGN field is still active, because the open issues are many. The previous notes tried to give a glimpse of the "common wisdom" picture of the main-

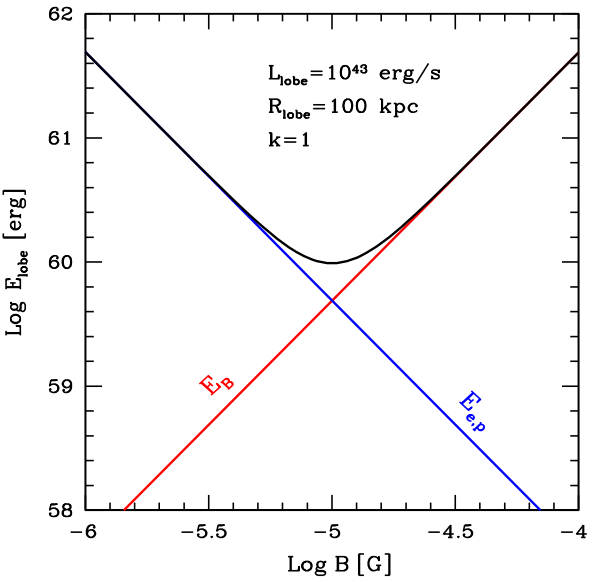


Fig. 8.16 The energy contained in the lobe in magnetic field (E_B) and in particles ($E_{e,p}$). The *black line* is the sum. We have assumed that the lobe of 100 kpc in size emits synchrotron luminosity $L_{lobe} = 10^{43}$ erg s^{-1} and that protons have the same energy of the emitting electrons (i.e. $k = 1$). For the particle distribution, we have assumed $\gamma_{min} = 1$, $\gamma_{max} = 10^5$ and $p = 2.5$ [i.e. $N(\gamma) \propto \gamma^{-2.5}$]

frame about AGNs, but we should avoid to take it as absolutely not controversial. The following is an incomplete list of open problems.

- **Black hole masses.** We have several ways to estimate the black hole masses, but the uncertainties are still large. Knowing the mass more precisely, we could know all the quantities in Eddington units, which is more physical.
- **Black hole growth.** When did the supermassive black hole form? It takes time to build them up. Can we live with black hole seeds of stellar size or do we need something more exotic?
- **Accretions modes.** When the density is small, protons cannot interact efficiently with electrons (responsible for the emitted radiation and the cooling). The energy remain in the protons, that do not cool. The pressure increases, and the disk puffs up, and the density becomes smaller still. At what accretion rate is there the transition? Are Coulomb collisions the only way for protons and electrons to interact?
- **What is the broad line region?** We still do not know if it is an ensemble of clouds in Keplerian motion, or some form of inflow or outflow.
- **The infrared "torus".** It should be unstable. Is it formed by a clumpy medium? Can it be, instead, a tilted disk? Where does it begin: is it a separate structure or just a continuation of the disk?
- **The acceleration mechanisms in the jet.** Shocks are the best bet, but shocks accelerate protons more than electrons. Accounting for hot (and relativistic) protons would increase the estimates for the jet power. What is the role of magnetic reconnection?

- **The power of jets.** We just started to estimate them in a reliable way, but we are still far from robust conclusions. Main uncertainties: the amount of electron–positron pairs, and the contribution of hot protons.
- **The spin of the black hole.** The rotational energy of the black hole is a huge energy reservoir that can be extracted. Does the black hole spin rapidly? Is it the spin energy that is used to accelerate relativistic jets? Is the spin at the root of the radio-loud/radio-quiet dicotomy?

References

1. Antonucci, R.R.J., Miller, J.S.: Spectropolarimetry and the nature of NGC 1068. Astrophys. J. **297**, 621 (1985)
2. Bonnoli, G., Ghisellini, G., Foschini, L., Tavecchio, F., Ghirlanda, G.: The γ-ray brightest days of the blazar 3C 454.3. Mon. Not. R. Astron. Soc. **410**, 368 (2011)
3. Donato, D., Ghisellini, G., Tagliaferri, G., Fossati, G.: Hard X-ray properties of blazars. Astron. Astrophys. **375**, 739 (2001)
4. Fabian, A.C., Miniutti, G.: The X-ray spectra of accreting Kerr black holes. In: Wiltshire, D.L., Visser, M., Scott, S.M. (eds.) Kerr Spacetime: Rotating Black Holes in General Relativity, Cambridge University Press, Cambridge (2005). astro-ph/0507409
5. Fossati, G., Maraschi, L., Celotti, A., Comastri, A., Ghisellini, G.: A unifying view of the spectral energy distributions of blazars. Mon. Not. R. Astron. Soc. **299**, 433 (1998)
6. Giacconi, R., Gursky, H., Paolini, F., Rossi, B.: Evidence for X-rays from sources outside the solar system. Phys. Rev. Lett. **9**, 439 (1962)
7. Gilli, R., Vignali C, C.A., Hasinger, G.: Compton-thick AGN and the synthesis of the cosmic X-ray background: The Suzaku perspective. In: Proceedings of "The Extreme Universe in the Suzaku Era". Prog. Theor. Phys. Suppl. (2007). astro-ph/0704.1376
8. Greenstein, J.L., Matthews, T.A.: Red-shift of the unusual radio source: 3C 48. Nature **197**, 1041 (1963)
9. Hazard, C., Mackey, M.B., Shimmins, A.J.: Investigation of the radio source 3C 273 by the method of lunar occultations. Nature **197**, 1037 (1963)
10. Lynden-Bell, D.: Galactic nuclei as collapsed old quasars. Nature **223**, 690 (1969)
11. Oke, J.B.: Absolute energy distribution in the optical spectrum of 3C 273. Nature **197**, 1040 (1963)
12. Salpeter, E.E.: Accretion of interstellar matter by massive objects. Astrophys. J. **140**, 796 (1964)
13. Schmidt, M.: 3C 273: a star-like object with large red-shift. Nature **197**, 1040 (1963)
14. Schmidt, M.: In: Bertotti, E.B., Balbinot, R., Bergia, S. (eds.) Modern Cosmology in Retrospect, p. 347. Cambridge University Press, Cambridge (1990)
15. Shakura, N.I., Sunjaev, R.A.: Black holes in binary systems. Observational appearance. Astron. Astrophys. **24**, 337 (1973)
16. Zeldovich, Ya.B.: Dokl. Akad. Nauk SSSR **157**, 67 (1964)

Further Reading

In the following I list some books about high energy astrophysics and Active Galactic Nuclei that can be useful to explore in more detail the issues discussed in these notes.

G.B. Rybicki and A.P. Lightman. *Radiative Processes in Astrophysics*. Wiley & Sons (New York)

J.D. Jackson. *Classical Electrodynamics*. Wiley & Sons (New York)

C.D. Dermer & G. Menon. *High Energy Radiation from Black Holes. Gamma Rays, Cosmic Rays and Neutrinos*. Princeton Series in Astrophysics. Princeton University Press (Princeton, New Jersey)

F. Melia. *High-Energy Astrophysics*. Princeton Series in Astrophysics. Princeton University Press (Princeton, New Jersey)

M.S. Longair. *High Energy Astrophysics*. Cambridge University Press (Cambridge, UK)

F.A. Aharonian. *Very High Energy Cosmic Gamma Radiation. A Crucial Window on the Extreme Universe*. World Scientific

J. Krolik. *Active Galactic Nuclei. From the Black Hole to the Galactic Environment*. Princeton Series in Astrophysics. Princeton University Press (Princeton, New Jersey)

J. Frank, A.R. King & D.J. Raine. *Accretion Power in Astrophysics*. Cambridge University Press (Cambridge, UK)

A.K. Kembhavi & J.V. Narlikar. *Quasars and Active Galactic Nuclei. An Introduction*. Cambridge University Press (Cambridge, UK)

D. De Young. *The Physics of Extragalactic Radio Sources*. The Univ. of Chicago Press (Chicago & London)

G. Ghisellini, *Radiative Processes in High Energy Astrophysics*,
Lecture Notes in Physics 873, DOI 10.1007/978-3-319-00612-3,

© Springer International Publishing Switzerland 2013

Index

Symbols
3C 48, 112, 113
3C 273, 112, 113
3C 454.3, 130

A
Aberration, 36, 37, 51
Absorption, 9, 11
Absorption coefficient, 6, 25, 62
Absorption optical depth, 63
Acceleration field, 19
Accretion disk, 41, 42, 106, 113, 115, 120, 137
Accretions modes, 139
Active galactic nuclei, 107
Adiabatic losses, 138
AGNs, 41
Angular distance, 41
Angular radius of the source, 56
Angular resolution, 93
Annihilation line, 71
Ariel 5, 111
Auger effect, 123
Average gain per scattering, 83
Average number of scatterings, 83

B
Beaming, 31
Beaming angle, 51
Beaming cone, 51
Beaming factor, 41
Bessel function, 52
BL Lac objects, 130
Black body, 26, 27
Black hole, 95, 111, 113
Black hole growth, 139
Black hole masses, 139
Black-body, 10
Black-body radiation, 116
Blazar sequence, 131
Blazars, 95, 109, 113, 129, 137
Blob, 38, 40
Bolometric luminosity, 1
Bremsstrahlung, 23, 26, 121
Brightness temperature, 28, 41, 57
Broad emission lines, 118
Broad line clouds, 42, 125
Broad Line Region (BLR), 41, 113, 119
Bulge, 114
Bulk kinetic energy, 128
Bulk Lorentz factor, 41, 45, 109

C
Causality argument, 95
Classic electron radius, 66
Classical electron radius, 60, 97
Clocks, 31
Collisions, 14, 17
Column of hydrogen, 127
Comoving energy density, 136
Comoving frame, 38
Compactness, 77, 100
Compactness parameter, 103, 105
Compton Gamma Ray Observatory, 107
Compton hump, 120
Compton reflection, 120, 122
Compton reflection hump, 127
Compton scattering, 65
Compton thick sources, 127
Comptonization, 13
Comptonization parameter, 82
Comptonization spectra, 85
Continuity equation, 105
Contraction, 32
Cooling rate, 106

G. Ghisellini, *Radiative Processes in High Energy Astrophysics*,
Lecture Notes in Physics 873, DOI 10.1007/978-3-319-00612-3,
© Springer International Publishing Switzerland 2013

Cooling time, 50, 76
Cosmic IR background, 109
Cosmic rays, 32
Coulomb collisions, 15, 60
Covering factor, 119
Cross section, 16, 102
Cut-off power law, 120
Cyclotron, 54

D
Dead leptons, 105, 106
Dilation, 32
Direct Compton scattering, 68
Disk luminosity, 115
Doppler broadening, 121
Doppler effect, 33
Doppler factor, 36, 40, 42, 91
Doppler shift, 118
Downscattering, 78, 85
Dust, 126
Dusty torus, 125

E
Eddington limit, 115
Eddington luminosity, 45, 71, 115
Effective cross section, 74
Einstein coefficients, 8, 11, 57
Einstein satellites, 111
Electric field, 66
Electric field of a moving charge, 18
Electromagnetic wave, 68
Electron radius, 49
Electron–positron pair production, 95
Electron–positron pairs, 45, 115
Electron–positrons, 136
Emission lines, 41, 117
Emission time, 44
Emissivity, 2, 11, 24, 39, 55, 61, 89
Emitted power, 47
Emitting time, 52
Energy density, 3, 28
Energy density of the radiation, 75
Energy exchange, 14
Energy gains, 105
Energy losses, 105
Energy reservoirs, 137
Energy spectrum, 79
Energy threshold, 97
Equipartition, 138
Equivalence principle, 37
Equivalent width of a line, 130
Escape time, 3
Exchange of photons, 14
External Compton, 135

F
Fe line, 120
Fine structure constant, 97
Flat radio spectrum, 129
Flat spectrum quasars, 92
Flat Spectrum Radio Quasars, 130
Fluorescent Iron line, 121, 127
Fluorescent line, 120
Flux, 2, 38
Flux density, 43
Forbidden line, 118
Fourier transform, 51, 54
Fourier transformation, 55
FR I radio-galaxies, 128
FR II radio-galaxies, 128
Free–free absorption, 25
Full width at half maximum, 118
Funnel, 126

G
Gamma Ray Bursts, 95, 103, 108
Gaunt factor, 24
General relativity, 124
Giant ellipticals, 128
Gravitational light bending, 123
Gravitational redshift, 123
Gyration, 48
Gyration frequency, 49
Gyration period, 54
Gyroframe, 54

H
Harmonic, 54, 55
HEAO–1, 111
Heating, 76, 105
Host galaxy, 114

I
Impact factor, 24
Impact parameter, 16, 23
Injection rate, 106
Intensity, 2, 38
Interferometric technique, 112
Interstellar scintillation, 41
Intra-Day Variable (IDV) sources, 41
Inverse Compton, 137
Inverse Compton frequency, 78
Inverse Compton process, 89, 106
Inverse Compton scattering, 60, 69, 72, 105
Ionization parameter, 119
Iron line, 123

J
Jet, 38, 41, 44, 92, 113, 128, 135

K
Keplerian motions, 119
Kerr black hole, 124
Kirchoff law, 25, 57
Klein–Nishina cross section, 68, 69, 71, 101
Klein–Nishina effects, 122
Klein–Nishina regime, 65, 76

L
Landau levels, 54
Larmor formula, 20, 23, 47, 48, 65, 66
Larmor frequency, 49, 52, 61
Larmor radius, 48, 49
Larmor wavelength, 60
Length contraction, 33
Lift, 36, 37
Light crossing time, 77
Limits of validity, 53
Lobe emission, 129
Lorentz force, 47, 48
Lorentz invariant, 47
Lorentz transformations, 31
Luminosity, 1, 38
Luminosity distance, 41
Luminosity of a typical galaxy, 1
Lyα line, 134

M
Magnetic energy density, 49
Magnetic moment, 17
Mass accretion rate, 115
Maxwellian, 25, 26, 57, 60, 82, 83, 105
Maxwellian distribution, 13
Maxwellian-like, 13
Mean free path, 11
Mesons, 32
Microwave background, 111
Minimum energy, 138
Misaligned jets, 129
Momenta, 13
Moving bar, 32
Moving square, 34, 33
Multiple Compton, 86
Multiple Compton scatterings, 88
Multiple scattering, 82

N
Narrow emission lines, 119
Narrow Line Region (NLR), 113
Narrow Line Seyfert 1 Galaxies, 128
Negative absorption, 11
NGC 1068, 125
Non-relativistic Maxwellian distribution, 13
Non-thermal, 13
Non-thermal pairs, 101
Non-thermal particle distribution, 15
Non-thermal plasmas, 15, 101
Non-thermal spectrum, 120
Nova Muscae, 71

O
Obscuration, 125
Optical depth, 101
Optically thin, 2

P
Pair annihilation rate, 97
Pair balance, 98
Pair plasmas, 99
Pair production mechanism, 97
Pair production process, 104
Pairs, 95
Pattern, 21
Pattern of the scattered radiation, 67
Peanut shape, 66
Photon spectrum, 79
Photon–photon, 101
Photon–photon absorption, 103, 104
Photon–photon collision, 95, 105
Photon–photon cross section, 102
Photon–photon interaction, 97
Pitch angle, 48, 49, 61
Pitch angle averaged absorption coefficient, 62
Pitch angle averaged synchrotron emissivity, 61
Pitch angles, 50
Polarization, 67
Power law distribution, 55
Power of jet, 135, 140
Poynting flux, 92, 128, 136, 137
Poynting vector, 20
Proton–proton collisions, 105
Pulsars, 111

Q
Quasars, 111
Quasi-saturation, 87
Quasi-thermal, 82

R
Radiation energy density, 42, 137
Radiation patterns, 51
Radiation pressure, 115
Radiation transfer, 58
Radiative energy density, 2
Radiative transfer, 63, 103
Radiative transport, 5, 99

Radio knots, 44
Radio lobes, 50, 128, 137
Radio loud quasar, 50
Radio maps, 44
Radio-galaxies, 113
Radio-loud AGN, 90, 92, 128
Radio-loud quasars, 44
Radio-loud sources, 91, 135
Raleigh–Jeans, 25, 116
Raleigh–Jeans law, 27
Random Lorentz factor, 63
Random walk, 12
Re-isotropization process, 73
Received power, 48, 50
Recoil of the electron, 68
Redshift, 112, 113
Reference frames, 31
Relativistic bulk motion, 91, 136
Relativistic transformations, 45
Relativistically broadened lines, 123
Reprocessing, 108
Reprocessing of pairs, 106
Reverberation mapping, 119
Rotation, 34
Ruler, 31

S
Saturated pair cascade, 106
Scattering, 12, 13
Scattering angle, 68
Scattering orders, 86
Scattering plane, 68
Schwarzschild radius, 95, 103, 115, 116
Seed photons, 80, 134
Self absorption frequency ν_t, 134
Self-absorbed, or thick, regime, 63
Self-absorption frequency, 59, 63, 135
Seyfert galaxies, 124
Seyfert Type 1, 125
Shock acceleration, 15
Sloan Digital Sky Survey, 118
Special relativity, 31, 35
Specific intensity, 63
Spectral index, 103
Spin of the black hole, 124, 140
Spontaneous emission, 8
SSC, 135
SSC flux, 91
SSC spectrum, 90
Steep radio spectrum, 129
Stefan–Boltzmann constant, 27, 116
Stimulated emission, 9, 11
Sun, 13, 28, 111
Sun luminosity, 1
Superluminal, 44
Superluminal motion, 43, 112, 135
Synchrotron absorption, 57, 59
Synchrotron absorption cross section, 59, 60, 63
Synchrotron cooling, 76
Synchrotron flux, 56
Synchrotron frequency, 56
Synchrotron peak, 64
Synchrotron power, 49
Synchrotron self absorption, 47
Synchrotron self-Compton, 89, 132

T
Targets, 103
Temperature, 14
The X-Ray Corona, 120
Thermal, 13
Thermal broadening, 118
Thermal comptonization, 82, 121
Thermal pairs, 96
Thermalization, 60
Thick spherical source, 5
Thomson cross section, 68
Thomson regime, 72
Thomson scattering, 45
Thomson scattering cross section, 49, 60
Threshold energy, 101
Time contraction, 36
Time dilation, 35, 36
Torus, 113
Total absorption, 11
Total cross section, 66, 68
Total loss rate, 74
Transit time, 99
Travel paths, 32
Type 1 Seyferts, 124
Type 2 Seyferts, 125

U
Uhuru, 111
Unification scheme, 124
Upscattering, 78

V
Variability time-scale, 41
Velocity field, 19
Very Long Baseline Interferometry, 43
Virial temperature of protons, 95
VLBI, 41, 92, 93

W
Wien bump, 88
Wien distribution, 84, 97

Wien law, 27
Wien peak, 87
Wien plasmas, 99, 100
Wien spectrum, 87

X
X-ray background, 112, 127
X-ray cavity, 135
X-ray corona, 113